いるかの30年のい 300600でのひかのか 0で965年の 535年0300い 35060 PROCEEDINGS OF THE NATIONAL ACADEMY OF SCIENCES OF GEORGIA

qimiis seria CHEMICAL SERIES

ISSN - 0132 - 6074

2025, ტომი Volume 45

თბილისი – TBILISI

しらもらめの30
 この
 しらもらめの30
 この
 この

qimiis seria

CHEMICAL SERIES

ISSN - 0132 - 6074

2025, <mark>ტომი</mark> Volume 45

> ჟურნალი დაარსდა 1975 წელს The Journal is founded in 1975

თბილისი – TBILISI

2025

საქართველოს მეცნიერებათა ეროვნული აკადემიის მაცნეს ქიმიის სერიის ეს ტომი მოიცავს 2023 წლის 23-25 წოემბერს ქ.თბილისში ჩატარებული მე-2 საერთაშორისო სამეცნიერო კონფერენციისა და სეზონური სკოლის "მეცნიერება, განათლება, ინოვაციები და ქიმიური ტექნოლოგიები – იდეიდან დანერგვამდე" მასალებს.

რედაქტორები: აკადემიკოსი ვ. ციციშვილი, წევრ-კორესპონდენტი გ. ტატიშვილი
საქართველოს მეცნიერებათა ეროვნული აკადემია,
ქიმიისა და ქიმიური ტექნოლოგიების განყოფილება,
0108, თბილისი, შ. რუსთაველის გამზ. #52
პასუხისმგებელი მდივანი ქ. ებრალიძე,
ივანე ჯავახიშვილის სახ. თბილისის სახელმწიფო უნივერსიტეტის
პეტრე მელიქიშვილის სახ. ფიზიკური და ორგანული ქიმიის ინსტიტუტი,
0186 თბილისი, ა. პოლიტკოვსკაიას ქ. #31, ტელ. 254-15-62, e-mail: ketevan.ebralidze@tsu.ge
რ.აგლაძის
პასუხისმგებელი მდივანი ლ. კვინიკაძე,
ივანე ჯავახიშვილის სახ. თბილისის სახელმწიფო უნივერსიტეტის
რაფიელ აგლაძის სახ. არაორგანული ქიმიისა და ელექტროქიმიის ინსტიტუტი,
ოაფიელ აგლაბის მამ. არაორგაბული ქიმიისა და ელექტორქიმიის იმმტიტუტი,
0186 თზილისი, ე. მინდელის #11, ტელ. 577 5353 78, e-mail: <u>lela.kvinikadze@tsu.ge</u>
0186 თბილისი, ე. მინდელის #11, ტელ. 577 5353 78, e-mail: lela.kvinikadze@tsu.ge This volume of Proceedings of the National Academy of Sciences of Georgia includes the materials of the 2 nd International Scientific Conference and Seasonal School "Science, Education, Innovations and Chemical Technologies – From Idea to Implementation" held on November 23-25, 2023, in Tbilisi.
0186 თბილისი, ე. მინდელის #11, ტელ. 577 5353 78, e-mail: lela.kvinikadze@tsu.ge This volume of Proceedings of the National Academy of Sciences of Georgia includes the materials of the 2 nd International Scientific Conference and Seasonal School "Science, Education, Innovations and Chemical Technologies
0186 თბილისი, ე. მინდელის #11, ტელ. 577 5353 78, e-mail: lela.kvinikadze@tsu.ge This volume of Proceedings of the National Academy of Sciences of Georgia includes the materials of the 2 nd International Scientific Conference and Seasonal School "Science, Education, Innovations and Chemical Technologies – From Idea to Implementation" held on November 23-25, 2023, in Tbilisi.
0186 თბილისი, ე. მინდელის #11, ტელ. 577 5353 78, e-mail: lela.kvinikadze@tsu.ge This volume of Proceedings of the National Academy of Sciences of Georgia includes the materials of the 2 nd International Scientific Conference and Seasonal School "Science, Education, Innovations and Chemical Technologies – From Idea to Implementation" held on November 23-25, 2023, in Tbilisi. Editors: Academician V.Tsitsishvili, Corresponding Member G.Tatishvili Georgian National Academy of Sciences, Department of Chemistry and Chemical Technologies 52 Rustaveli av., Tbilisi 0108 Executive Secretary K.Ebralidze,
0186 თბილისი, ე. მინდელის #11, ტელ. 577 5353 78, e-mail: lela.kvinikadze@tsu.ge This volume of Proceedings of the National Academy of Sciences of Georgia includes the materials of the 2 nd International Scientific Conference and Seasonal School "Science, Education, Innovations and Chemical Technologies – From Idea to Implementation" held on November 23-25, 2023, in Tbilisi. Editors: Academician V.Tsitsishvili, Corresponding Member G.Tatishvili Georgian National Academy of Sciences, Department of Chemistry and Chemical Technologies 52 Rustaveli av., Tbilisi 0108
0186 თბილისი, ე. მინდელის #11, ტელ. 577 5353 78, e-mail: lela.kvinikadze@tsu.ge This volume of Proceedings of the National Academy of Sciences of Georgia includes the materials of the 2 nd International Scientific Conference and Seasonal School "Science, Education, Innovations and Chemical Technologies – From Idea to Implementation" held on November 23-25, 2023, in Tbilisi. Editors: Academician V.Tsitsishvili, Corresponding Member G.Tatishvili Georgian National Academy of Sciences, Department of Chemistry and Chemical Technologies 52 Rustaveli av., Tbilisi 0108 Executive Secretary K.Ebralidze, Ivane Javakhishvili Tbilisi State University
0186 თბილისი, ე. მინდელის #11, ტელ. 577 5353 78, e-mail: lela.kvinikadze@tsu.ge This volume of Proceedings of the National Academy of Sciences of Georgia includes the materials of the 2 nd International Scientific Conference and Seasonal School "Science, Education, Innovations and Chemical Technologies – From Idea to Implementation" held on November 23-25, 2023, in Tbilisi. Editors: Academician V.Tsitsishvili, Corresponding Member G.Tatishvili Georgian National Academy of Sciences, Department of Chemistry and Chemical Technologies 52 Rustaveli av., Tbilisi 0108 Executive Secretary K.Ebralidze, Ivane Javakhishvili Tbilisi State University Petre Melikishvili Institute of Physical and Organic Chemistry
O186 თბილისი, ე. მინდელის #11, ტელ. 577 5353 78, e-mail: lela.kvinikadze@tsu.ge This volume of Proceedings of the National Academy of Sciences of Georgia includes the materials of the 2 nd International Scientific Conference and Seasonal School "Science, Education, Innovations and Chemical Technologies – From Idea to Implementation" held on November 23-25, 2023, in Tbilisi. Editors: Academician V.Tsitsishvili, Corresponding Member G.Tatishvili Georgian National Academy of Sciences, Department of Chemistry and Chemical Technologies 52 Rustaveli av., Tbilisi 0108 Executive Secretary K.Ebralidze, Ivane Javakhishvili Institute of Physical and Organic Chemistry 31 Politkovskaia str., Tbilisi 0186; tel.: 254-15-62; e-mail: ketevan.ebralidze@tsu.ge Executive Secretary L. Kvinikadze , Ivane Javakhishvili Tbilisi State University
O186 თბილისი, ე. მინდელის #11, ტელ. 577 5353 78, e-mail: lela.kvinikadze@tsu.ge This volume of Proceedings of the National Academy of Sciences of Georgia includes the materials of the 2nd International Scientific Conference and Seasonal School "Science, Education, Innovations and Chemical Technologies – From Idea to Implementation" held on November 23-25, 2023, in Tbilisi. Editors: Academician V.Tsitsishvili, Corresponding Member G.Tatishvili Georgian National Academy of Sciences, Department of Chemistry and Chemical Technologies 52 Rustaveli av., Tbilisi 0108 Executive Secretary K.Ebralidze,

CONTENT

V. Tsitsishvili - Reasons for Using Natural Zeolites of Georgia				
V. Tsitsishvili, N. Mirdzveli, N. Dolaberidze, M. Nijaradze, Z. Amiridze, B. Khutsishvilili - Identification of Impurities in Paper Made from Waste Paper	22			
S. Stefanov, L. Ljutzkanov, V. Beschkov – Performance of Sulfide-Driven Fuel Cell at Different Catodes and Processes				
V. Majidzade, S. Javadova, S. Jafarova, A. Aliyev, D. Tagiyev - Electrodeposition and Determination of the Bandgap of Thin Films Fe-Se	32			
T. Paikidze, Sh. Japaridze, G. Tatishvili, E. Kachibaia - Selection of Starting Reagents, Reactor Material and Synthesis Method for Semi-Industrial Production of Promising Cathode Materials for Lithium-Ion Batteries	35			
V. Varazashvili, M. Tsarakhov, T. Mirianashvili, M. Khundadze, T. Machaladze – Magnetic Heat Capacity Anomalies of Lanthanide-Iron Complex Oxides				
M. Avaliani, V. Chagelishvili, E. Shapakidze, G. Todradze Gulnara, N. Barnovi, K. Chikovani – A Comparative Study of Synthesis from Solution-Melts with Thermal Synthesis for obtention of Condensed Phosphates Avaliani Marina				
E. Shapakidze, M. Avaliani, M. Nadirashvili, V. Maisuradze, I. Gejadze, T. Petriashvili – Features of the Synthesis of Metakaolin Based on Calcined Shales				
M. Kapanadze, M. Mshvildadze, N. Kebadze, T. Loladze – Pecularities of Glaze Production Using Technogenic Raw Materials				
L. Bagaturia, T. Chakhunashvili – On the Issue of Safe Recycling of Amortizied Lead Batteries	54			
V. Tsitsishvili, N. Dolaberidze, N Mirdzveli, M. Nijaradze, Z. Amiridze, B. Khutsishvilili- Heat-Acid Treatment of Natural Georgian Heulandite				
N. Gabitashvili, M. Tsintsadze, N. Gegeshidze, N. Kilasonia, T Tsintsadze, D Lochoshvili - Coordination Capabilities of Olanzapine: A Semi-Empirical Approach	66			
T. Qamushadze, E. Khutsishvili, N. Kobulashvili, M. Darchiashvili - Development of Graphene Poduction Technology	70			

სარჩევი

ვ. ციციშვილი - საქართველოს ბუნებრივი ცეოლითების გამოყენების მიზეზები	6
ვ. ციციშვილი, წ. მირძველი, წ. დოლაბერიძე, მ. ნიჟარაძე, ზ. ამირიძე, ბ. ხუციშვილი - ნარჩენებისგან დამზადებულ ქაღალდში მინარევების იდენტიფიცირება	22
ს. სტეფანოვი, ლ. ლუცკანოვი, ვ. ბეშკოვი – სულფიდზე მომუშავე საწვავის უჯრედის მუშაობა სხვადასხვა კათოდებსა და პროცესების პირობებში	26
ვ. მაჯიზადე, ს. ჯავადოვა, ს. ჯაფაროვა, ა. ალიევი, დ. ტაგიევი – Fe-Se თხელი ფენების ელექტროდეპონირება და ზოლის განსაზღვრა	32
თ. პაიკიძე, შ. ჯაფარიძე, გ. ტატიშვილი, ე. ქაჩიბაია – ლითიუმ-იონური აკუმულატორებისთვის პერსპექტიული კათოდური მასალების ნახევრად ინდუსტრიული წარმოებისთვის საწყისი რეაგენტების, რეაქტორის მასალის და სინთეზის მეთოდის შერჩევა	35
ვ. ვარაზაშვილი, მ. ცარახოვი, თ. მირიანაშვილი, მ. ხუნდაძე, თ. მაჩალაძე – ლანთანიდ-რკინის კომპლექსური ოქსიდების მაგნიტური სითბოტევადობის ანომალიები	38
მ. ავალიანი, ვ. ჩაგელიშვილი, ე. შაფაქიძე, გ. თოდრაძე, წ. ბარნოვი, ქ. ჩიქოვანი – კონდენსირებული ფოსფატების მისაღებად ხსნარიდან ნალექების სინთეზის შედარებითი კვლევა თერმული სინთეზით	41
ე. შაფაქიძე, მ. ავალიანი, მ. ნადირაშვილი, ვ. მაისურაძე, ი. გეჯაძე, თ. პეტრიაშვილი — კალცინირებული ფიქლების საფუძველზე მეტაკაოლინის სინთეზის თავისებურებები	46
მ. კაპანაძე, მ. მშვილდაძე, ნ. ქებაძე, თ. ლოლაძე – ტექნოლოგიური ნედლეულის გამოყენებით მინანქრის წარმოების თავისებურებები	51
ლ. ბაღათურია, თ. ჩახნაშვილი – ამორტიზებული ტყვიის აკუმულატორების უსაფრთხო გადამუშავების საკითხზე	54
ვ. ციციშვილი, ნ. დოლაბერიძე, ნ. მირძველი, მ. ნიჟარაძე, ზ. ამირიძე, ბ. ხუციშვილი - ნატურალური ქართული ჰეულანდიტის თერმული მჟავით დამუშავება	59
წ. გაბიტაშვილი, მ. ცინცაბე, წ. გეგეშიბე, წ. კილასონია, თ. ცინცაბე, დ. ლოჩოშვილი - ოლანზაპინის კოორდინაციული შესაძლებლობები: ნახევრად ემპირიული მიდგომა	66
თ. ქამუშაძე, ე. ხუციშვილი, ნ. ქობულაშვილი, მ. დარჩიაშვილი - გრაფენის მიღების ტექნოლოგიის შემუშავება	70

Reasons for Using Natural Zeolites of Georgia

V. Tsitsishvili*

¹ Georgian National Academy of Sciences, 52 Rustaveli Av., Tbilisi, 0108, Georgia

Abstract. Zeolites, natural and synthetic hydrated crystalline aluminosilicates with an open three-dimensional framework that forms cavities and channels, have molecular-sieve, sorption, ion exchange and catalytic properties, due to which they are widely used in industry, agriculture, medicine and other sectors. Georgia is rich in natural zeolites, their occurrences have been studied by geologists, and research into their rational use is ongoing. The article presents an overview of the results of studies conducted by Georgian scientists in recent years on the possibility of using natural zeolites such as heulandite-clinoptilolite, analcime, laumontite, mordenite, phillipsite and scolecite. It has been shown that Georgian zeolites can be used in agriculture as feed additives and fertilizer components, as adsorbents for capturing antibiotics and volatile nitrosamines, as catalysts for the synthesis of aspirin and methyl salicylate, as ion exchangers for wastewater treatment from heavy metals, as carriers of biologically active metals for obtaining bactericidal fillers and filter materials, as well as in other industries.

Keywords: analcime, heulandite-clinoptilolite, laumontite, mordenite, phillipsite, scolecite

ვ. ციციშვილი - საქართველოს ბუნებრივი ცეოლითების გამოყენების მიზეზები

რეზიუმე. ცეოლითები, ბუნებრივი და სინთეზური ჰიდრატირებული კრისტალური ალუმინოსილიკატები ღია სამგანზომილებიანი ჩარჩოებით, რომლებიც ქმნიან ღრუებს და არხებს, აქვთ მოლეკულურ-საცრული, სორბციული, იონმიმოცვლითი და კატალიზური თვისებები, რის გამოც ისინი ფართოდ გამოიყენება მრეწველობაში, სოფლის მეურნეობაში, მედიცინასა და სხვა სექტორებში. საქართველო მდიდარია ბუნებრივი ცეოლითებით, მათი გამოვლინებები შესწავლილია გეოლოგების მიერ და მიმდინარეობს მათი რაციონალური გამოყენების კვლევა. სტატიაში წარმოდგენილია ქართველი მეცნიერების მიერ ბოლო წლებში ჩატარებული კვლევების შედეგების მიმოხილვა ისეთი ბუნებრივი ცეოლითების გამოყენების შესაძლებლობის შესახებ, როგორიცაა ჰეილანდიტ-კლინოპტილოლიტი, ანალციმი, ლომონტიტი, მორდენიტი, ფილიპსიტი და სქოლეციტი. ნაჩვენებია, რომ ქართული ცეოლითები შეიძლება გამოყენებულ იქნას სოფლის მეურნეობაში, როგორც საკვების დანამატები და სასუქის კომპონენტები, როგორც ადსორბენტები ანტიბიოტიკების და აქროლადი ნიტროზამინების დასაჭერად, როგორც კატალიზატორები ასპირინისა და მეთილის სალიცილატის სინთეზისთვის, როგორც იონმიმომცვლელები მძიმე მეტალებისაგან ჩამდინარე წყლების გასაწმენდად, როგორც ბიოლოგიურად აქტიური ლითონების მატარებლები ბაქტერიციდული შემავსებლების და მფილტრავი მასალების მისაღებად, ისევე როგორც სხვა სფეროებში.

Introduction

The famous American geologist and mineralogist F.A. Mumpton, in an article published at the end of the 20^{th} century [1], called zeolites "La Roca Magica – a magic stone" and predicted the rapid development of research and applications of zeolites in the 21^{st} century. Zeolites are hydrated crystalline aluminosilicates of general formula $M_x[Al_xSi_yO_{2(x+y)}]$ ·mH₂O (where M^+ is compensating singly charged ion), built from alternating SiO₄ and AlO₄–tetrahedra and forming an open 3D framework with cages and channels. Due to this structure, zeolites have a complex of molecular-sieve, sorption, ion exchange and catalytic properties. Today the Database of Zeolite Structures of the International Zeolite Association [2] includes 256 different types of frameworks, of which less than 40 occur in Nature, the rest are obtained synthetically.

The scientist's prediction came true, as evidenced not only by numerous reviews of studies on the possibilities of using natural and synthetic zeolites in industry, agriculture, medicine, environmental protection and other fields, but also by the actual implementation of the results of these studies in practice and everyday life.

Georgia is rich in natural zeolites such as heulanditeclinoptilolite, analcime, mordenite, laumontite and phillipsite; scolecite, chabazite and others are also found. Deposits and manifestations of zeolites in Georgia were studied by famous Georgian geologists Alexander Tvalchrelidze, Giorgi Gvakharia and Nikoloz Skhirtladze, the results were summarized in a monograph [3]. The composition, structure and properties of natural zeolites of Georgia have been studied since the 1960s under the guidance of famous Georgian chemists Giorgi Tsitsishvili and Teimuraz Andronikashvili, the results were included in a review monograph [4].

The purpose of this publication is to analyze the results of studies of Georgian natural zeolites obtained in recent years mainly using samples of zeolite rocks from newly investigated plots [5], including natural zeolites such as heulandite-clinoptilolite, analcime, laumontite, mordenite, phillipsite and scolecite.

Heulandite-Clinoptilolite

Heulandite-clinoptilolite with the crystal chemical data $M_8(H_2O)_{24}[Al_8Si_{28}O_{72}]$ -**HEU** and structure shown in Fig. 1 is the most common natural zeolite found mainly in sedimentary rocks of volcanic origin.

^{*}E-mail v.tsitsishvili@gmail.com

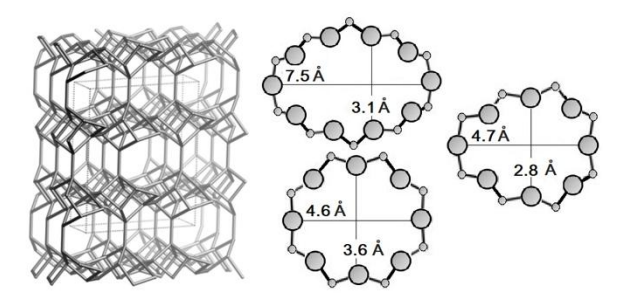


Fig. 1. HEU framework constructed from 10- and 8-membered rings viewed along [001], and small 8-ring viewed along [100].

Such deposits are of strong commercial interest because heulandite-clinoptilolite tuffs are often quite pure and can be mined by simple methods. At the turn of the century, in North America and Europe, most production went into animal hygiene applications, including cat litter and other animal bedding, with the remainder divided between applications in animal feed, fertilizers, and building materials (dimension stones, pozzolanic cements and concrete, and lightweight aggregates) [6]. Over the past twenty years, the consumption of HEU tuffs for the production of animal feed, fertilizers and cement has increased significantly, mainly due to the rapid development of agriculture and construction in China and other countries in the region.

A large deposit of sedimentary HEU zeolite-bearing tuffs is located in the Tedzami River valley in eastern Georgia, its reserves amount to at least 36 million tons, during the years of liquidation of the consequences of the 1986 Chernobyl disaster up to 120 thousand tons per year were mined there, currently production is limited to several hundred tons and is used for cement production. The properties of a typical sample of zeolite-containing rock from the Tedzami deposit are summarized in Table 1, the amounts of framework (Ti atoms instead of Al atoms) and mineral (iron oxides and calcium carbonate) impurities are given per atom of aluminum.

Table 1. Properties of zeolite-containing rock from the Rkoni plot of the Tedzami deposit.

mon plot of the reazum deposit.				
Zeolite phase content, %	90			
Empirical formula	$Na_{0.25}K_{0.06}Ca_{0.19}Mg_{0.15} \\ [AlSi_{3.6}O_{9.2}] \cdot 3H_2O$			
Framework impurity	Ti _{0.005}			
Mineral impurity	Fe _{0.2} , Ca _{0.14}			

According to the data of powder X-ray diffraction patterns, the zeolite phase consists of high-silica heulandite (Si/Al=3.6) and chabazite ($|M_{12}(H_2O)_{40}|$ [Al $_{12}Si_{24}O_{72}$]-CHA) in a molar ratio of 1:8 [7].

It is important to note that this tuff fully complies with the requirements of European legislation [8]: the content of the zeolite phase exceeds 80%, and among the mineral impurities there are no quartz or fibrous minerals, so that the tuff of the Tedzami deposit can be used as feed for any kind of animal. It is believed that zeolite additives provide an increase in live weight by 8-12% and survival of young animals up to 99% for poultry, cattle, etc. These results were obtained by Georgian scientists who used both the zeolitic tuff from the Tedzami deposit itself and its combination with methionine complexes [9]. It was also established that Tedzami tuff can

be successfully used for long-term conditioning and structuring of soil and substrates, mechanical support of plant roots, pH optimization, as well as a water depot, to improve ion exchange properties, prolong the action of nutrients, and provide a favorable microbial background [10].

The feasibility of activating natural zeolite by its simple and inexpensive modification, as well as combining tuff with low-calorie brown coal, was demonstrated. Thus, if the introduction of untreated tuff into the soil increased the dry green mass of barley by approximately three times, then the introduction of modified tuff led to an increase in mass by approximately six times, while the simultaneous introduction of modified tuff and brown coal increased the mass by more than nine times [11].

By fusing Tedzami tuff with ammonium dihydrogen phosphate NH₄H₂PO₄ and adding potassium nitrate and microelements (Fe, Ca, Mn, Zn, Mg, Cu, Mo, Co, Sn), an anionic zeolite nanomaterial was obtained, which was successfully tested as an environmentally friendly complex fertilizer with a prolonged action for wheat and other grain crops [12].

The use of zeolites in construction has a long history, the most extensive example being the construction of the 240-mile Los Angeles Aqueduct early in the last century (1907-13), when more than 25% of the required Portland cement was replaced by inexpensive clinoptilolite-rich tuff quarried near Tehachapi, CA [13]. However, Georgian scientists managed to say a new word in this industry. Thus, it was proposed to use clinoptilolite-containing tuff, saturated with kiln gases of cement clinker such as CO₂, SO_x, NO_x, as additives in building materials [14].

The molecular sieve properties of HEU were used in the development of a method for the adsorption "capture" of frequently used fluoroquinolone anti-biotics (moxifloxacin and norfloxacin, see Fig. 2) from wastewater [15].

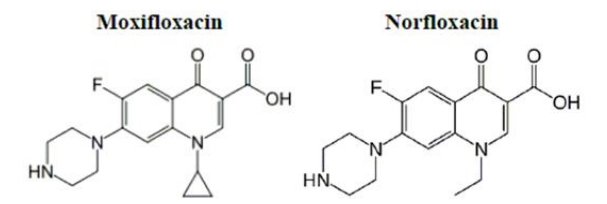


Fig. 2. Structural formulas of moxifloxacin and norfloxacin.

Adsorption measurements were carried out under static and dynamic conditions, using both natural tuff and its acid-treated form as adsorbent. The highest static adsorption capacities (2.7 and 4.14 mg/g for moxifloxacin and norfloxacin, respectively) were observed at a low initial concentration (0.2 mg/mL) of the antibiotic solution, the highest dynamic adsorption capacities (1.2 and 2.1 mg/g) were observed at a low flow rate (1.5 mg/mL) and low input concentration (0.2 mg/mL). While untreated and hydrochloric acid-activated tuff showed the same adsorption capacity for capturing moxifloxacin and norfloxacin, β -lactam broad-spectrum antibiotic ceftriaxone (see Fig. 3) was captured from aqueous solutions more successfully using acid-treated samples [16].

Fig. 3. Structural formula of ceftriaxone.

Natural heulandite has also been used to trap potent carcinogens such as volatile N-nitrosamines from tobacco smoke [17]. The experiments were carried out on the setup shown in Fig. 4, and a validated gas chromatography-mass spec-trometry (GC-MS, Agilent 6890/MSD 5975 system) method for the quantitative assessment of volatile Nnitrosamines such as N-nitrosodimethylamine (NDMA), Nnitrosomethyl-ethylamine (NMEA), N-nitrosodiethylamine (NDEA). N-nitrosodipropylamine (DPNA). nitrosodibutyl-amine (NDBA), N-nitrosopiperidine (NPIP), N-nitro-sopyrrolidine (NPYR), N-nitrosomorpholine (NMPA), N-nitrosodiphenylamine (NDPA) was developed.

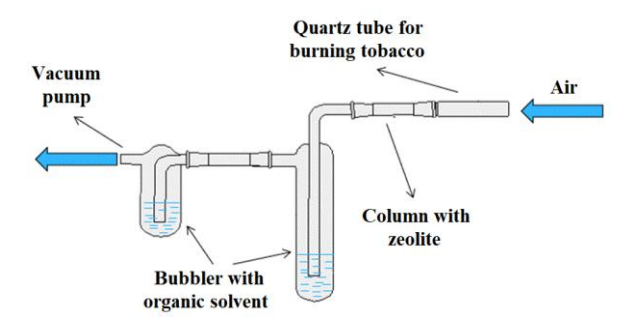


Fig. 4. Equipment for production of tobacco smoke and capture volatile N-nitrosamines.

Modified natural HEU zeolite successfully used as catalyst in aspirin production [18]. Typically, aspirin (acetylsalicylic acid, ASA) is produced in a two-step process called the salicylic acid/acetic anhydride method [19]. In the first stage, salicylic acid (SA) is obtained using the Kolbe-Schmitt reaction; in the second stage, acetylation of SA with acetic acid anhydride (AAA) occurs (see Fig. 6) either in a solvent or in the presence of basic or acid catalysts; the most effective acid catalysts are considered to be concentrated sulfuric or phosphoric acid at 60-80 °C.

The widely used sulfuric and phosphoric acids have extremely harmful and corrosive effects on the environment, and heterogeneous low-temperature and completely environmentally friendly new catalysts, namely decationized and dealuminated forms of natural clinoptilolite (Si/Al=4.4) from Dzegvi and heulandite (Si/Al=3.8) from Akhaltsikhe, have been proposed as an alternative.

In the catalytic reaction of esterification of salicylic acid with methanol to methyl salicylate (see Fig. 6), the best catalyst was ultra-dispersed crystallites (300-325 nm) of the acid-modified form of natural clinoptilolite from the Dzegvi deposit, obtained by exposure to ultrasound H-CL(US). It was found that the conversion of the salicylic acid and the selectivity to methyl salicylate on H-CL(US) are 90 and 95 %, respectively, at 120 °C [20], which is which is higher

than the values obtained when using sulfuric acid (85 and 90 %, at 100Prepara $^{\circ}$ C), and significantly higher than the results obtained on synthetic zeolites H-Beta and H-ZSM-5 (49, 44 and 82 %, at 135 $^{\circ}$ C).

Fig. 5. Scheme of reaction for obtaining of acetylsalicylic acid, ASA.

Simultaneously decationized dealuminated forms of catalysts were prepared by acid leaching of initial zeolites. It was demonstrated using the methods of gravimetric, UV, FTIR spectral and HPLC analysis, also by catalysts acidity measurements the symbatic change of ASA yield in the amount of proton acid centers (A1-(OH)-Si)of catalysts: $(Si/Al=10.7) > H-HEU (Si/Al=5.4) \ge H-HEU-M$ (Si/Al=4.1); yield of ASA on H-CL was about 92% and on heulandites – 75% at 80 $^{\circ}$ C.

Fig. 6. Scheme of reaction of the esterification of salicylic acid with methanol into methyl salicylate.

By modifying natural clinoptilolite using

- **≡Si-OH+BrCH**₂COOH→**≡**Si-O-CH₂COOH+HBr and
- **■Si-OH+C1CH**₂CH₂COOH →
- **■Si-O-CH**₂CH₂COOH + HCl

reactions, crystalline ionites were obtained [21].

Natural zeolites can be used in the production of synthetic zeolites as sources of silicon and aluminum. A synthetic mordenite-type ($|M_8(H_2O)_{24}|$ [Al $_8Si_{40}O_{96}$]-MOR) zeolite material was prepared from natural heulandite from the Tedzami deposit by hydrothermal crystallization in the absence of seeds and organic templates [22]. Recrystallization of HEU in MOR was carried out in the following steps:

- Preparation of raw materials included treating the tuff with a 20% aqueous solution of HCl, rinsing with water until the Cl⁻ ions completely disap-peared, and drying in an oven at a temperature of 100–105 °C;
- Suspension was prepared at a solid to liquid ratio of 1:3;

- **Gel formation**: the prepared suspension was treated with 10% aqueous NaOH solution, solid to liquid ratio 1:6, gel homogenization takes 30 minutes. Chemical composition of the gel prepa-red for aging and crystallization: SiO₂/Al₂O₃ = 9.8, Na₂O/SiO₂ = 0.08, H₂O/Na₂O = 250:
- Aging of the gel at room temperature took 7 days;
- Crystallization of the aged gel was carried out in Teflon flasks at a temperature of 100-110 °C; the duration of the process was up to 90 hours;
- Separation of the obtained crystalline material was carried out by filtration of the mother liquor, the solid material was washed with water to pH 8.0-8.5 and dried at a temperature of 90-100 °C.

The MOR-type framework of the obtained material is confirmed by powder X-ray diffraction patterns, no additional diffraction peak at $2\Theta=16.3$ indicating the formation of analcime was observed. The developed microporous structure of zeolite crystals in the synthesized samples is also confirmed by the relatively high average value (5.30 mmol/g) of water absorption capacity under static conditions at "plateau" pressure.

The resulting prismatic mordenite crystals have a width in the range of 0.15–0.45 μm and a length of up to 3 μm (see Fig. 7).

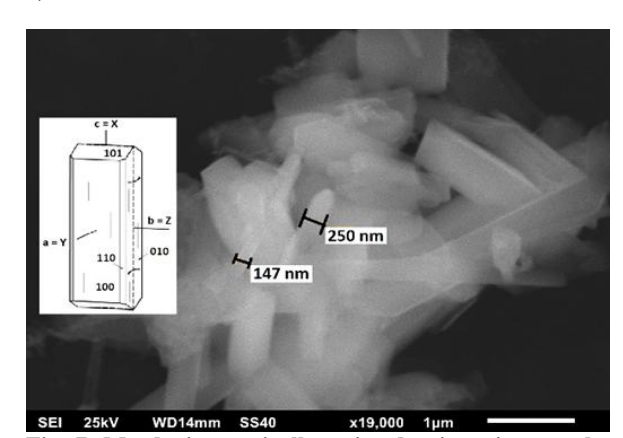


Fig. 7. Mordenite vertically striated prismatic crystals; magnification -19,000x.

The fibrous aggregates of mordenite obtained as a result of rapid recrystallization are characterized by a fiber diameter from 40 nm to 90 nm and a length of up to 10 μ m (see Fig. 8).

Thus, preliminary acid treatment of raw materials (tuff with a zeolite structure NEU) provides the possibility of a relatively fast and simple method for obtaining high-quality crystalline material of various morphologies, both prismatic crystals and nanosized fibrous aggregates.

Heulandite-bearing tuff from Tedzami deposit has a relatively low silicate modulus (Si/Al=3.6) and can be used as an ion exchanger. Silver-, copper- and zinc-containing microporous materials were synthesized using ion exchange reactions between acid-pretreated (0.025 mol/L HCl) zeolite microcrystals and a salt of the corresponding transition metal in the solid phase, followed by rinsing with distilled water [27]

According to X-ray energy dispersive spectra, powder X-ray diffraction patterns and Fourier transform infrared spectra, the obtained materials retain the crystalline structure of HEU

zeolite and contain more than 130 mg/g silver, 65-72 mg/g copper and 30-58 mg/g zinc. Prepared silver and coppercontaining materials show bacteriostatic activity towards Gram negative bacterium *Escherichia coli*, Gram positive bacteria *Staphylococcus aureus* and *Bacillus subtilis*, fungal pathogenic yeast *Candida albicans*, and a fungus *Aspergilus niger*; zinc-containing zeolite is active against *Bacillus subtilis*, weak against fungi and inactive against *E. coli* and staphylococcus. The most active is a silver-containing zeolite, but from a practical point of view, the most promising for applications is copper-containing heulandite.

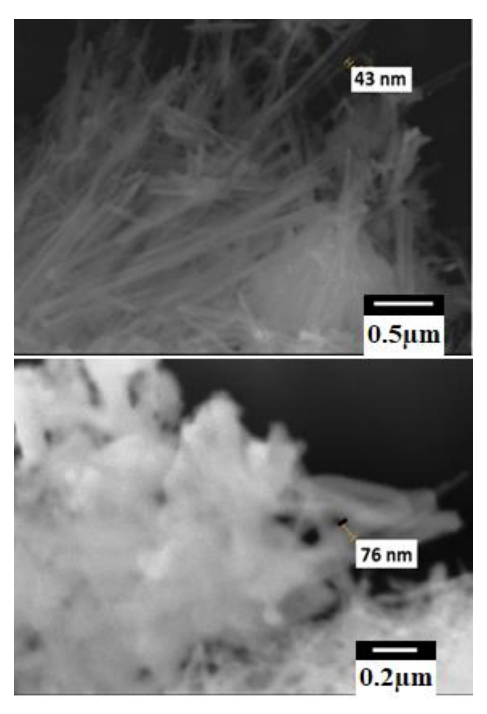


Fig. 8. Mordenite fibrous aggregates; magnification – 33,000x (top), 60,000x (bottom).

It was later shown [28] that the bacteriostatic activity of metal-containing samples is determined not only by the bioactive metal ions released into the liquid medium, but also by the type of zeolite. A synergistic effect was established: against E. coli and hay bacilli, as well as against yeast and black fungus, a mixture of zinc and copper forms of heulandite is most effective, and against staphylococcus, any binary mixture of silver, copper and zinc forms in a molar ratio of 1:1 relative to metals [29].

The obtained metal-containing heulandite samples were successfully tested as bactericidal fillers in the production of paper under factory conditions; the introduction of zeolite fillers was carried out on the paper web during the coating process, by adding a zeolite suspension to a boiled starch binder [30,31]. It was found that the introduction of coppercontaining (70 mg/g) filler in an amount of about 3 g/m² makes the paper waterproof and gives it bactericidal properties in particular against staphylococcus, and the introduction of zinc-containing (50 mg/g) filler in the same amount makes the paper bactericidal against E. coli.

The aim of the subsequent study [32] using the Tedzami heulandite-bearing tuff was to establish the possibility of imparting antimicrobial properties to packaging paper in a simpler way by introducing into the paper pulp not ready-

made zeolite fillers, but a mixture of zeolite and a salt of a bioactive metal.

Zeolitic tuff was crushed, fractionated to a particle size of less than 0.044 mm (325 US mesh), washed with a hydrochloric acid solution (0.025 mol/l) to remove clay impurities and "open" micropores, and dried to constant weight at a temperature of 95-100 °C. The cation exchange capacity (CEC) of the obtained sample was ≈ 3 mg-Eq/g; for comparison, a partially amorphized sample calcined at a temperature of 400 °C for one hour was used, in which the CEC was reduced to ≈ 2 mg-Eq/g.

Paper samples were prepared in the laboratory from shredded commercial tissue paper, which was placed in a glass laboratory crystallizer, covered with boiling water, hand shredded, and allowed to stand, after which boiled starch glue was added to the resulting mass, the paper pulp and glue were mixed, after which the resulting mixture was transferred to a polyethylene mesh (18 US mesh), evenly distributed on it, and dried at room temperature to constant weight. Metal salts and/or zeolite were added to the starch glue and applied to the surface of the wet paper.

It was found that the introduction of silver nitrate into the paper pulp leads to the reduction of silver cations Ag^+ and the formation of Ag^0 nanoparticles with an average size of 38 nm, which is facilitated by the introduction of crystalline (unheated) zeolite. Copper chloride dihydrate introduced into the paper pulp forms both large (>200 nm) crystallites and nanoparticles (<20 nm), zinc chloride forms nanoparticles.

The bacteriostatic properties of paper samples were studied by the disk diffusion method using cultures of *E. coli*, *Salmonella enteritidis*, *Staphylococcus aureus* and *Bacillus subtilis*, as well as fungal microorganisms *Candida albicans* and *Aspergilus niger*. Ag-containing paper without zeolite fillers has the lowest activity, and with the introduction of fillers, Zn-containing paper demonstrates the highest activity with respect to all microorganisms. Crystalline zeolite filler enhances the effect of silver with respect to *Salmonella* and *Bacillus subtilis*, and amorphized filler enhances the effect of zinc with respect to gram-positive bacteria and fungi; both zeolite fillers weaken the effect of copper.

Thermally and acid-modified heulandite was also used as carriers of bioactive metals. Acid treatment of natural zeolites is considered an effective method of "improving" their structure and properties, and under the influence of heat, the zeolite loses water molecules and undergoes structural changes.

It was found [33] that the acidic environment leads to significant

dealumination (the Si/Al ratio molar increases from 3.6 to decationization (the total charge of metal ions per Al atom decreases from 1 to 0.68) of heulandite from Tedzami. while hydrochloric acid solutions do not lead to the amorphization of microporous crystalline structure. but gradually dissolve it. Acid treatment also results in a sharp increase in the volume of micropores accessible to large molecules (from ≈7 to $80-90 \text{ mm}^3/\text{g}$) and the active surface area (from ≈ 13 to 120-175 m²/g), as well as changes in the mesoporous system, leading to the predominance of pores with a diameter of up to 4 nm.

Heating of heulandite results in stepwise dehydration occurring up to ≈800 °C, amorphization starting at ≈250 °C, and structural changes: the transition to the metastable phase of heulandite B at ≈340 °C is not recorded, but mineral wairakite (Ca(Al₂Si₄O₁₂) 2H₂O) is formed at \approx 500 °C; at temperatures above ≈1000 °C, the amorphous aluminosilicate contains crystalline inclusions of cristobalite (SiO₂ polymorph), αquartz, albite (Na(AlSi₃O₈), hematite (Fe₂O₃), and magnetite (FeO·Fe₂O₃); changes in the mesopore system upon heating are insignificant. It has also been shown that heat treatment increases the acid resistance of heulandite, which is expressed in a decrease in the degree of dealumination after acid treatment of calcined samples.

The enrichment of zeolite samples with biometals was carried out by ion exchange reactions in solutions of silver nitrate, copper chloride and zinc chloride; enrichment of untreated heulandite yields samples containing over 240 mg/g silver, about 43 mg/g copper and 60 mg/g zinc; in pre-treated samples, the metal content is usually lower, with the exception of pre-calcined samples, in which the copper content is 65-80 mg/g. According to the results of tests carried out by the disk diffusion method, pre-treatment does not increase the bacteriostatic activity of samples enriched with silver and copper, but acid treatment followed by the introduction of zinc initiates inhibition of the growth of Escherichia coli, Staphylococcus aureus and the fungal microorganisms Candida albicans and Aspergillus niger, and also slightly increases the activity with respect to Bacillus subtilis, the activity with respect to Salmonella enteritidis remains virtually unchanged [34].

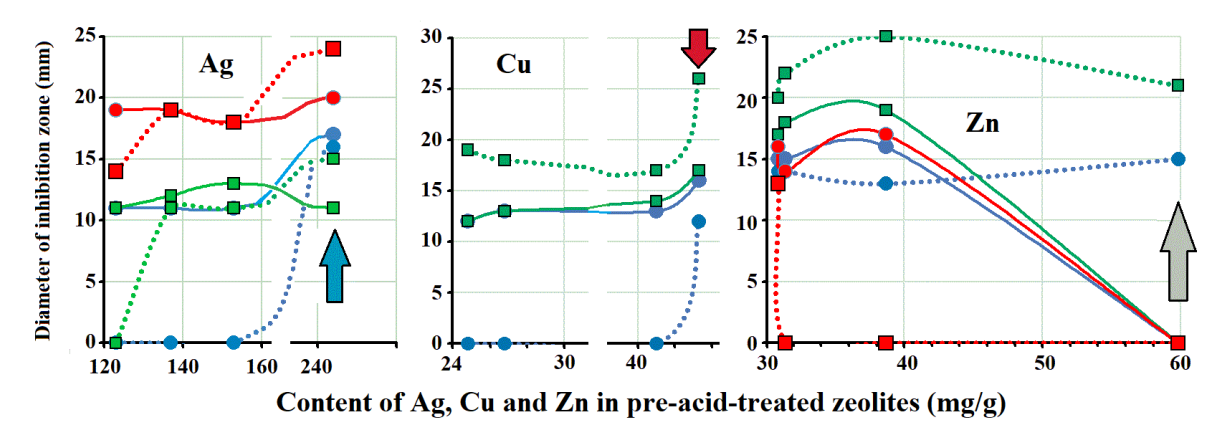


Fig. 9. Dependence of the diameter of the inhibition zones of the growth of microorganisms (1 - E. coli, 2 - Salmonella, 3 - Staphylococcus, 4 - Bacillus, 5 - Candida, 6 - Aspergillus) on the content of metals in pre-acid-treated samples; arrows show the metal content in the untreated samples.

Analcime

Analcime is characterized by the crystal chemical data $M_{16}(H_2O)_{16}[Al_{16}Si_{32}O_{96}]$ -**ANA**, its structure (see Fig. 10) is built from irregular channels formed by highly distorted 8-membered rings.

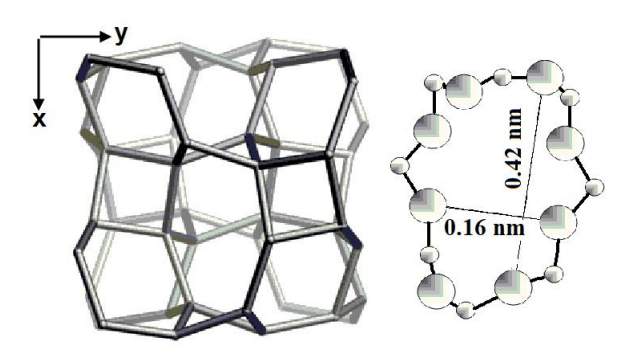


Fig. 10. Unit cell (left) and 8-membered ring (right) of analcime, ANA.

Analcime deposits are found in many areas of Georgia. Abundance of analcime associated with volcanogenicsedimentary rocks is observed in the Middle Eocene massifs of the Achara-Trialeti folded system, starting from the Mtskheta region, including the Borjomi Valley and to the west in the Bagdadi and Vani districts. Stratified rocks containing analcime are known in western Georgia in the deposits of the Jurassic carbonaceous and non-ferrous suites of the Kutaisi region [3]. Analcime from a basalt geode in the vicinity of Tbilisi, chemically crystallized analcime in sedimentary rocks in the vicinity of Kutaisi, and analcime of diagenetic origin in volcanogenic-sedimentary rocks of the Akhaltsikhe deposit have been well studied and characterized [3]. In addition, the properties of analcime-containing rocks from newly explored plots of deposits have been studied [5]: sedimentary analcime from the Chachubeti area of the Tedzami deposit and volcanogenic-sedimentary analcime from the Gelati deposit, Western Georgia.

Analcime is usually considered one of the most commonly used natural zeolites, but its use is limited due to the peculiarities of its crystal structure. Thus, the geometry of the entrance windows to the analcime channels makes it difficult for even such small molecules as water to pass through them,

and the adsorption capacity for water vapor of analcime is quite low, at room temperature not exceeding 2 mmol/g.

Typically, to increase the adsorption capacity of zeolites, acid treatment in dilute solutions is used, which allows the removal of large cations "closing" the entrance windows and an increase in the size of the windows due to moderate dealumination. However, analcime is characterized by rapid and significant removal of aluminum from the crystal structure even at low acid concentrations, but a high degree of dealumination (Si/Al>7) is unattainable even with long-term treatment in highly concentrated acid solutions. The removal of aluminum at an acid concentration of more than 0.5 mol/L can be expressed through the relative aluminum content CAI(N) by empirical formula

$$C_{Al}(N)=D_{max} [1+k\cdot exp(-c\cdot N)],$$

where N is the normality of the solution, maximum degree of dealumination $D_{\rm max}{=}0.42{\pm}0.02$, coefficients $k{=}1.38{\pm}0.07$, c=0.20±0.02 [34]. The process of acid dealumination in analcime is general in nature and does not depend on the cationic composition, but the removal of alkaline and alkaline earth cations is specific to samples of different origins. Figure 11 shows the dependence of water adsorption capacity of acid-treated analcime samples on the acid concentration and the number of treatments lasting one hour at room temperature.

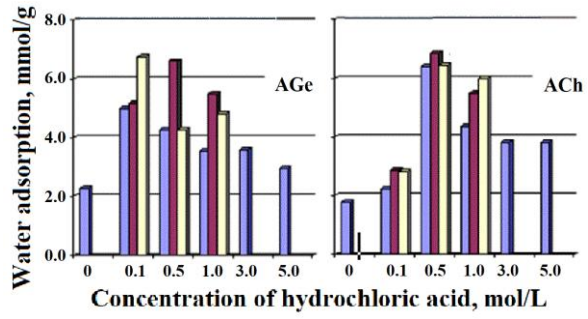


Fig. 11. Water adsorption of acid-treated analcime samples from Gelati (AGe) and Chachubeti (ACh).

For the sample from Gelati, the highest adsorption capacity ($\approx 7 \text{ mmol/g}$) is achieved after three treatments in a solution with a

concentration of 0.1 mol/L, and for the sample from Chachubeti after two treatments in a solution with a concentration of 0.5 mol/L [35].

Compared to heulandite, analcime has a higher specific aluminum content and, therefore, a higher ion-exchange capacity. The total ion exchange capacity for crude analcimes from Gelati and Chachubeti was found [36] to be in the range of 3.2–3.6 mEq/g and *approx*. 4.1 mEq/g for distilled water washed samples, which is comparable to 4.3 mEq/g for the ideal ANA structure taking into account the zeolite phase content (95 and 90% for washed samples from Gelati and Chachubeti, respectively).

Ion exchange isotherms for the sodium-enriched form of analcime sample from Chachubeti Na-ACh with the participation of monovalent (Li⁺, K⁺, NH₄⁺, Ag⁺) and divalent (Ca⁺², Sr⁺²) ions are shown in Fig. 12.

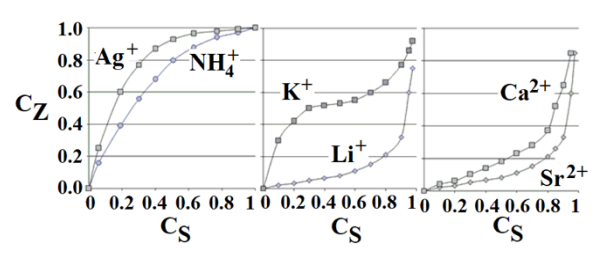


Fig. 12. Ion exchange isotherms $C_Z = f(C_S)$, where C_Z is the ion concentration in the zeolite, and C_S is its concentration in the solution, on Na-ACh at 20 °C and a solid: liquid ratio of 1:20 [36].

The selectivity sequence for the sodium-rich form, derived from ion exchange isotherms, is as follows: $NH_4^+>Ag^+>Li^+>Ca^{+2}>K^+\sim Sr^{+2}$. Na-ACh and sodium-rich forms of other natural analcimes can be successfully used to purify water contaminated with ammonium. Raw natural analcimes have lower ion exchange capacity and also a different selectivity series (Na+>K+>Ag+>NH_4+>Ca+2>Sr^+2>Li+, [36]), but they can also be used for ammonium absorption.

In order to clarify the possibilities of agricultural use of analcime-containing rocks and their modifications, the effect of analcime, its ammonia-enriched form and their mixtures with manure on the yield of cucumbers and scallop was studied in comparison with the results of using mineral fertilizers [37]. Good results were obtained using mixtures of analcime with manure - the yield of cucumbers increases by 60-70%, and scallops – by about 100%, while the application of mineral fertilizers increases the yield by 35 and 70%, respectively. An increase in seed growth was noted in areas with the introduction of zeolite, as well as an improvement in the appearance and quality of plant products. In particular, cucumber from such areas retains stable moisture during long-term storage at room temperature. Thus, the use of analcime mixtures with manure can be an alternative to the use of mineral fertilizers, and both raw analcime and analcime ion exchangers used to purify water contaminated with ammonia can be used.

Preliminary acid treatment of natural analcime enables the preparation of commercially valuable Linde Type A zeolite (crystal chemical data |Na₁₂ (H₂O)₂₇|8[Al₁₂Si₁₂O₄₈]8-**LTA**) by simple hydrothermal crystallization. Processing of the raw material into the target material also includes the stages of

suspension of the treated analcime, gelation and aging followed by crystallization at temperatures up to 90 °C.

The reaction mixture with the chemical composition $3.4\mathrm{Na}_2\mathrm{O}: \mathrm{Al}_2\mathrm{O}_3: 1.1\mathrm{SiO}_2$ yields a product with the molar ratio $\mathrm{Si/Al} \approx 1$ and characterized by an XRD pattern (see Fig. 13) and IR spectrum typical for the LTA framework; the number of water molecules in the resulting synthetic zeolite differs from that established in the ideal LTA structure (H₂O:Na=9:4) and depends on the crystallization conditions: hydrated materials (H₂O:Na=9:5.5) are produced at low temperature, high temperature results in dehydration (H₂O:Na=9:3).

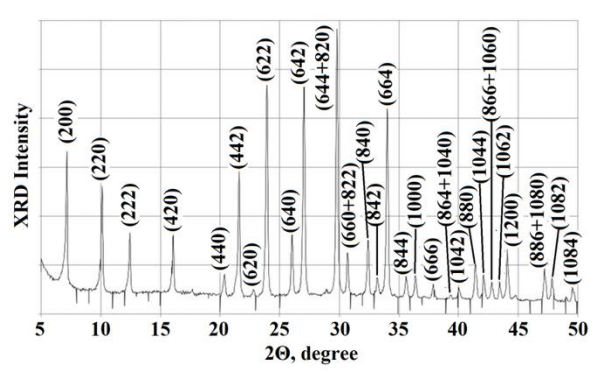


Fig. 13. Powder XRD pattern of the material obtained by the recrystallization of analcime; numbers in parentheses are Miller indices (hkl).

Rapid crystallization produces nanosized crystals and aggregates, whereas slow crystallization at relatively low temperatures produces micrometric crystallites (Fig. 14).

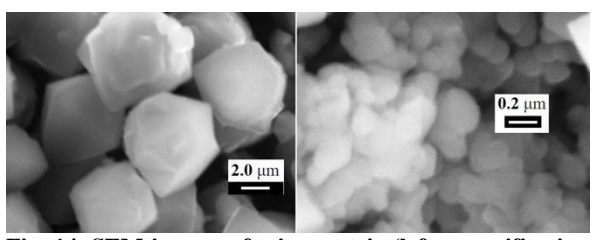


Fig. 14. SEM images of micrometric (left, magnification 5,500x) and nano (right, 55,000x) crystals of LTA zeolites recrystallized from analcime.

The resulting material has a fairly high ion exchange capacity of 4.5 mEq/g and can be used as a component in washing powders and water softening tablets [38].

Analcime from Chachubeti was used as a carrier of biometals, the materials obtained by the method of "dry" ion exchange contain up to 180 mg/g silver, 50 mg/g copper and 62 mg/g zinc, the silver form showed bacteriostatic activity against a wide range of microorganisms, the zinc form – against *Bacillus subtilis* and *Aspergillus niger*, and the copper form was inactive [39].

Synergism was found for mixtures of these forms of analcime: a mixture of copper and zinc forms showed weak activity against staphylococcus, a mixture of copper and silver forms was active against bacteria and fungal microorganisms, and a mixture of silver and zinc forms was

characterized by increased activity with a twofold decrease in silver content [28].

Laumontite

Laumontite (crystal chemical data $|M_8 (H_2O)_{16}|$ [Al $_8Si_{16}O_{48}$]-LAU, see Fig. 15) is one of the most common zeolite minerals known in Georgia; in some manifestations, its concentration in rocks reaches 85-90%, while the thickness of the laumontite layer exceeds 500 meters [3]. However, laumontite did not attract much attention and its research began only in the 21^{st} century [39].

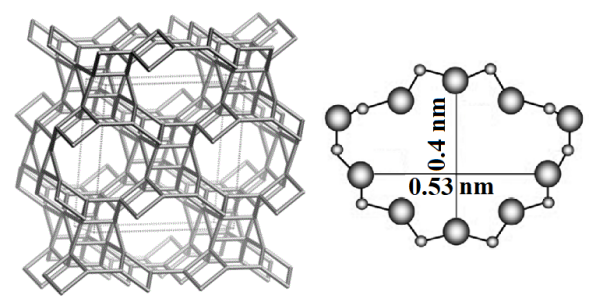


Fig. 15. Unit cell (left) and 10-membered ring (right) forming 1D system of laumontite channels [100]-10.

The phase and chemical composition, as well as the adsorption and ion exchange properties of seven samples of laumontite-containing rocks collected in the vicinity of Tbilisi (Botanical Garden, Bagebi, Ponichala), in the Gupta (Java region), Ateni Sioni, and the Khvedureti and Chkherimela rivers gorges were studied. The highest content of the zeolite phase was recorded in samples collected in the Botanical Garden and the Ateni Sioni gorge, 60-90% and 60-85%, respectively; in the first manifestation the capacity of the rock is 25 m, in the second – up to 700 m.

Although powder X-ray diffraction patterns and IR spectra confirm that the studied samples belong to LAU-type zeolites, the Si/Al molar ratio significantly exceeds the Si/Al=2 value accepted for this type. Probably, the high silicon concentration is due to the presence of quartz impurity, but X-ray diffraction does not provide the possibility of quantitatively assessing its content, since the quartz peak is overlapped by the intensive peak (002) at 2Θ =25.2°. Chemical analysis also shows the presence of impurities in the form of iron and manganese oxides. Calcium predominates in the cationic composition of all samples, although the sample taken in the Chkherimela gorge is characterized by a fairly high sodium content, and the sample taken in Gupta contains a significant amount of potassium.

Treatment in a dilute hydrochloric acid solution results in significant dealumination of laumontite. Thus, after treatment in a 0.1 mol/L solution, the aluminum content decreases by 1.4 times, while a further increase in the acid concentration affects the removal of the remaining aluminum to a lesser extent and after treatment in a 3 mol/L solution, the aluminum content decreases by only 1.8 times. The crystalline microporous structure of laumontite is preserved when treated in hydrochloric acid solutions with a concentration of less than 0.25 mol/L; at higher concentrations, the structure is destroyed, while when treated in ammonium chloride NH4Cl solutions with a concentration of up to 3 mol/L, the structure is preserved. When heated, the crystalline structure of laumontite is preserved up to a temperature of 450 °C,

complete destruction of the structure occurs at 800 $^{\circ}$ C; acid treatment reduces thermal stability and a change in structure occurs at 310 $^{\circ}$ C.

The values of ion exchange capacity for different cations, measured under static and dynamic conditions, indicate the following selectivity series for single-charged cations $Cs^+>Ru^+>NH_4^+>Li^+$ and divalent cations $Ba^{+2}>Sr^{+2}>Ca^{+2}>Mg^{+2}$, and this allows laumontite to be recommended for the extraction of radioactive cesium and strontium.

Studies were conducted on the possibility of using laumontite in plant growing [40], and it was found that the introduction of laumontite-containing rocks into the soil has a significant and dose-dependent effect of the introduced zeolite on the growth of the yield of wheat grain and on the straw mass output, and also, to a lesser extent, on the mass of wheat grains. There is also an increase in the mass of plant roots and an improvement in the biometric indicators of wheat.

Mordenite

Sedimentary deposits of mordenite (crystal chemical data $|M_8 (H_2O)_{24}|$ $[Al_8Si_{40}O_{96}]$ - \mathbf{MOR} , see Fig. 16) are present in many countries including Georgia. where the main explored reserves of mordenite are concentrated in the Akhaltsikhe deposit.

Synthetic mordenite is one of the "Big Five" zeolites (BEA, FAU, FER, MOR, and MFI) used in the modern chemical industry, in particular, conversions of petrochemical, for instance, the production of gasoline and volatile, flammable liquid hydrocarbons such as propylene, as well as aromatics productions (for example, ethylbenzene and cumene).

Synthetic mordenite differs from natural mordenite in that its channels allow ions or molecules with a diameter of up to ≈ 0.7 nm to pass through, while natural mordenites adsorb molecules with a diameter of no more than 0.45 nm.

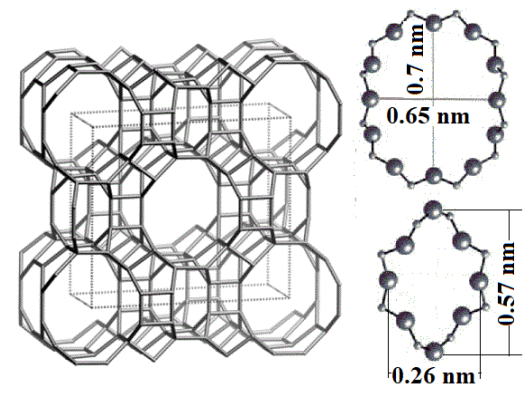


Fig. 16. Unit cell (left) and 8-, 12-membered rings (right) forming 2D system of mordenite channels [001]-12*↔[001]-8***.

The industrial, agricultural and other uses of natural mordenite have been reviewed by Colella [41]. Mordenite crystallizes in the form of fibrous aggregates, masses and vertically striated prismatic crystals, and handling fibrous mordenite minerals may pose health risks similar to erionite and asbestos [42, 43]. Therefore, mordenite-bearing

sedimentary rocks should be carefully examined by SEM to determine the crystalline morphology before use.

Mordenite has wider pores than heulandite, they can accommodate spherical molecules or their fragments with a diameter of up to 0.67 nm. Thus, mordenite can be used to trap both antibiotics moxifloxacin and norfloxacin from the aquatic environment [44] and N-nitrosamines from tobacco smoke [45].

In both cases, the hydrochloric acid-treated form of mordenite was shown to be a more effective adsorbent. According to the authors [44], the increase in the adsorption activity of mordenite as a result of its treatment with acid is associated with an increase in pore size due to the unblocking of the channels of the aluminosilicate framework of the adsorbent during the dealumination process.

As expected, mordenite was found to be somewhat more effective as a N-nitrosamine adsorbent [45] than heulandite, although both zeolites were significantly more effective than the conventional acetyl cellulose (ACC) filter (see Fig. 17).

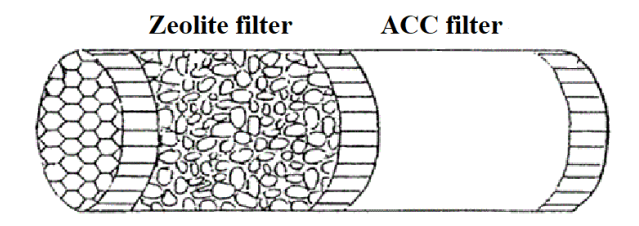


Fig. 17. Model cigarette filter consisting of acetyl cellulose and zeolite parts used in the study [45].

Thus, if after passing to bacco smoke through the ACC filter the NDMA concentration is $1.88~\mu g/mL$, then after passing smoke through zeolite filters the NDMA content decreases to 0.65~ and $0.56~\mu g/ml$ for H-HEU and H-MOR filters, respectively.

PHILLIPSITE

Phillipsite (crystalline chemical data $|M_6(H_2O)_{12}|$ [Al₆Si₁₀O₃₂]-**PHI**) is structurally built up of layers of 4- and 8-membered rings (see Fig. 18) forming double crankshaft chains, the framework contains 3D system of systems parallel to the crystallographic axes a, b and c: [100]-b* \leftrightarrow [010]-b*.

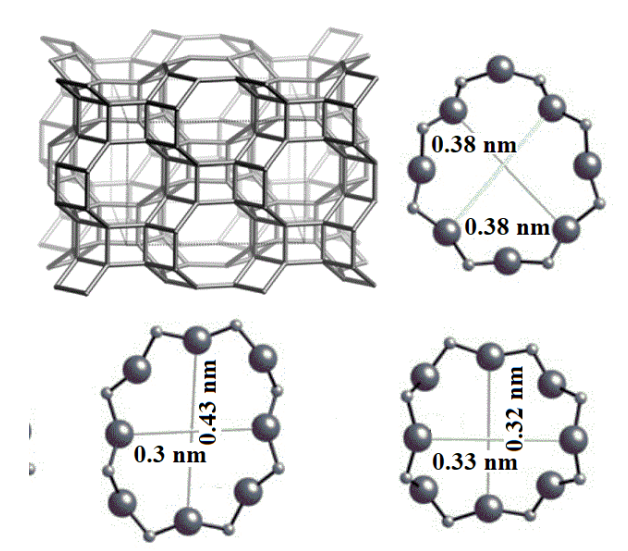


Fig. 18. Unit cell (top, left) and three 8-membered rings forming 3D system of phillipsite channels.

The applications of phillipsite are not as widespread as heulandite-clinoptilolite, but it has been used for ammonia adsorption [46] and removal of various heavy metals from wastewater [47], Ca-enriched phillipsite have been found to exhibit the ability to adsorb humic acids [48], and phillipsite has been shown to be effective in removing picolines from aqueous solutions over a wide range of concentrations [49]. Eocene rocks containing phillipsite were discovered in Georgia, first on the northern edge of the Akhaltsikhe Depression together with other zeolites, and then in the Guria Range [3], near the village of Shukhuti. The content of the zeolite phase in the rocks of the Akhaltsikhe deposit fluctuates within 60-70%, the main impurities are chlorite and montmorillonite; in the phillipsite-containing rocks of Shukhuti with a high potassium content, the zeolite phase is 60-80%, the main impurity in yellow-green samples is heulandite.

The total ion exchange capacity estimated from the results of chemical analysis [50] is in the range of 2.6–3.3 mEq/g for PA and 2.2–3.2 mEq/g for phillipsite from Shukhuti PS, which is at least 30% lower compared to 4.5 mEq/g for the synthetic P sample used in the preparation of the surfactant-modified material [51] as a standard.

In surfactant-modified zeolites (SMZ) charge-balan-cing ions M^+ located at the surface are replaced by high-molecular-weight quaternary amines, typically alkyltrimethylammonium halides, that form admicelles as a monolayer or a bilayer, and change SMZ surface charge from negative to positive. It is believed that SMZs are effective sorbents for removing from water not only inorganic cations, but also anions, as well as large non-polar organic substances that do not pass through the micropores of zeolite [52].

For the production of SMZ, clinoptilolite-containing tuffs are usually used, while phillipsite is characterized by a higher ion-exchange capacity and a developed mesopore system, which can also be an important factor in terms of immobilization of long-chain quaternary alkylamines on the outer surface of the zeolite.

Modification of clinoptilolite from the Tedzami deposit and phillipsite from Shukhuti was carried out in solutions of cetyltrimethylammonium C₁₆H₃₃(CH₃)₃NBr bromide (CTMA-Br) with a concentration of 0.45 to 60 mEq/L; the solid-to-liquid ratio was 1:4; each sample was treated at room temperature for 8 hours [51]. As a result of the conducted study of the composition, structure and properties of the obtained materials, it was established that when modifying natural zeolites with surfactants, the microporous structure and the properties of its cation exchange centers, which determine the bond energy between organic molecules and the surface, as well as the secondary porosity, which determines the conditions for the formation monomolecular and double layers, are of greater importance, while the total ion exchange capacity of the zeolite is of lesser importance.

Thus, phillipsite is characterized by a stronger bond between the cation exchange centers and the positively charged amine heads of (CH₃)₃N⁺ than in the case of clinoptilolite, but the distribution and immobilization of hydrophobic organic matter in the relatively small mesopores of phillipsite with a diameter of less than 10 nm are associated with certain difficulties, and SMZ based on phillipsite does not have any particular advantages in trapping nonpolar organics compared to SMZ based on clinoptilolite, which has mesopores with a diameter of 20 to 100 nm [53].

On the other hand, the strong bond between the zeolite surface and the surfactant may be an obstacle to the use of phillipsite-based SMZs for water purification from pathogenic microorganisms using the Bowman method [54], but this issue requires further study.

The cation exchange capacities of sodium-, potassium- and ammonium-enriched forms obtained from natural phillipsites are given in Table 1; the PS sample, which is characterized by a high potassium content in nature, demonstrates the highest capacity not only with respect to potassium.

Table 1. Cation exchange capacities (CEC) of phillipsite cationic forms.

Comple -	CEC (mEq/g)					
Sample -	Na-form	K-form	NH ₄ -form			
PA	1.5	1.9	2.2			
PS	1.2	3.3	3.2			

The PS sample was successfully used in agriculture: its introduction into the soil in the amount of 200 g/m^2 led to almost the same increase in the yield of cucumbers and scallop as the introduction of mineral fertilizers [37].

The ion exchange isotherms obtained experimentally on PA (equilibrium at 20 °C is justified by a constant solution concentration, a solid to liquid ratio of 1:20) are shown in Fig. 19.

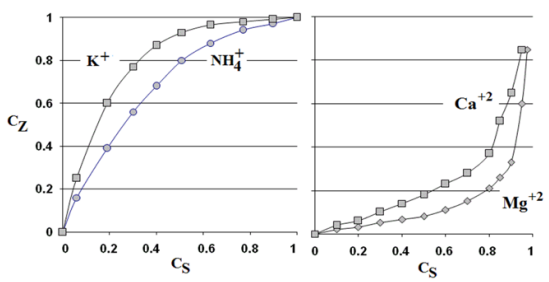


Fig. 19. Ion exchange isotherms $C_Z = f(C_S)$ on PA.

The selectivity sequences depend on the origin of zeolite: $K^+ > NH_4^+ >> Ca^{+2} > Mg^{+2}$ for PA with low content of potassium and high content of calcium and magnesium, and $NH_4^+ > K^+ > Na^+ >> Ca^{+2} > Mg^{+2}$ for PS with comparatively high content of potassium.

In the temperature range of 140-180 °C, phillipsite loses water and transforms into metaphillipsite, the thermal stability of which strongly depends on the cationic composition and silicate modulus Si/Al: calcium samples with a low silicon content decompose at 300 °C, while sodium-potassium samples with a high silicon content retain the metaphillipsite structure up to 450-500 °C; after cooling, metaphillipsite easily hydrates in air for several hours, and the original structure is restored [4].

According to XRD patterns (three merging peaks at 2Θ =12.35-12.5° of reflections 001, 020 and 110, as well as a peak at 2Θ =27.9° of reflection 041) and infrared spectra (the intertetrahedral oscillation band at 615 cm⁻¹) of PA samples heated for 4 hours, the content of the crystalline phase does not change as a result of heating to 200 °C, but decreases by 10% after heat treatment at 300 °C, by 13% at 400 °C and by 40% at 500 °C. Treatment in a dilute solution (0.1 mol/L) of hydrochloric acid at 90 °C for 2 hours at a solid to liquid phase ratio of 1:40 causes minor changes in the XRD pattern and IR spectrum, the content of the crystalline phase decreases by 35% after treatment in a solution with a concentration of 0.5 mol/L, by about 55-60% in a solutions with a concentration of 1 to 2 mol/L, and by 85% in a 5 mol/L solution [55].

Phillipsite from Akhaltsikhe PA and its acid-treated forms have been used in the catalytic conversion of methanol in the presence of oxygen, proceeding in the following directions: dehydration to dimethyl ether (DME), dehydrogenation to formaldehyde, and oxidation to carbon monoxide and carbon dioxide. The experimental results are shown in Fig. 20 [55]. Untreated phillipsite is characterized by low dehydration activity, methanol is mainly converted into formaldehyde and carbon oxides. The highest dehydration activity is demonstrated by the sample treated in a 0.5 mol/L hydrochloric acid solution, the DME yield is 80% at about 350 °C. The highest formaldehyde yield (40%) is provided at a temperature of about 500 °C by phillipsite treated in a 0.1 mol/L solution. Despite the low content of the crystalline phase for sample P-1, it is characterized by pronounced dehydration and dehydrogenation activity: the DME yield is 55% at 350 °C and 30% formaldehyde at 450 °C [55].

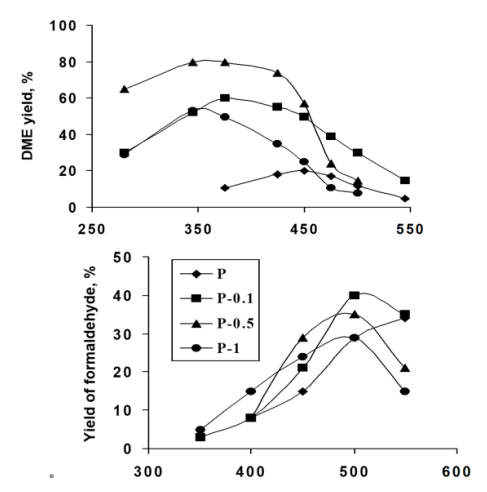


Fig. 20. Yield of DME (top) and formaldehyde (bottom) vs temperature of catalytic reaction on untreated PA (P) and acid-treated forms (P-concentration in mol/L).

Phillipsite from the Akhaltsikhe deposit PA was recrystallized to produce synthetic zeolite faujasite of the FAU type $(M_{58}(H_2O)_{240}|$ [Al₅₈Si₁₃₄O₃₈₄]-FAU), one of the "Big Five" zeolites [56]. Phillipsite powder was suspended in Teflon flack placed in shaking water bath controlling temperature at 90-95 °C; suspension was processed with a 12% hydrochloric acid solution at the rate of 5 mL/g of the solid raw material; activated suspension was diluted with water and treated by adding of a 25% sodium hydroxide solution, followed by the formation of a homogeneous gel for about one hour. The aging of the gel with the chemical composition SiO2/Al2O3 = 3.8, Na2O/Al2O3 = 12 and H2O/Na2O = 55 was carried out at room temperature for four days; crystallization was carried out in a temperaturecontrolled water bath; the temperature (up to 95 °C) and duration (up to 55 hours) were selected to obtain micrometric single crystals with a diameter of 2-8 μm, shown in Fig. 21. The chemical composition of the obtained product corresponds to the formula $|Na_{66(3)}[Me]_{12(1)}$ $(H_2O)_{248(10)}|$ $(Al_{78(3)}Si_{114(4)}O_{384})$, Me=K, ½Ca, ½Mg, ½Cu and ½Zn, Si/Al=1.46±0.07, so this product is attributed to FAU type zeolite NaX, which is confirmed by the assignment of peaks in the powder XRD pattern and its comparison with the XRD pattern of commercial zeolite NaX (see Fig. 22).

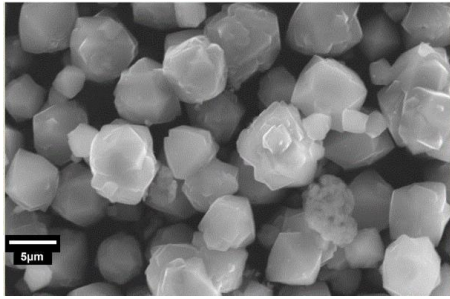


Fig. 21. SEM image of FAU zeolite recrystallized from phillipsite, magnification 5,500x.

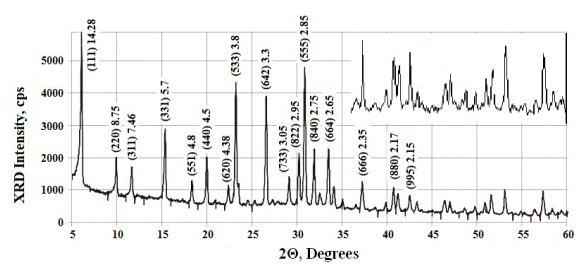


Fig. 22. XRD pattern of the phillipsite recrystallization product; numbers in parentheses are Miller indices (hkl), after the parenthesis are d-spacings (Å).

The specific surface area of 589 m²/g calculated from low-temperature (77 K) nitrogen adsorption-desorption isotherms is comparable to 573 m²/g for zeolite X obtained from coal fly ash [57] and is higher than the specific surface area of 453 m²/g reported for NaX obtained from diatomite [58].

The total pore volume of the prepared NaX is 0.578 cm³/g, the volume of micropores with a diameter of less than 8 Å is 0.301 cm³/g, which is slightly higher than the micropore volume in X zeolites obtained from coal fly ash (0.281 cm³/g, [57]) and from diatomite (0.284 cm³/g, [58]), and also significantly higher than the micropore volume in NaX zeolites synthesized using structure-forming reagents that block part of the channels [59].

The mesopores have a volume of about $0.28~\rm cm^3/g$, and their filling is reflected in the nitrogen adsorption-desorption isotherms as a very narrow hysteresis loop at high relative pressures (from 0.9 to 0.99). Such a loop of the H_1 type, according to the Sing classification, indicates the presence of well-defined cylindrical pore channels, the diameter of which, calculated using the Barrett-Joyner-Halenda method from the desorption isotherm, is 53 nm.

The loop observed in the synthesized zeolite NaX is different from the wide hysteresis loops described for some synthetic zeolites [58,60](Ltaief et al., 2015; Yao et al., 2018) and corresponding to the filling of disordered pores (type H_2) or uniform slit-shaped (type H_3) intercrystal mesopores of non-rigid aggregates of plate-like particles, ascribed to the packing of zeolite crystals.

It has been shown previously [53] that raw natural phillipsite from Shukhuti is inert to *E. coli* and *Staphylococcus aureus*, while acid-treated samples exhibit high bactericidal activity. It should be noted that back in the Soviet period, Pylev et al. [61] reported the carcinogenicity of phillipsite, but later the International Agency for Research on Cancer (IARC) assessed their study as inadequate [62].

Recently, bactericidal phillipsites containing up to 230 mg/g of silver, 66 mg/g of copper, and 86 mg/g of zinc silver and zinc have been obtained using ion-exchange reactions between grinded and washed by dilute HCl solution zeolite and a salt of a corresponding metal in the solid phase followed by washing with distilled water [63]. The obtained silver-, copper- and zinc-containing phillipsites exhibit bactericidal and bacteriostatic activity towards E coli regardless of whether the amount of released bioactive metal ions reaches the minimum inhibitory concentration in the solution. The dry ion-exchange synthesis procedure increases the dispersion of the material, but does not affect the developed mesoporous system of phillipsite and the total pore volume, which averages 0.285 cm³/g. The compliance of the proposed method for obtaining silver-, copper- and zinccontaining forms of phillipsite with high environmental

standards is confirmed by its low Sheldon factor E compared to similar indicators of green chemistry of traditional ion exchange methods in solutions.

Later [28,29] biometal-enriched phillipsites were tested for bacteriostatic activity against other microorganisms, and it was found that copper- and zinc-containing phillipsites were more active against hay bacillus than the silver-containing form, and mechanical mixtures exhibited synergism. In particular, a mixture of silver and copper forms was maximally active against *E. coli*, and a mixture of copper and zinc forms was most active against mold (see Fig. 23).

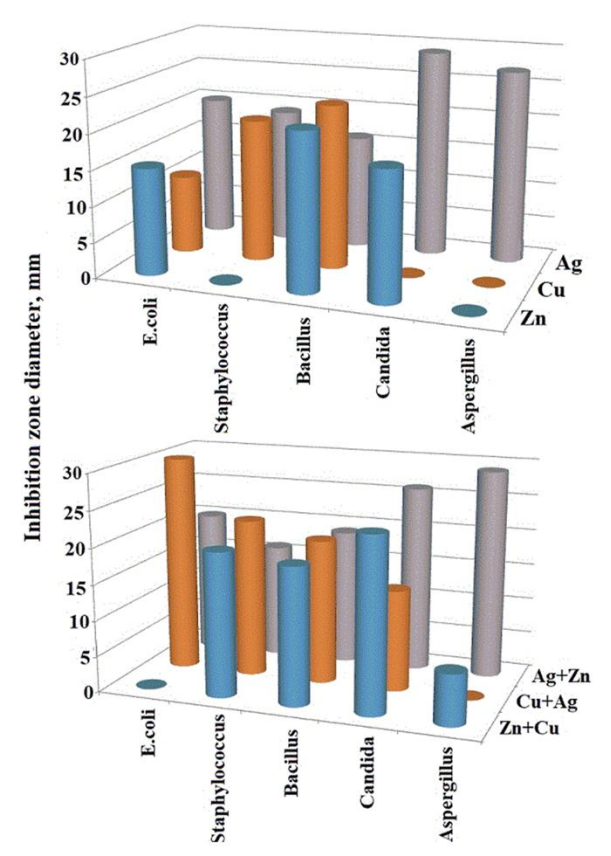


Fig. 23. Inhibition of growth of microorganisms by silver-(Ag), copper- (Cu) and zinc-containing (Zn) phillipsites and their mixtures.

Scolecite

Scolecite is a tectosilicate mineral isostructural with the sodium-calcium zeolite mesolite and the sodium zeolite natrolite, that belong to the **NAT** type zeolites (crystal chemical data |M₁₆ (H₂O)₁₆| [Al₁₆Si₂₄O₈₀]-**NAT**). Scolecite is a common zeolite, but it is a hydro-thermal mineral of secondary origin derived from low temperature alteration of basalts and related rocks, and occurs with other zeolites in the amygdaloidal cavities of weathered basalts, also in gneisses and amphibolites, in laccoliths and dikes derived from syenitic and gabbroic magmas, and in contact metamorphic zones. Scolecite associated with other zeolites, calcite, quartz and prehnite is widespread in Georgia, but a promising manifestation for industrial use is found only near the village of Kursebi, located in western Georgia, in the Tkibuli municipality [64].

The framework of **NAT** zeolites (see Fig. 24) includes a twodimensional system of channels with narrow entrance windows in the form of 8- and 9-rings with dimensions of 0.26 nm x 0.39 nm and 0.25 nm x 0.41 nm, respectively; channels are variable due to considerable flexibility of framework.

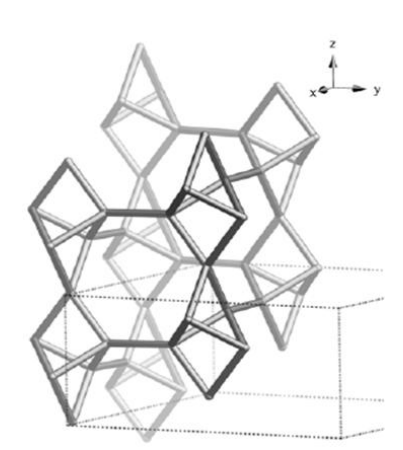


Fig. 24. Scolecite framework.

The relatively high aluminum content (Si/Al=1.5) allows these minerals to be used as ion exchangers, and Brazilian [65] and Sudanese [66] scolecites have been successfully used to remove heavy metal ions from industrial wastewater. It is also known that natural scolecite from India has proven to be an effective catalyst for the one-pot synthesis of 2,4,5-triarylimidazole derivatives via a three-component reaction using benzyl or benzoin, aldehydes and ammonium acetate [67].

In accordance with the results obtained [68], the chemical composition of the aluminosilicate framework of the Georgian scolecite from Kursebi is described by the empirical formula Na_{0.025(15)} ·K_{0.015(8)} ·Ca_{0.50(3)}·[AlSi_{1.68}O_{5.36}], so that the molar ratio Si/Al slightly exceeds the value determined for the NAT-type zeolites, and the prevalence of calcium in the cationic composition is fully consistent with published data [65-68] on natural scolecites from different countries.

The transformations of Georgian scolecite when heated are similar to those described by Peng back in 1955 [68]: at ≈ 350 °C, some water molecules are lost and *metascolecite* is formed by the reaction CaAl₂Si₃O₁₀·3H₂O \rightarrow CaAl₂Si₃O₁₀·2H₂O+H₂O \uparrow , and at a temperature of 500-520 °C, the framework loses the remaining H₂O molecules and is completely destroyed.

The same effect of microstructure destruction occurs as a result of acid treatment of scolecite with concentrated HCl solutions, and the decationization process is more intensive than dealumination. Thus, after treatment in a solution with a concentration of 3 mol/l, the content of calcium cations decreases more than tenfold, while the content of aluminum atoms decreases by 3.5 times [64].

Ion exchange properties of Georgian scolecite were studied under dynamic conditions in model solutions of alkali, alkaline earth and some heavy metal chlorides. It was found that the dynamic cation exchange capacity (DCEC) depends on the solution concentration, the maximum DCEC value is achieved at a concentration of about 1 mol/L, while scolecite

absorbs strontium cations Sr2+ to the greatest extent (DCEC = 3-4 mEq/g), while doubly charged cations of heavy metals $(Co^{2+},\ Ni^{2+},\ \text{etc.})$ are absorbed to a lesser extent (DCEC ≈ 1.3 mEq/g); exchange capacity for Cs+ ions at a flow rate of 5 mL/min and room temperature is 2/5 mEq/g. The DCEC increases with the temperature of the solution passing through the zeolitefilled column, but insignificantly, so the purification process can be carried out quite effectively at room temperature. The DCEC decreases with the flow rate of the purified solution, the optimal flow rate should be selected empirically.

CONCLUSION

Heulandite-clinoptilolite meets European safety standards and can be used in livestock farming as a feed additive, as well as in crop farming as a fertilizer component in combination with organic waste or such cheap mineral raw materials as brown coal. In construction, this zeolite can be used as an additive to concrete, and in the pharmaceutical industry as a substitute for sulfuric acid. Heulandite-clinoptilolite effectively absorbs antibiotics from water and volatile nitrosamines from tobacco smoke, can be used as a carrier of biologically active metals, and also as an aluminosilicate raw material for the production of synthetic mordenite and ionites.

Acid treatment of analcime allows obtaining effective adsorbents, the sodium form of analcime can be used to purify water from ammonium, and a mixture of analcime with manure can partially replace mineral fertilizers.

Laumontite can be used to purify water from heavy metals, including radioactive ones, especially cesium ions Cs⁺.

Mordenite absorbs pharmaceutical pollutants (e.g., antibiotics moxifloxacin and norfloxacin) from water, and after acid treatment it very effectively absorbs volatile N-nitrosamines from tobacco smoke.

Phillipsite can be used in plant growing to replace mineral fertilizers, as a catalyst for methanol conversion, as an ion exchanger for water purification from ammonium, as a carrier of biologically active metals, and also as an aluminosilicate raw material for obtaining valuable synthetic zeolite faujasite.

Scolecite can be used without any treatment to purify water contaminated with radioactive elements such as cesium and, in particular, strontium.

Acknowledgement

The author thanks Nanuli Dolaberidze for synthesis of zeolites, Maya Alelishvili, Manana Nijaradze and Nato Mirdzveli for modifications, sorption and ion exchange studies, Giorgi Tsintskaladze for helping with characterization of zeolites by IR spectroscopy, and Vakhtang Gabunia for help with X-ray studies.

REFERENCES

- Mumpton F.A. "La Roca Magica a magic stone". Proc. Natl. Acad. Sci. USA, 1999, vol. 96, pp. 3463-3470
- Database of Zeolite Structures: http://www.izastructure.org/databases/
- 3. Skhirtladze N.I. Sedimentary Zeolites of Georgia, Tbilisi State University: Tbilisi, 1991, 144 p.
- Tsitsishvili G.V, Andronikashvili T.G., Kirov G.N, Filizova L.D. Natural Zeolites. Ellis Horwood: London, 1992, 224 pp.
- Tsitsishvili V., Dolaberidze N., Alelishvili M., Tsintskaladze G., Sturua G., Chipashvili D., Nijaradze M., Khazaradze N. "Adsorption and thermal properties of zeolitic rocks from newly investigated deposit plots in Georgia". Georgian Engineering News, 1998, no 2(6), pp. 61-65.
- Ambruster T. "Clinoptilolite-heulandite: applications and basic research". Stud. Surf. Sci. Cat., 2001, vol. 135 (Zeolites and Mesoporous Materials at the Dawn of the 21st Century, edited by A. Galarnau, F. Di Renzo, F. Faujula and J. Vedrine), pp. 13-27.
- Tsitsishvili V., Panayotova M., Miyamoto M., Dolaberidze N., Mirdzveli N., Nijaradze M., Amiridze Z., Klarjeishvili N., Khutsishvili B., Dzhakipbekova N., Harutyunyan L. "Characterization of Georgian, Kazakh and Armenian natural heulandite-clinoptilolites". *Bull. Georg. Natl Acad. Sci.*, 2022, vol. 16, no 4, pp. 115– 122...
- Regulations. Commission Implementing Regulation (EU) No 651|2013 of 9 July 2013, concerning the authorization of clinoptilolite of sedimentary origin as a feed additive for all animal species and amending Regulation (EC) No 1810|2005. Official Journal of the European Communities, L 189/1, 10.7.2013, Brussels. (Available at http://eur-lex.europa.eu/legal-content/EN/TXT/?uri=CELEX%3A32013R0651)
- Beshkenadze I., Urotadze S., Tsitsishvili V., Zhorzholiani N., Gogaladze M., Begheluri G. "Application of methionine-containing complexes and their composites with clinoptilolite in poultry nutrition". Bull. Georg. Natl. Acad. Sci., 2015, vol 9, no 2, pp. 110-115
- Eprikashvili L.G., Dzagania M.A., Kekelia G.V., Pirtskhalava N.B., Kordzakhia T.N., Zautashvili M.G. "Effect of the using of combined environmentally friendly methods on increasing the yield of agricultural products". *Annals of Agrarian Science*, 2020, vol. 18, no 2, pp. 195-200.
- Eprikashvili L., Zautashvili M., Kordzakhia T., Dzagania M., Pirtskhalava N. "Use of coal industry wastes and zeolitic tuffs to increase the bio-productivity of agro-landscapes". *Journal Chemical & Environmental Research*, 2019, vol. 7, no 1, pp. 23-28.
- 12. Tsintskaladze G., Sharashenidze T., Zautashvili M., Burdjanadze M., Antia G., Mumladze N. "Anionic zeolite nanomaterial environmentally safe complex fertilizer with prolonged action". *Bull. Georg. Natl. Acad. Sci.*, 2021, vol 15, no 3, pp. 210-218.
- 13. F.A. Mumpton F.A. "La roca magica: Uses of natural zeolites in agriculture and industry". Proc. Natl. Acad. Sci. U.S.A., 1999, vol. 96, no 7, pp. 3463-3470,
- Kordzakhia T., Skhvitaridze R., Tsintskaladze G., Giorgadze I., Verulava Sh., Skhvitaridze A.

- "Perspectives of usage of natural zeolite saturated with kiln gases of cement clinker". *International Journal of Advanced Research*, 2019, vol 6, no 10, pp. 1282-1287.
- Rubashvili I., Eprikashvili L., Kordzakhia T., Zautashvili M., Pirtskhalava N., Dzagania M. "Adsorptive removal study of the frequently used fluoroquinolone antibiotics – moxifloxacin and norfloxacin from wastewaters using natural zeolites". Mediterranean Journal of Chemistry, 2019, vol. 9, no 2, pp. 142-154.
- Eprikashvili L., Kordzakhia T., Zautashvili M., Rubashvilia I., Pirtskhalava N., Dzagania M., Tsintskaladze G., Antia G. "Effect of clinoptilolite acid activation on ceftriaxone sorption from wastewaters". Research Journal of Chemistry and Environment, 2021, vol. 25, no 5, pp. 80-86.
- 17. Rubashvili I., Tsitsishvili V. "Quantitative estimation of volatile N-nitrosamines in tobacco smoke using validated GC-MS method and its uncertainty evaluation, illustrated by determination of Nnitrosomethylethylamine". *Bull. Georgian Nat. Acad. Sci.*, 2015, vol. 9, no 1, pp. 85-92.
- Ramishvili Ts.M., Tsitsishvili V.G., Kokiashvili N.G., Gabunia V.M., Inanashvili N.M. "Modified forms of natural zeolites – clinoptilolite and heulandite as an effective catalysts for synthesis of acetylsalicylic acid". *Asian J. Sci. Techn.*, 2017, vol. 08, is. 06, pp. 4985-4995.
- Rainsford K.D., "Aspirin and related drugs," in Occurrence, Properties and Synthetic Developments of Salicylates (Ed.: K.D.Rainsford), CRC Press, Taylor & Francis: London and New-York, 2004, ch. 3, pp. 70-120.
- 20. Ramishvili Ts., Tsitsishvili V., Chedia R., Sanaia E., Gabunia V., Kokiashvili N. "Preparation of ultradispersed crystallites of modified natural clinoptilolite with the use of ultrasound and its application as a catalysts in the synthesis of methyl salicylate". Am. J. Nano Res. Appl., 2017, vol. 5, no 3-1, pp. 26-32.
- Papava G., Gurgenishvili M., Chitrekashvil I., Gavashelidze E., Gelashvili N. "Ionites on the basis of clinoptilolite". *International Academy Journal Web of Scholar*, 2019,
- Tsitsishvili V., Dolaberidze N., Mirdzveli N., Nijaradze M. "MOR type synthetic zeolite material". *Proc. Georgian Nat. Acad. Sci., chem. ser.*, 2016, vol. 42, no 1, pp. 35-39.
- 23. Mignoni M.L., Petkowicz D.I., Fernandes Machado N.R.C., Pergher S.B.C. "Synthesis of mordenite using kaolin as Si and Al source". *Applied Clay Science*, 2008, vol. 41, is. 1-2, pp. 99-104.
- 24. Merdekawati R., Ediati R., Prasetyoko D. "Effect of silica to alumina molar ratio on crystallinity of mordenite synthesized using rice husk ash and kaolin from Bangka Belitung", in: *Proc. Internat. Conf. Satya Wacana Uni.*, Indonesia, pp. BC.84-89, 2015.
- 25. Bajpai P.K. "Synthesis of mordenite type zeolite". *Zeolites*, 1986, vol. 6, is. 1, pp. 2-8.
- Ailing Lv, Hao Xu, Haihong Wu, Yueming Liu, Peng Wu. "Hydrothermal synthesis of high-silica mordenite by dual-templating method". *Microporous and Mesoporous Materials*, 2011, vol. 145, is. 1-3, pp. 80-86.

- Tsitsishvili V., Dolaberidze N., Mirdzveli N., Nijaradze M., Amiridze Z. "Properties of Georgian natural heulandite-clinoptilolite and its silver, copper, and zinc-containing forms". *Bull. Georgian Natl Acad. Sci.*, 2021, vol. 15, no 2, pp. 60-67.
- Tsitsisvili V.G., Dolaberidze N.M., Mirdzveli N.A., Nijaradze M.O. "Bactericidal materials based on natural and synthetic zeolites" *Uspekhi v khimii I khimicheskoi* tekhnojogii (ISSN 1506-2017), 2021, vol. XXXV, no 13(248), pp. 98-100 (in Russian).
- Tsitsishvili V., Dolaberidze N., Nijaradze M., Mirdzveli N., Amiridze Z., Khutsishvili B. "Bactericidal activity of materials based on synthetic and natural zeolites", in: "Modern Pharmacy - Science and Practice", Kutaisi, Georgia, pp. 287-295, 2023.
- Tsitsishvili V., Dolaberidze N., Mirdzveli N., Nijaradze M., Amiridze Z. "Preparation of bactericidal fillers from Georgian heulandite-clinoptilolite and their application for paper production. I. Bactericidal fillers". Scientific Collection «InterConf+», 2021, vol. 67, pp. 340-358.
- Tsitsishvili V., Dolaberidze N., Mirdzveli N., Nijaradze M., Amiridze Z. "Preparation of bactericidal fillers from Georgian heulandite-clinoptilolite and their application for paper production. II. Bactericidal paper". Scientific Collection «InterConf+», 2021, vol. 67, pp. 359-374.
- Tsitsishvili V.G., Dolaberidze N.M., Doula M.K., Gemishev O.T., Mirdzveli N.A., Nijaradze M.O., Amiridze Z.S., Khutsishvili B.T. "The role of zeolite in imparting bacteriostatic properties to paper". *Chemistry*, *Physics and Technology of Surface*, 2024, vol. 15, no 4. pp. 467-477.
- 33. Tsitsishvili V.G., Dolaberidze N.M., Nijaradze M.O., Mirdzveli N.A., Amiridze Z.S., Khutsishvili B.T. "Acid and thermal treatment of natural heulandite". *Chemistry, Physics and Technology of Surface*, 2023, vol. 14, no 4. pp. 519-533.
- 34. Tsitsishvili V., Dolaberidze N., Nijaradze M., Mirdzveli N.. "Modification of natural analcime". In: "Achievements and perspectives of modern chemistry", Chisinau, Moldova, p. 28, 2019.
- Tsitsishvili V., Dolaberidze N., Alelishvili M., Chipashvili D., Tsintskaladze G., Sturua G., Nijaradze M., Gigolashvili N., Mirdzveli N. "Adsorbents on the base of modified forms of analcime". *Georgian Eng. News*, 1999, no 1, pp. 102-104.
- Tsitsishvili V., Dolaberidze N., Urotadze S., Alelishvili M., Mirdzveli N., Nijaradze M. "Ion exchange properties of Georgian natural zeolites". *Chemistry Journal of Moldova*, 2017, vol. 12, no 1, pp. 95-101.
- 37. Alelishvili M, Andronikashvili T., Tsitsishvili V., Dolaberidze N. "On the possibility of growing cucumber and scallop without application of traditional fertilizers". *Chemical & Environmental Research*, 2003, vol. 12, no 1&2, pp. 121-134.
- Tsitsishvili V., Dolaberidze N., Mirdzveli N., Nijaradze M., Amiridze Z. "Natural analcime as a raw material for ion exchangers", in: "Modern technologies and methods of inorganic materials science", Tbilisi, Georgia, pp. 188-191, 2021.
- Urotadze S., Tsitsishvili V., Osipova N., Kvernadze T.
 "Laumontite natural zeolite mineral of Georgia". Bull. Georgian Nat. Acad. Sci., 2016, vol. 10, no 1, pp. 32-37.
- 40. Tsitsishvili G.V., Urotadze S.L., Andronikashvili T.G., Osipova N.A., Kvernadze T.K., Tsitsishvili V.G.

- "Application of laumontite for wheat crop increase", in: *Zeolite 2010*, Sofia, Bulgaria, pp. 265-266, 2010.
- Colella C. "Natural zeolites". Stud. Surf. Sci. Cat., 2005, vol. 157 (Zeolites and Ordered Mesoporous Materials: Progress and Prospects, edited by J.Čejka, H. van Bekkum), pp. 13-40.
- Lilis R. "Fibrous zeolites and endemic mesothelioma in Cappadocia, Turkey". J. Occup. Med., 1981, vol. 23, pp. 548-550.
- Stephenson D.J., Fairchild C.I., Buchan R.M., Dakins M.E. "A fiber characterization of the natural zeolite, mordenite: A potential inhalation health hazard. *Aerosol Science and Technology*, 1999, vol. 30, pp. 467-476.
- 44. Eprikashvili L.G., Kordzakhia T.N., Zautashvili M.G., Rubashvili I.M., Pirtskhalava N.V., Dzagania M.A., Tsintskaladze G.P. "Feability study for use of natural mordenite in purification processes of wastewaters from pharmaceutical pollutants". *International Journal of Advances Research*, 2021, vol. 9, no 03, pp. 683-691.
- 45. Rubashvili I., Eprikashvili L., Kordzakhia T. "Removal of volatile N-nitrosamines from tobacco smoke using local natural zeolites", in: *International Congress on Chemical, Biological and Environmental Sciences*, Osaka, Japan, pp. 577-578, 2016.
- Sherman J.D., Ross R.J. "Phillipsite-type zeolites for ammonia adsorption device for elementary analyses". USA Patent No. 4344851A, 1982.
- 47. Kallo D, "Applications of natural zeolites in water and wastewater treatment". *Reviews in Mineralogy and Geochemistry*, 2001, vol. 45, pp. 519-550.
- Salvestrini S., Iovino P., Canzano S., Capasso S., "Use of natural zeolites for organic compounds removal from water," in *Application of Adsorbents for Water Pollution Contro*, (Ed. Bhatnagar A.), Bentham Science Publishers: Sharjah, Oak Park, Bussum, pp. 363–381, 2012.
- 49. Rawajfih Z., Al Mohammad H., Nsour N., Ibrahim K. "Study of equilibrium and thermodynamic adsorption of α-picoline, β-picoline, and γ-picoline by Jordanian zeolites: phillipsite and faujasite". *Microporous and Mesoporous Materials*, 2010, vol. 132, pp. 401-408.
- Dolaberidze N., Tsitsishvili V., Panayotova M., Mirdzveli N., Nijaradze M., Amiridze Z., Kapanadze T., Virsaladze K. "Characterization of Georgian natural phillipsites", in: 2nd International Eurasian Conference on Biological and Chemical Sciences, Ankara, Turkey, pp. 398-404, 2019.
- 51. Tsitsishvili V., Alelishvili M., Dolaberidze N., Nijaradze M., Mirdzveli N. "Surfactant-modified clinoptilolite and phillipsite". *Bull. Georgian Acad. Sci.*, 2003, vol. 167, no 3, pp. 457-459.
- 52. Bowman R.S., Sullivan E.J., Li Z. "Uptake of cations, anions, and nonpolar organic molecules by surfactant-modified clinoptilolite-rich tuff," in *Natural Zeolites for the Third Millenium*, (Eds. Collela C., Mumpton F.A.), De Frede Editore, Naples, Italy, 2000.
- 53. Tsitsishvili G., Tsitsishvili V., Dolaberidze N., Alelishvili M., Suladze M. "Natural zeolites: potential applications," in: *Chemistry of Advanced Compounds and Materials*, (Eds Lekishvili N., Zaikin G.E.), Nova Science Publishers, New-York, pp. 115-122, 2008.
- 54. Bowman R.S. "Applications of surfactant-modified zeolites to environmental remediation". *Micropor. Mesopor. Mat.*, 2003, vol. 61, no 1-3, pp. 43-56.

- 55. Tsitsishvili G., Tsintskaladze G., Tsitsishvili V. "Catalytic activity of natural phillipsite from akhaltsikhe deposit of Georgia", in 6th International Conference on the Occurrence, Properties and Utilization of Natural Zeolites, Aristotle University, Thessaloniki, Greece, 2002.
- Tsitsishvili V., Dolaberidze N., Mirdzveli N., Nijaradze M., Amiridze Z., Sinauridze N., Kapanadze T., Virsaladze K. "Transformation of natural analcime and phillipsite during their hydrothermal recrystallization into zeolites A and X". *International Journal of Advanced Research*, 2019, vol. 7, no 2, pp. 219-230.
- 57. Hu T., Gao W., Liu X., Zhang Y., Meng, C. "Synthesis of zeolites Na-A and Na-X from tablet compressed and calcinated coal fly ash". *Royal Society Open Science*, 2017, vol. 4, no 10, pp. 170921-170934.
- Yao G., Lei J., Zhang X., Sun Z., Zheng, S. "One-step hydrothermal synthesis of zeolite X powder from natural low-grade diatomite". *Materials*, 2018, vol. 11, pp. 906-920.
- Chen Y., Xu T., Xie C., Han H., Zhao F., Zhang J., Song H., Wang, B. "Pure zeolite Na-P and Na-X prepared from coal fly ash under the effect of steric hindrance".
 J. Chem. Technol. Biotechnol., 2016, vol. 91, pp. 2018-2025
- 60. Ltaief O.O., Siffert S., Fourmentin S., Benzina, M. "Synthesis of faujasite type zeolite from low grade Tunisian clay for the removal of heavy metals from aqueous waste by batch process: Kinetic and equilibrium study". *Comptes Rendus Chimie*, 2015, vol. 18, pp. 1123-1133.
- 61. Pylev L.N., Kulagina T.F., Grankina E.P., Chelishchev N.F., Berenstein B.G. "Carcinogenicity of zeolite phillipsite". *Gigiena i Sanitaria*, 1989, vol. 8, pp. 7-10 (in Russian).
- International Agency for Research on Cancer. "Zeolites other than erionite (Group 3)". *IARC Monographs*, 1997, vol. 68, pp. 307-333.
- 63. Tsitsishvili V.G., Dolaberidze N.M., Nijaradze M.O., Mirdzveli N.A., Amiridze Z.S. "Bactericidal adsorbents obtained by ion exchange modification of natural phillipsite". *Chemistry, Physics and Technology of Surface*, 2019, vol. 10. no 4, pp. 327-339.
- 64. Urotadze S., Osipova N., Kvernadze T., Tsitsishvili V. "Ion exchange properties of Georgian scolecite". *Proc. Georgian Natl Acad. Sci., chem. ser.*, 2016, vol. 42, no 4, pp. 570-574.
- Bosso S.T, Enzweiler J. "Evaluation of heavy metal removal from aqueous solution onto scolecite". Water Research, 2002, vol. 36, is. 19, pp. 4795-4800.
- Almalih M.A., Salih A., Dafaallah A.A., Magid S.A.A., Gizouli A.M.E., Tilal A.S. "Removal of heavy metal ions from industrial wastewater by scolecite". *Environmental & Analitical Toxicology*, 2015, vol. 5, is. 5, pp. 300-305.
- 67. Gadekar L.S., Mane S.R., Katkar S.S., Arbad B.R., Lande M.K. "Scolecite as an effective heterogeneous catalyst for the synthesis of 2,4,5-triarylimidazoles". *Central European Journal of Chemistry*, 2009, vol. 7, no 3, pp. 550-554.
- Peng C.J. "Thermal analysis study of the natrolite group". *American Mineralogist*, 1955, vol. 40, no 9-10, pp. 834-856.

Identification of Impurities in Paper Made from Waste Paper

V. Tsitsishvili, N. Mirdzveli, N. Dolaberidze, M. Nijaradze, Z. Amiridze, B. Khutsishvilili

- ¹ Georgian National Academy of Sciences, 52 Rustaveli Av., Tbilisi 0108, Georgia
- ² Petre Melikishvili Institute of Physical and Organic Chemistry, Tbilisi State University, 31 A.Politkovskaia Str., Tbilisi 0186, Georgia
 - *E-mail v.tsitsishvili@gmail.com

Abstract. Cardboard and paper made from waste paper contain various impurities along with the usual calcium carbonate filler. Samples of paper made from recycled materials on the production line of a three-layer corrugated cardboard factory, as well as in laboratory conditions, were studied. It has been shown that elemental analysis and elemental mapping using X-ray energy-dispersive spectrometry allow the identification of crystalline and amorphous impurities that are not visible in powder X-ray diffraction patterns.

Keywords: elemental mapping, impurity, X-ray energy-dispersive spectrum.

ვ. ციციშვილი, წ. მირძველი, წ. დოლაბერიძე, მ. წიჟარაძე, ზ. ამირიძე, ზ. ხუციშვილი - წარჩენებისგან დამზადებულ ქაღალდში მიწარევების იდენტიფიცირება

რეზიუმე. მაკულატურისგან დამზადებული მუყაო და ქაღალდი შეიცავს სხვადასხვა მინარევებს ჩვეულებრივ კალციუმის კარბონატის შემავსებელთან ერთად. შესწავლილი იქნა სამფენიანი გოფრირებული მუყაოს ქარხნის საწარმოო ხაზზე, ასევე ლაბორატორიულ პირობებში, გადამუშავებული მასალებისგან დამზადებული ქაღალდის ნიმუშები. ნაჩვენებია, რომ ელემენტური ანალიზი და ელემენტური რუქა რენტგენული გამოსხივების ენერგიის დისპერსიული სპექტრომეტრიის გამოყენებით იძლევა კრისტალური და ამორფული მინარევების იდენტიფიცირების საშუალებას, რომლებიც არ ჩანს რენტგენულ დიფრაქტოგრაშებში.

Introduction

During the coronavirus pandemic, demand for new antibacterial and antiviral materials has increased, especially for polymer and paper packaging for food and agricultural products, and this interest continues in the context of the post-pandemic period. On the other hand, the World Health Organization notes that infectious diseases caused by various microorganisms lead to millions of deaths worldwide, so interest in disinfectants is constantly growing and research is being conducted in many countries to create new liquid and powder antibacterial, antifungal and antiviral substances [1].

Among these substances are bactericidal powder materials that are used as fillers in the production of polymeric materials and paper to protect their surfaces from microbial contamination. To obtain such fillers, natural or synthetic zeolites (aluminosilicates of the general formula $M_x[Al_xSi_yO_{2(x+\ y)}]$ ·mH₂O) are used, in which the cations of alkali or alkaline earth metals M are partially replaced by ions of silver, copper, zinc or another biologically active metal [2,3]. Bactericidal compositions with metal-containing zeolites do not cause allergic and skin reactions in humans, are non-toxic, odorless, and are considered environmentally friendly [4-7].

Recently we have developed special zeolite fillers, containing up to 130 mg/g of silver, or up to 72 mg/g of copper, or up to 58 mg/g of zinc [8], and which give packaging paper bactericidal properties against gram-negative bacterium *Escherichia coli* and gram-positive bacterium *Staphylococcus aureus* [9]. Along with testing the bacteriostatic activity, the physicochemical properties of the obtained paper samples were investigated. The powder X-ray diffraction (XRD) patterns of paper samples both with and without fillers show broad peaks of cellulose in the range $12^{\circ}<2\Theta<25^{\circ}$ (double peak of reflections (101) and (10-1) at $2\Theta\approx15$ and 16° , shoulder of (021) at $2\Theta\approx21^{\circ}$ and intense peak of (002) at $2\Theta\approx22.5^{\circ}$), as well as narrow peaks at large 2Θ angles (see Fig. 1).

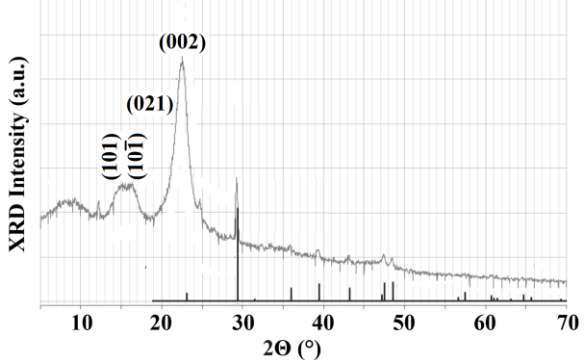


Fig. 1. Powder XRD pattern of paper.

According to the RRUFF database (see https://rruff.info/Calcite/R050128), these narrow peaks, the most intense of which is detected at $\approx 29.5^{\circ}$, indicate the presence of calcite (calcium carbonate CaCO₃) in the paper samples. Calcium carbonate is widely used in the paper industry [10], and its presence in paper is not surprising, especially since the filled papers were manufactured on the production line of the paper mill of the GPM company (2 Akhvlediani str., line 10, Tbilisi, Georgia), producing paper and three-layer corrugated paperboard from recycled waste.

As a rule, packaging paper and cardboard made from secondary raw materials — waste paper, along with calcium carbonate contain various amorphous and crystalline impurities, as evidenced by a wide band at 20≈9° and a narrow peak at 20≈12° in the powder XRD pattern, respectively (see Fig. 1). Identification of impurities is a necessary and important task, since they not only affect the quality of paper, but can also interact with ions of biologically active metals. Therefore, the aim of this study was to identify methods that can determine the nature and

chemical composition of impurities in paper made from waste paper.

Experimental

During the production of paper samples on the production line, the introduction of zeolite fillers was carried out on practically dry paper, during the coating process, by adding a zeolite suspension to a boiled starch binder, as shown in Fig. 2.

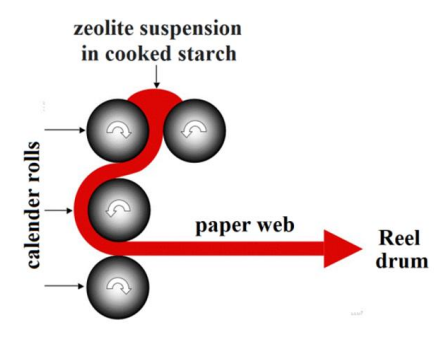


Fig. 2. Introduction of fillers on paper.

The paper samples for the study were also prepared in laboratory from commercial tissue paper made from recycled paper. The tissue paper, crushed to a size of 2 x 2 mm, was placed in a glass laboratory crystallizer, poured with boiling water in a ratio of 1:20 by weight, manually ground and kept for 15 minutes, after which boiled starch glue was added to the resulting mass (ratio of dry starch and water 1: 12, the ratio of dry tissue paper to glue is 1:4), the paper pulp and glue were mixed, after which the resulting mixture was transferred to an 18 US mesh polyethylene mesh measuring 30 x 30 cm, evenly distributed on it and dried at room temperature until a constant weight was achieved.

Powder XRD patterns were recorded on a moder-nized Dron-4 diffractometer (USSR) employing the Cu-K $_{\alpha}$ line ($\lambda=0.154056$ nm); scanning was carried out in the 2Θ range from 5° to 68° in steps of 0.02° at a scanning speed of 1° /min.

Scanning electron microscope (SEM) images and X-ray energy-dispersive (XR-ED) spectra were obtained on a JSM-6510LV scanning electron microscope (Jeol, Japan) equipped with a X-Max 20 analyzer (Oxford, UK), which was also used for elemental mapping, when an electron beam is two-dimensionally scanned over a specimen area, and the characteristic XR-ED spectra generated by the electron beam are acquired pixel by pixel. Elemental mapping visualizes the distribution of constituent elements in a sample by displaying characteristic X-ray intensities or element concentrations in two dimensions.

Results & discussion

Scanning electron micrograph (SEM) images of the paper surface show cellulose fibres ranging in thickness from a few micrometers to about 50-60 micrometers and lengths up to 1-2 millimeters, as shown in Fig. 3, as well as relatively small (ranging in size from fractions of a micrometer to several micrometers) and large (tens of micrometers) objects of various shapes, shown in the SEM images at different magnification provided in the Appendix.

With the exception of calcium carbonate, which is present in large quantities, powder XRD patterns of paper do not allow the identification of other crystalline and, especially, amorphous impurities, since the region of low-angle peaks ($2\Theta < 25^{\circ}$) is covered by cellulose peaks. However, to identify impurities, one should first turn to elemental analysis.

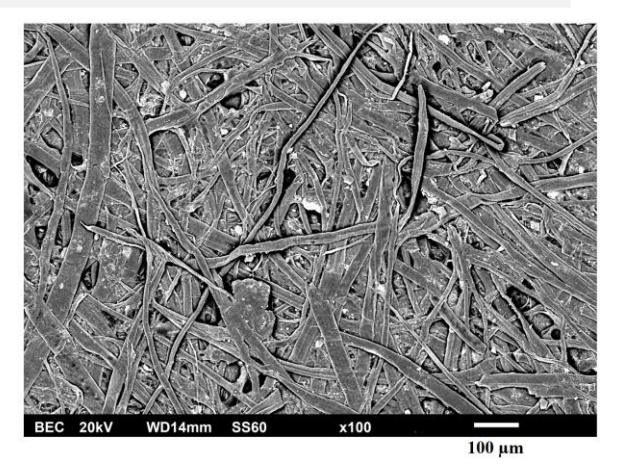


Fig. 3. Typical SEM images of paper prepared on the production line.

A typical XR-ED spectrum of unfilled paper contains intense peaks of cellulose $(C_6H_{10}O_5)_n$) carbon and oxygen, as well as weak peaks of calcium and other elements contained in the impurities, examples of XR-ED spectra showing peaks of silicon, aluminum, etc., are given in the Appendix.

Since paper made from waste paper is not a homogeneous material, the XR-ED spectra taken from different "sites" of the paper sample surface shown in Fig. 4 as Spectrum 0, Spectrum 1, etc., show different contents of impurity atoms; the results of elemental analysis for calcium, silicon and other impurity atoms are presented in Tables 1 and 2 in atomic percentages.

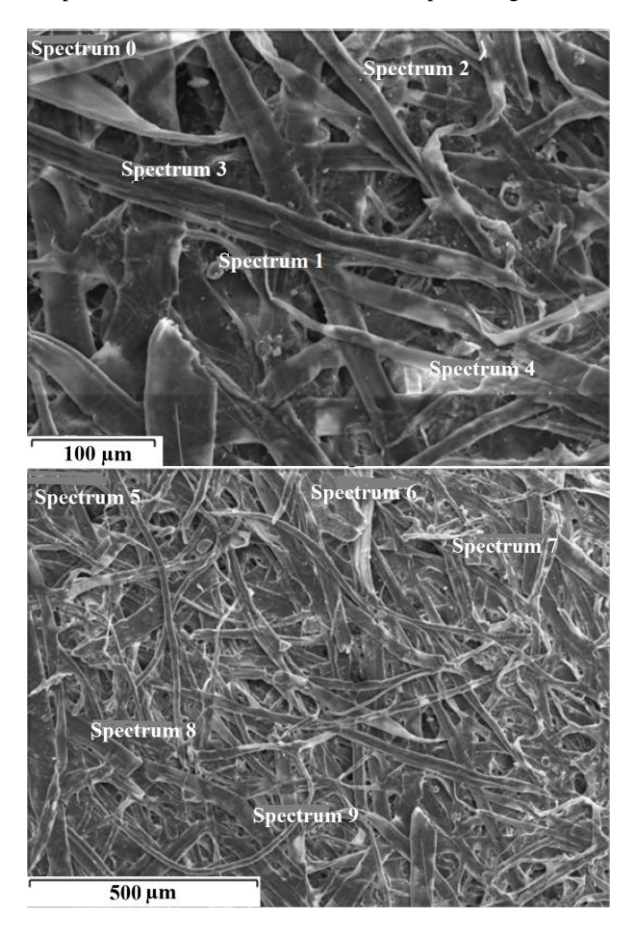


Fig. 4. SEM images of the paper surface indicating some of the sites (0-9) selected for scanning XR-ED spectra, the remaining sites (10-19) are shown in the Appendix.

The XR-ED mapping of carbon and oxygen atoms is shown in Fig. 5 in comparison with the SEM image; it can be seen that the mapping follows the contours of the cellulose fibers, while the oxygen-XR-ED-mapping image is characterized by a higher contrast compared to the carbon-XR-ED-mapping image.

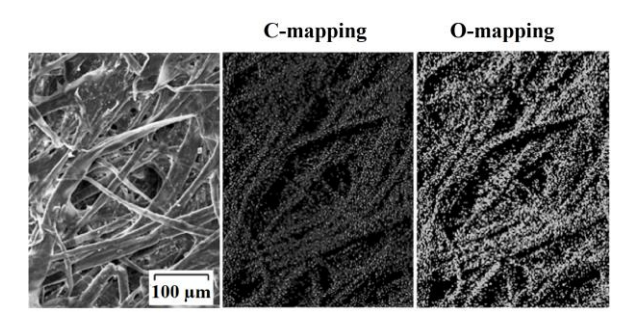


Fig. 5. SEM image (left) compared with C-XR-ED (middle) and O-XR-ED (right) mappings of sites corresponding to Spectra 0-4 (Fig. 3, top).

According to XR-ED elemental analysis, calcium is present in all sites, but its content varies within very wide limits from 0.06 to more than 11 atomic percent. A certain pattern is observed: for ten sites the spectra show a calcium content of less than 1 atomic %, and this corresponds to the usual content of calcium carbonate as a uniformly distributed filler, while at five sites (Spectra 4, 6, 7, 11 and 12) the calcium content exceeds 5 atomic %.

Table 1. Content of calcium, silicon & aluminum in paper prepared on the production line.

Spectrum	Atomic %		
No.	Ca	Si	Al
0	0.50	0.2	0.1
1	0.24	14.0	1.1
2	0.50	0.1	< 0.05
3	0.34	-	-
4	5.28	2.7	2.3
5	0.50	0.19	0.13
6	7.81	2.88	2.85
7	11.4	0.27	0.36
8	0.92	0.21	0.16
9	1.13	0.30	0.22
10	0.56	0.24	0.16
11	9.74	-	-
12	9.88	1.44	1.22
13	0.06	_	_
14	0.72	0.14	0.16
15			
16			
17			
18			
19			

Calcium-XR-ED mapping shows the non-uniform distribution of calcium on the paper surface and allows the identification of calcium carbonate conglomerates, marked by the circle and oval in Fig. 5, which compares the SEM image with the calcium XR-ED mapping result of the same area.

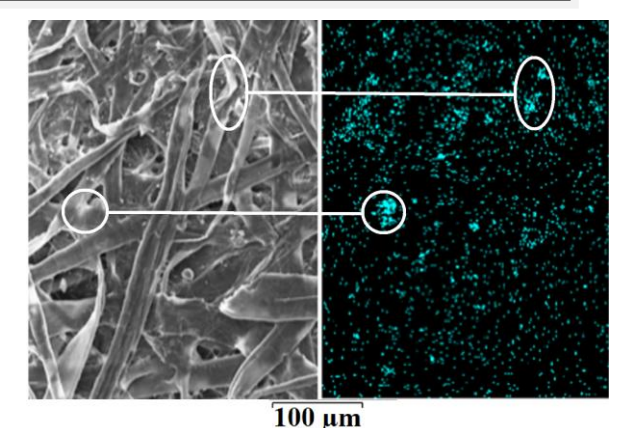


Fig. 5. SEM image (left) and Ca-XR-ED mapping (right) of "sites" corresponding to Spectra 11 and 12.

Seventeen of the twenty sites contain silicon and aluminum atoms on their surfaces, ranging in abundance from trace amounts to approximately 3 atomic percent, with the exception of site 1, which contains 14 atomic percent silicon (Spectrum 1).

The detection of silicon atoms indicates the possibility of the presence of such impurities as quartz sand (α -SiO₂) and glass (SiO₂ nNa₂O mCaO), as well as various silicates, natural chemical compounds with a complex silicon-oxygen radical [SiO₄]⁴⁻, etc. The simultaneous detection of aluminum atoms may indicate the presence of such basic rock-forming minerals as feldspars. However, in the presence of orthoclase (K[AlSi₃O₈]) or albite (Na[AlSi₃O₈]), the XR-ED spectra should show strong peaks of potassium and sodium, respectively, which is not observed.

The presence of calcium atoms may indicate feldspar anorthite $(Ca[Al_2Si_2O_8])$, in which case there should be matching points on the Ca-, Si- and Al-mappings. Such points are indeed found at two sites corresponding to Spectra 4 and 6, showing a relatively high content of calcium atoms and approximately equal amounts of silicon and aluminum atoms (see Table 1).

Apparently, the main silicon-containing impurities in paper are micrometric particles of quartz sand and glass, marked with a circle and oval in Fig. 7.

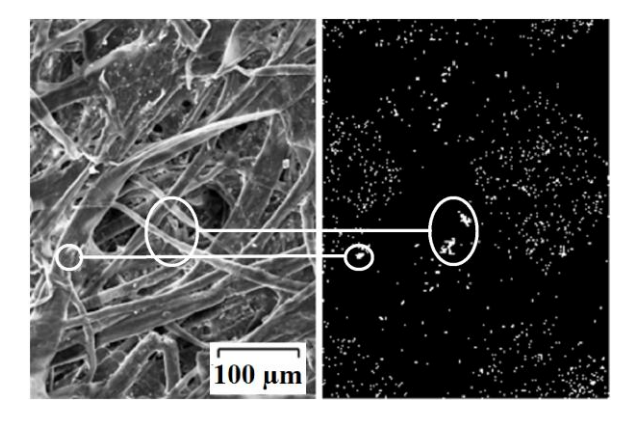


Fig. 7. SEM image (left) and Si-XR-ED mapping (right) of sites corresponding to Spectra 0-4.

Detection of aluminum atoms may also indicate the presence of aluminum oxide or metallic particles.

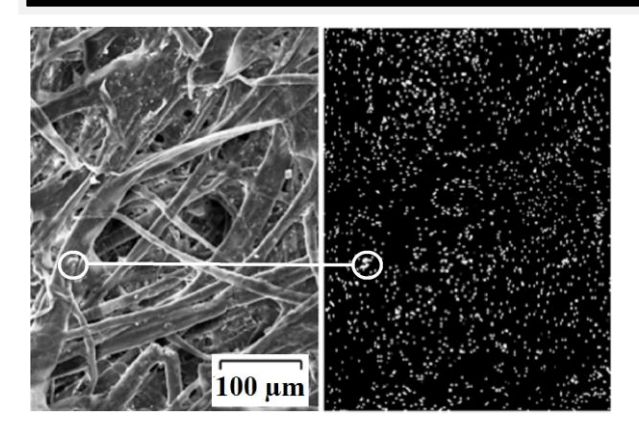


Fig. 8. SEM image (left) and Al-XR-ED mapping (right) of sites corresponding to Spectra 0-4.

The mapping of aluminum atoms (Fig. 8) shows a fairly uniform distribution of these atoms, mainly in relatively small particles, with larger aluminum particles highlighted by a circle.

Along with calcium, silicon and aluminum, XR-ED spectra at some sites detect atoms of magnesium, iron and zinc (see Table 2).

Table 2. Content of magnesium, iron & zinc in paper prepared on the production line.

Spectrum	Atomic %		
No.	Mg	Fe	Zn
1	0.4	0.1	0.1
4	0.1	1.1	0.3
6	0.28	0.08	-
7	0.07	_	=
11	0.23	_	_
12	0.21	_	_
16	3.13	_	_
18	0.08	_	-

High magnesium content is detected at only one site (Spectrum 16), where the SEM image (Fig. 9, top center) shows a large particle (3-5 $\,$ wide, 27 μm long) between the fibers, as well as other, slightly smaller impurity particles.

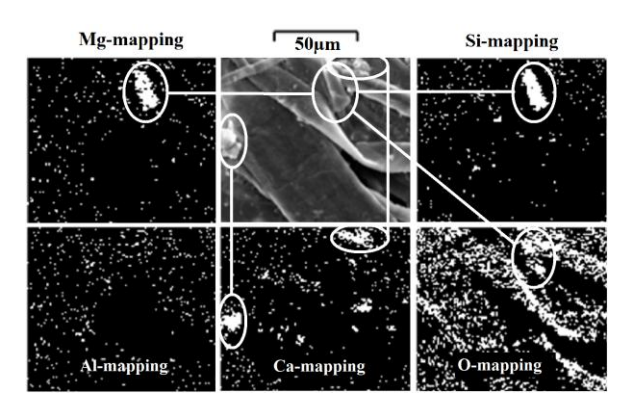


Fig. 9. SEM image (top, center) and Mg- (top, left). Si-(top. right), Al- (bottom, left), Ca- (bottom, center)m and O- (bottom, right) XR-ED mappings of site corresponding to Spectrum 16.

Mapping of this area shows that the outline of the large particle is reproduced by the Mg-, Si-, and O-XR-ED-mappings, indicating that the chemical composition of this impurity corresponds to silicate of magnesia (talc, (MgO)_n (SiO₂)_m, used as a filler in paper production [11]); other impurity formations at the left and upper edges of the site are visible in the Ca-XR-ED-mapping.

Iron and zinc atoms appear in XR-ED spectra in trace or small quantities; in XRD patterns, strong peaks of magnetite FeOFe_2O_3 , hematite Fe_2O_3 and zinc oxide ZnO at $20\approx 36^{\rm o}$ are not visible; XR-ED-mapping of iron and zinc atoms and, consequently, localization of the corresponding impurities is not possible.

Conclusion

The XR-ED spectra of the paper, in addition to the carbon and oxygen atoms of cellulose and the calcium atoms of calcite, also detect the presence of atoms of silicon, aluminum, magnesium, iron, and zinc. XR-ED mapping combined with SEM images allowed the identification of impurities such as quartz sand and talc

APPENDIX

The figures in the Appendix show the details of the study conducted.

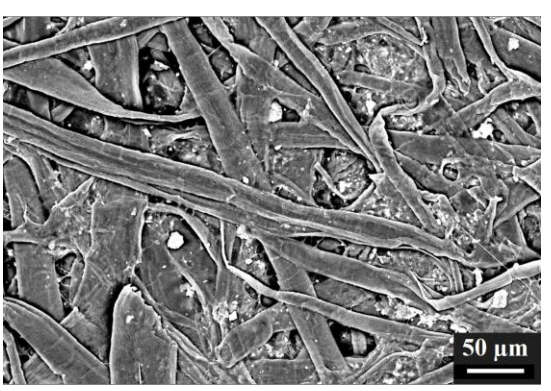


Fig. A1. SEM image of the paper surface at 270x magnification.

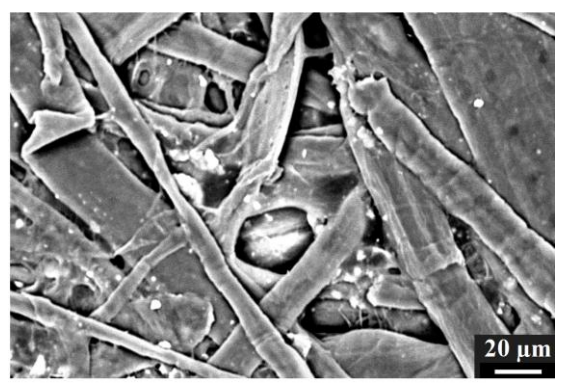


Fig. A2. SEM image of the paper surface at 550x magnification.

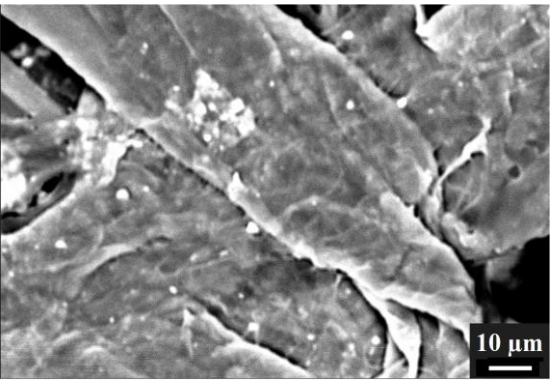


Fig. A3. SEM image of the paper surface at 1,000x magnification.

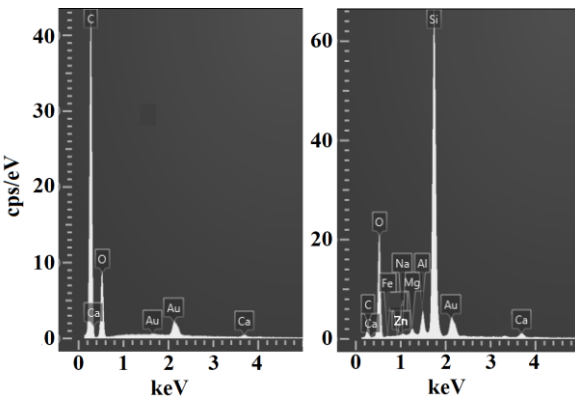
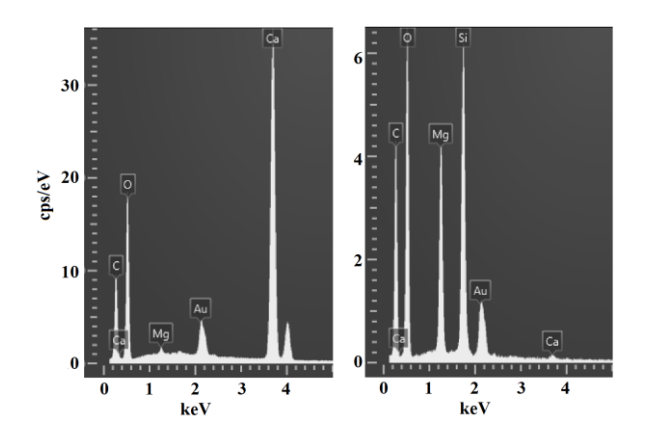


Fig. A4. XR-ED spectra of sites of paper with a small content of calcium impurity (left, Spectrum 3) and paper with a particle of quartz sand (right, Spectrum 1); the spectra record signals of contrasting gold atoms, but they are not taken into account in the calculations of the specific content of the elements.



REFERENCES

- [1] Salam M.A., Al-Amin M.Y., Salam M.T., Pawar J.S., Akhter N., Rabaan A.A., Alqumber M.A.A. "Antimicrobial resistance: A growing serious threat for global public health. *Healthcare* (Basel), 2023, vol. 11, no 13, #1946.
- [2] Nikolov A., Dobreva L., Danova S., Miteva-Staleva J., Krumova E., Rashev V., Vilhelmova-Ilieva N. "Natural and modified zeolite clinoptilolite with antimicrobial properties: A review". Acta Microbiologica Bulgarica, 2023, vol. 39, no 2, #147.
- [3] Villa C.C., Valencia G.A., Córdoba A.L., Ortega-Toro R., Ahmed Sh., Gutiérrez T.J. "Zeolites for food applications: A review". *Food Bioscience*, 2022, vol. 46, #101577.
- [4] Wakweya B., Jifar W.W. "In vitro evaluation of antibacterial activity of synthetic zeolite supported AgZnO nanoparticle against a selected group of bacteria". *J. Exp. Pharmacol.*, 2023, vol. 15, pp. 139-147.
- [5] Azizi-Lalabadi M., Alizadeh-Sani M., Khezerlou A., Mirzanajafi-Zanjani M., Zolfaghari H., Bagheri V., Divband B., Ehsani A. "Nanoparticles and zeolites: Antibacterial effects and their mechanism against pathogens". *Curr. Pharm. Biotechnol.*, 2019, vol. 20, no 13, pp. 1074-1086.

Fig. A4. XR-ED spectra of sites paper with a large calcium carbonate particle (left, Spectrum 11) and paper with a talc particle (right, Spectrum 16).

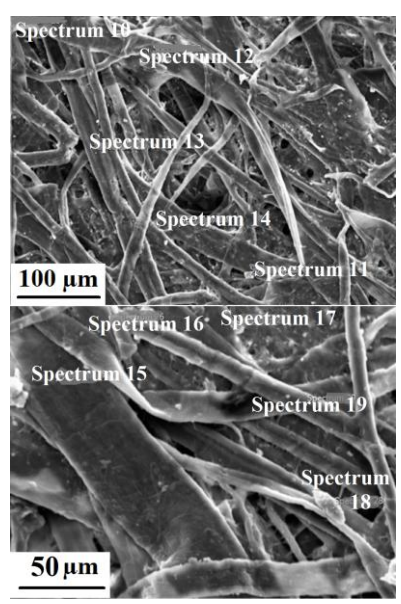


Fig. A4. SEM image of the paper surface indicating sites 10-19.

Acknowledgement

The authors express their gratitude to the Shota Rustaveli National Science Foundation of Georgia (SRNSF) supported this work under the project AR-22-610 "Production of paper with bactericidal and improved surface properties".

- [6] Król M., Syguła-Cholewińska J., Sawoszczuk T. "Zeolitesupported aggregate as potential antimicrobial agents in gypsum composites". *Materials*, 2022, 15: #3305.
- [7] Díez-Pascual A.M. "Antibacterial activity of nanomaterials". *Nanomaterials*, 2018, 8: #359.
- [8] Tsitsishvili V., Dolaberidze N., Mirdzveli N., Nijaradze M., Amiridze Z. "Preparation of bactericidal fillers from Georgian heulandite-clinoptilolite and their application for paper production. I. Bactericidal fillers". Scientific Collection «InterConf+», 2021, vol. 67, pp. 340-358.
- [9] Tsitsishvili V., Dolaberidze N., Mirdzveli N., Nijaradze M., Amiridze Z. "Preparation of bactericidal fillers from Georgian heulandite-clinoptilolite and their application for paper production. II. Bactericidal paper". Scientific Collection «InterConf+», 2021, vol. 67, pp. 359-374.
- [10] Schabel S., Putz H.J., Hamm U., Kersten A., Bobek B., Hirsch G., Voss D. "Calcium carbonate in the paper industry – Blessing for coated papermaking and curse for recycling processes", *TAPPI Journal*, 2014, vol. 13, no 11, pp. 47-54.
- [11] Chauhan V.S., Bhardwaj N.K. "Efficacy of dispersion of magnesium silicate (talc) in papermaking", *Arabian Journal* of Chemistry, 2017, vol. 10, supplement 1, pp. S1059-S1066.

Performance of sulfide-driven fuel cell at different catodes and processes

Institute of Chemical Engineering, Bulgarian Academy of Sciences, 111 Sofia, Bulgaria *E-mail: vbeschkov@gmail.com

Abstract. The fuel cells operating in liquid phase stand back to the traditional ones, operating at high temperatures. This problem is well manifested when oxygen is used as electron acceptor in the cathode space of the cell because of its low solubility in water and low mass transfer rate. The present work aims to find ways to enhance the cathode process in aqueous fuel cell. This study deals with the use of three different reduction processes and electrodes as cathode in a sulfide-driven fuel cell. First, metal titanium is tested as cathode. Next, a catalyst, enhancing the oxygen reduction with graphite as electrode. The catalyst consists of compounds of cobalt and manganese, embedded in activated carbon after pyrolysis of soot. Last, nitrate anions are used as oxidizer in a big excess to the sulfide initial concentration with graphite cathode. It was shown that the highest electric current density is obtained when catalyst was used. The excess of nitrate helps to increase the power density but nitrate are not compatible with environmentally sensitive systems, like marine water. The use of cathode of high electric conductivity is not sufficient to compensate the low oxygen solubility in aqueous media.

ს. სტეფანოვი, ლ. ლუცკანოვი, ვ. ზეშკოვი – სულფიდზე მომუშავე საწვავის უჯრედის მუშაობა სხვადასხვა კათოდებსა და პროცესების პირობებში

რეზიუმე. თხევად ფაზაში მომუშავე სათბობი ელემენტები განსხვავდებიან ტრადიციულებისგან, რომლებიც მუშაობენ მაღალ ტემპერატურაზე. ეს პრობლემა აშკარად ვლინდება, როდესაც ელემენტის კატოდურ სივრცეში ელექტრონის აქცეპტორად გამოიყენება ჟანგბადი მისი წყალში დაბალი ხსნადობის და მას-ტრანსფერის მცირე სიჩქარის გამო. წარმოდგენილი ნაშრომი მიზნად ისახავს წყლის სათბობ ელემენტში კატოდური პროცესის კვლევაში განხილულია სამი განსხვავებული აღდგენითი პროცესი და გაუმჯობესების გზების ძიებას. ელექტროდების კატოდად გამოყენება სულფიდებზე მომუშავე_ სათბობ ელემენტში. თავდაპირველად, კატოდად მეტალური ტიტანი იყო გატესტილი. შემდეგ-კატალიზატორი, რომელიც აძლიერებდა ჟანგბადის აღდგენას, ელექტროდად გრაფიტი იყო გამოყენებული. კატალიზატორი შედგებოდა გააქტიურებულ ნახშირბადში კობალტისა და მანგანუმის ნაერთების ჩანართებისგან, რომლებიც ჭვარტლის პიროლიზის შედეგად იყო მიღებული. დაბოლოს, დამჟანგავად, სულფიდის საწყის კონცენტრაციასთან შედარებით ჭარბი რაოდენობის ნიტრატ-ანიონები იყო გამოყენებული, გრაფიტის. კატოდით. ნაჩვენებია, რომ ელექტრული დენის ყველაზე მაღალი სიმკვრივე მიიღწევა კატალიზატორის გამოყენებისას. ნიტრატის სიჭარბე ხელს უწყობს დენის სიმკვრივის ზრდას, მაგრამ ნიტრატი არაა თავსებადი ეკოლოგიურად მგრმნობიარე სისტემებთან, ისეთებთან, როგორიცაა მაგალითად ზღვის წყალი. წყლის გარემოში მაღალი ელ-გამტარობის მქონე კატოდის გამოყენება საკმარისი არ არის ჟანგბადის დაბალი ხსნადობის კომპენსირებისთვის.

Keywords: cathode process, catalyst, electron acceptor, cathode space, graphite electrode, reductio, sulfide-driven fuel cell. Introduction

This research arose some years ago when experience accumulated during the work on sulfide driven fuel cells. Hydrogen sulfide can be used as a reductor (fuel) in this type of operation. Its amount in the Black Sea waters was estimated to be about 4.6 billion tons [1] with annual additions of at least 5 million tons [2]. Having in mind that the enthalpy of oxidation of hydrogen sulfide to sulfate is 833.6 kJ/mole at 25 °C, one can calculate that the total amount of hydrogen sulfide for the Black Sea is equivalent to 33,000 TWh electric energy. Some time ago a method for direct electricity production was proposed [3,4. It is based on the direct oxidation of sulfide to sulfite and sulfate in the anode compartment of aqueous fuel cell.

Other application of fuel cells operating in gaseous phase is the treatment of hydrogen sulfide released during oil desulphurization [5]. The disadvantage in this case consists in the elemental sulfur accumulation and the blockage of the anode. There is a recent paper claiming the sulfide utilization as electricity from sulfide containing caustic stream using gas-diffusion electrode [6]. In this case, however, the alkalinity of the feeding solution is very high, i.e. pH 13.9 and it is inadmissible from environmental point of view. On the other hand in this case the sulfide oxidation stops with elemental sulfur as oxidation product.

Kim &Han [7] attained high current density in a liquid phase sulfide fuel cell, but in very strong alkaline media, which is also inadmissible for environmental purposes.

There are also efforts to use the sulfide-driven fuel cell for hydrogen peroxide production based on the energy generated by electrochemical processes [8].

Some obstacles before the practical use of this type of fuel cells are known. First, it is the low sulfide concentrations in natural ponds, e.g. reaching almost 22 g/m3 in the Black Sea at biggest depths. Another hinder is the low concentration of oxygen in the cathode aqueous streams. In these cases the concentration of oxygen is very low, i.e. 5-10 g/m3 at atmospheric pressure and ambient temperatures. These factors together with the low mass transfer rate in liquid phase lead to shortage in oxygen supply and therefore sluggish kinetics of the cathode oxygen reduction and low fuel cell efficiencies are expected [9].

There are different methods to facilitate oxygen mass transfer in cathode space of liquid phase fuel cell: to use pure oxygen under pressure, to use cathodes of high electro-conductivity, gas-diffusion electrodes [10], catalysts to enhance oxygen reduction or to replace oxygen by other oxidizers at higher concentrations, e.g. nitrate.

Ipsakis et al. [11] proposed an electro-catalytic membrane reactor for hydrogen sulfide oxidation in aqueous media using solid electrolyte membrane.

The present work summarizes our efforts in these directions. We present own experimental data on sulfide oxidation in sulfide-driven fuel cell by these three cathode modifications:

- Use of titanium as cathode;
- Use nitrate at high concentration as oxidizer;
- Use of catalyst embedded in electro-conductive support.

Materials and methods

1. Materials

Experiments either with and without catalyst were carried out. The sulfide solutions were prepared by sodium sulfide nona-hydrate ACS reagent ≥.98% (Sigma-Aldrich production) or by sodium hydrosulfide, NaHS. As supporting electrolyte for the sulfide solution sodium chloride aqueous solution (16 g dm-3), the same as it is in the Black Sea water, was used. The initial solution pH varied between 7.3 and 12.6 depending on the chosen sulfide concentration from 20 to 240 mg dm⁻³.

Sodium nitrate in the experiments with nitrate as oxidizer, was used. The nitrate concentration was around 500 mg dm⁻³, i.e. in large excess compared to the sulfide concentration.

Two types of electrodes were used: square sheets of sintered graphite of 100 sq. cm area and rectangular sheets of titanium same size. The EDX-spectrum of the graphite plates showed contamination of silicon only.

When catalyst in the cathode space was used, graphite plates as electrodes were applied. The catalyst consisted of oxides of manganese, iron and cobalt. It was prepared by pyrolysis of waste soot of tires production, soaked by salts of the listed metals. The obtained char particles were electro-conductive. The cathode space was packed by these particles with size ca. 0.2 mm, thus to increase the contact area of the electrode. The XRD-diagram of the catalyst is shown in the **Fig. 1**.

Zinc oxide, as well as sulfides, sphalerite and wurtzite were detected too. Probably the zinc compounds are present as components of the substrate.

2. Methods

The expected scheme of the fuel cell for the considered case is shown in Fig. 2.

Both cases of anode reactions involving proton or hydroxylic anion exchange are presented.

$$SO_4^{2-} + 8H^+ + 8e = S^{2-} + 4H_2O$$
 anode reaction $O_2 + 4H^+ + 4e^- = 2H_2O$ cathode reaction or

$$SO_4^{2-} + 4H_2O + 8e^- = S^{2-} + 8OH^-$$
 anode reaction $O_2 + H_2O + 4e^- = 4OH^-$ cathode reaction

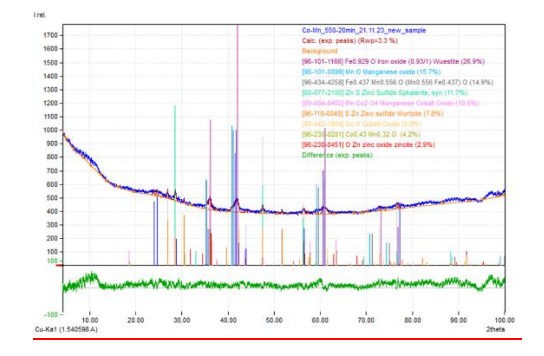


Fig. 1. A XRD-diagram of the prepared and used catalyst.

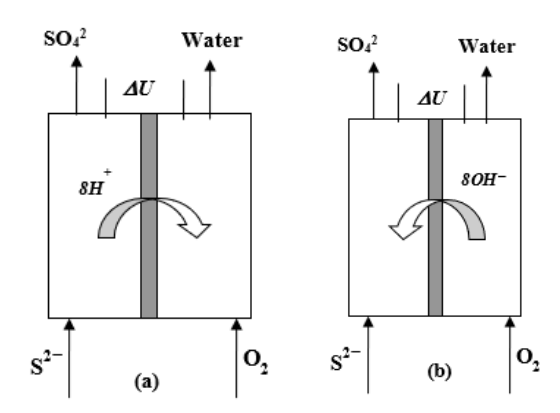


Fig. 2. Scheme of the operation mode of sulfide driven fuel cell; (a) – proton exchange; (b) – hydroxylic anion exchange.

Experiments were carried in a lab-scale fuel cell designed for the present purpose (Fig 3).

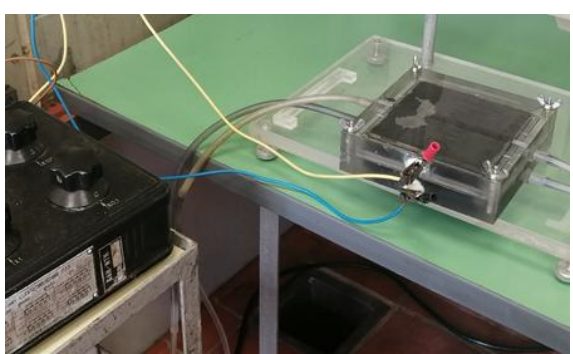


Fig. 3. A picture of the lab-scale fuel cell

The cell consisted of two rectangular compartments with plane electrodes separated by ion-exchange membrane. In all cases anion exchange membrane (DSVN, a Selemion production, Japan) was used. The slot of the anode compartment was 0.5 cm and of the cathode one -0.8 cm. The cross section of each compartment was 100 sq.cm.

The cathode space was fed by the same supporting electrolyte preliminary aerated by air.

Both batch and continuous processes for the anode compartment were studied. In the case of batch processes the cathode electrolyte was supplied continuously by peristaltic pump.

During the continuous experiments the sulfide solutions were purged by nitrogen prior to supplying to the fuel cell to avoid or at least to minimize the parasite bulk oxidation of sulfide. The feeding was accomplished by peristaltic pump.

The current efficiencies were calculated from the measures electric current according to the Faraday's law and compared to the converted sulfide according to the analysis.

$$\frac{m}{t} = \frac{Mi}{nF}, m = \frac{M}{nF} \int_0^t i \cdot dt$$

$$\frac{m}{t} = \frac{Mi}{nF}, m = \frac{M}{nF} \int_0^t i \cdot dt$$
(1)

where:

• i—electric current, A; •

- m—mass of reacting substance, g;
- t—time, s;
- M—molar mass of reacting substance, g;
- n—number of exchanged electrons;
- $F = 96,484 \text{ C mol}^{-1}$, Faraday constant.

The number of exchanged electrons n depends on the reactions on the anode. In the case of sulfide oxidation these reactions are very sensitive to the sulfide concentration and a large variety of exchanged electrons for different electrochemical reactions are possible. We shall constraint ourselves to some of them, more probable at lower sulfide concentrations, as it is in our case. Table 1, excerpt of broader one [Suhotin, A.M. Guidebook on Electrochemistry (in Russian); Himia: Leningrad, Russia, 1981] is shown below.

Table 1. Short excerpt of sulfide oxidation reactions, taken from [12]

No.	Reversible anode reaction	Number of	Standard electrode
		exchanged	potential, 25oC, V
		electrons, n	
1	$SO_4^{2-} + H_2O + 2e = SO_3^{2-} + 2OH^-$	2	-0.91
2	$SO_3^{2-} + 3H_2O + 6e = S^{2-} + 6OH^{-}$	6	-0.66
3	$S_2^{2-} + 2e = 2S^{2-}$	1	-0.524
4	$S + 2e = S^{2-}$	2	-0.48
5	$S_2O_3^{2-} + 6H^+ + 8e = 2S^{2-} + 3H_2O$	4	-0.006

Note, that the oxidation of sulfide to sulfate involving 8 exchanged electrons passes through two steps: first, oxidation to sulfite involving 6 electrons and second, oxidation of sulfite to sulfate, with 2 exchanged electrons.

3 Analyses

Samples from the solutions in the inlet and outlet solution were taken regularly. They were analyzed for sulfide, sulfite and sulfate. The pH values of the feeding solutions and the outlet ones were measured by pH-meter. Sulfide was analyzed quantitatively by photometry [13]. Sulfite was analyzed iodometrically. Sulfate ions were analyzed qualitatively by addition of barium chloride. Formation of polysulfides was checked qualitatively by acidification of the reaction mixture and deposition of elemental sulfur. The presence of thiosulfates was checked qualitatively by ferric chloride yielding intensive purple complex.

When nitrate as oxidizer was used, nitrate concentration was determined photometrically using a method described in [14]

4. Polarization experiments

The polarization curves for the fuel cell performance were evaluated varying the current by external Ohmic resistance and measuring the corresponding cell voltage. The current was calculated by the Ohm's law from the measured cell voltage and the current Ohmic resistance. Then the generated power was calculated.

5. Experiments with fuel cell discharge

These experiments were carried out in a batch and continuous modes. The generated electromotive force was discharged through external ohmic resistance selected by the optimum current density evaluated at the polarization experiments.

At the continuous process, both compartments were fed by peristaltic pumps with a constant flow rate. In the case of batch processes in the anode compartment the cathode electrolyte was also supplied continuously to the cathode compartment by peristaltic pump.

Results and discussion

1. Control experiments with dissolved oxygen

Example of polarization curve for control experiment is shown in Fig. 4. In these cases, no catalysts were used, nor nitrate as electron acceptor. Sintered graphite sheets served as electrodes. It is seen that both current and power densities are extremely low. The maximum current density is 0.03 A/m2 and the power density is about 6 mW/m2.

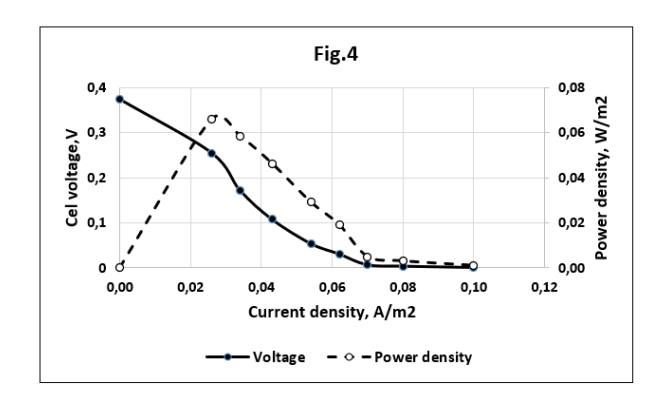


Fig. 4. Polarization curve for experiment when no catalyst, no nitrate were added. Continuous process, feed flow rates 0.3 dm³ h⁻¹ for both compartments. Inlet sulfide concentration 202.4 g dm⁻³. Supporting electrolyte 16.5 g dm⁻³ NaCl for both compartments.

2. Fuel cell performance at titanium cathodes

Some experimental results obtained by the use of titanium as cathode are shown in Fig.5. The straight line on Fig.4b shows that there are no overpotential at low current densities and no mass transfer limitations at higher ones. There is a stable continuous process of sulfide oxidation soon after the process starts.

A comparison of the calculated oxidation rates to the determined ones by analysis is shown in Table 2. One can see that the reaction, involving polysulfide formation with one exchanged electron (reaction 3) is not admissible. Reactions 1 and 4 seem suitable for the obtained results, with 67% conversion rate. However, no elemental sulfur corresponding to reaction 4 was observed, nor thiosulfate were observed. The complete conversion of sulfide to sulfate, involving 8 exchanged electrons seems negligible, i.e. about 15% only. A possible explanation of this result is that a parasite bulk

A possible explanation of this result is that a parasite bulk reaction of sulfate to sulfite oxidation may take place and that the purging the inlet sulfide solution with nitrogen is not sufficient.

Table 2. Comparison of the calculated by the Faraday's law and the determined by analysis oxidation rates with titanium as cathode, $mg\ h^{-1}$

Number of exchanged electrons		1	2	4	6	8
Analysis	1.83					
Faraday's	-	2.44	1.22	0.61	0.31	0.15
law, <u>Eq.(</u> 1)						

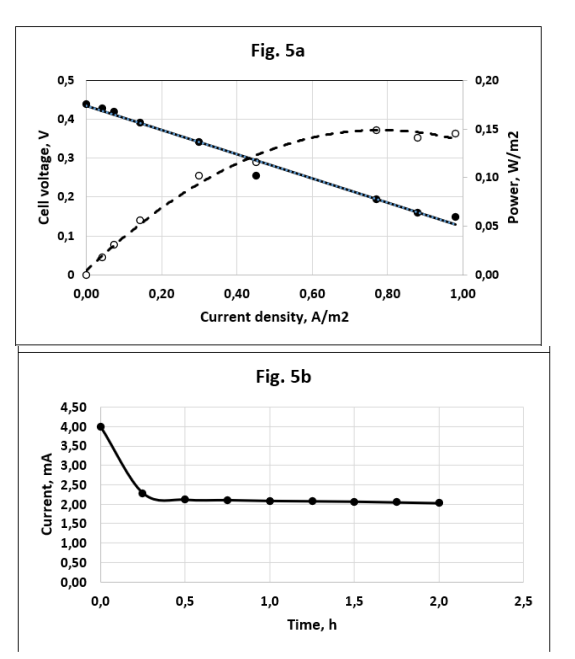


Fig. 5. Polarization curve (5a) and fuel cell discharge (5b) in continuous process.

Initial sulfide concentration, 21.5 g dm⁻³; feed flow rate for anode compartment $0.76 \text{ dm}^3 \text{ h}^{-1}$; graphite sheet as anode. Titanium sheet as cathode; feed flow rate for cathode compartment $0.72 \text{ dm}^3 \text{ h}^{-1}$. Supporting electrolyte 16.5 g dm^{-3} NaCl for both compartments. External ohmic resistance $30 \land (\text{Fig. 5b})$.

3. Fuel cell performance with nitrate as oxidizer

Nitrate anions of concentration ca. 500 mg dm⁻³ were used as electron acceptor. The excess of nitrate was chosen to avoid mass transfer and kinetic limitations as it happened when oxygen dissolved in aqueous solution was used.

When nitrate is used as oxidizer, the cathode reaction in the fuel cell is as follows:

$$NO_{3}^{-} + H_{2}O + 2e^{-} = NO_{2}^{-} + 2OH^{-}$$

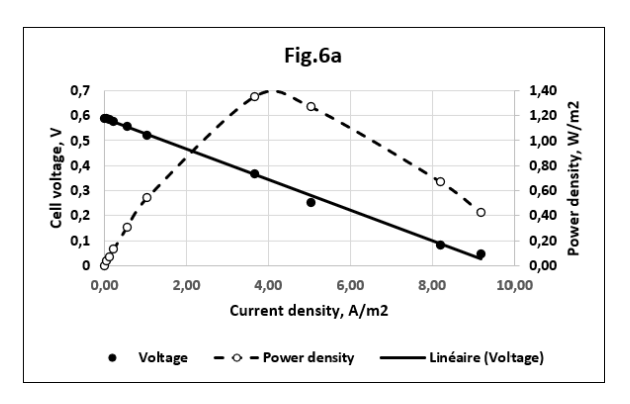
The results for fuel cell performance under static conditions are shown in Fig. 5. When nitrate is used in excess as electron acceptor, the current and power densities are much higher than in the case of dissolved oxygen use. Nitrate depletion was about 50% of its initial amount, thus keeping the nitrate concentration sufficiently high compared to the sulfide one.

Under batch conditions the fuel cell was discharged and exhausted within 1 hour. During this time the current efficiency according to the Faraday's law corresponds to different number of exchanged electrons, as shown in the Table 3.

Table 3. Comparison of the calculated by the Faraday's law and the determined by analysis oxidation rates with nitrate as oxidizer in the cathode compartment, mg.

Number of		1	2	4	6	8
exchanged						
electrons						
Analysis	3.09					
Faraday's	-	5.75	2.87	1.43	0.96	0.72
law, Eq.(1)						

Again, the reaction involving one exchanged electron is not admissible. The reactions 1 and 4, involving exchange of 2 electrons gives very high agreement with the result of the analysis, i.e. about 93%. It seems very high compared with other data for the fuel cell efficiencies. The reaction 2 of sulfite formation with exchange of 6 electrons seems reasonable, with agreement of 31% with the result of the analysis.



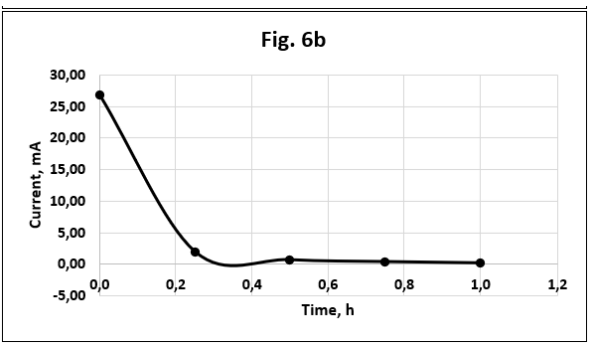


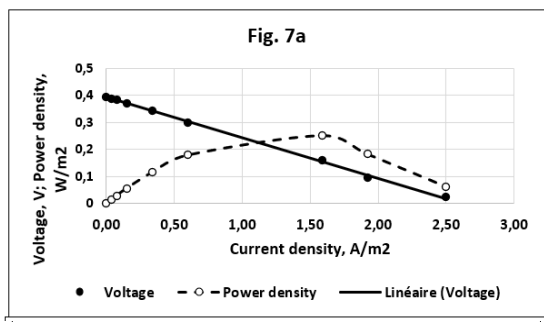
Fig. 6. Polarization curve (6a) and fuel cell discharge (6b) in batch process. Initial sulfide concentration, 67.4 g dm⁻³; graphite sheets as electrodes. Initial nitrate concentration, 480 mg dm⁻³. Supporting electrolyte 16.5 g dm⁻³ NaCl for both compartments. External ohmic resistance 10 ∧ (Fig. 6b).

4. Fuel cell performance with catalytic oxygen reduction

At these experiments the cathode space of the fuel cell was packed with the catalyst. The inlet sulfide concentrations were within 200 and 220 mg dm $^{-3}$. The experiments were carried out in continuous mode. Both compartments were fed with flow rate of 0.3 dm $^{-3}$ /h.

Some experimental results are shown in Fig.7. The best results for current density and power density are obtained by the Co-Mn catalyst. The latter causes an additional effect, facilitating the conversion of sulfide to polysulfide as observed qualitatively.

The comparison of the analytical results and the values calculated by the Faraday's law confirms that the reaction of sulfide to polysulfide is the most probable one. Sulfite anions are also detected. These controversial results can be explained by the catalyst activity and the relatively high inlet sulfide concentrations. The most probable reactions for this case are reactions 1 (sulfite oxidation) and reaction 3 (polysulfide formation), cf. Table 4.



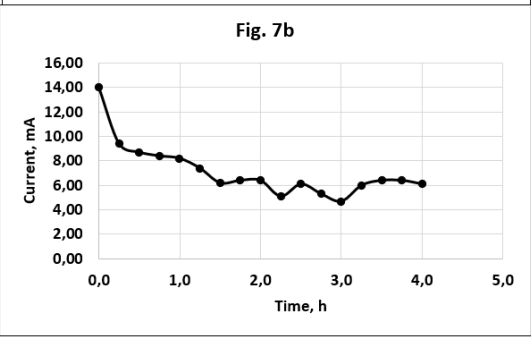


Fig 7. Polarization curve (7a) and fuel cell discharge (7b) in continuous process. Initial sulfide concentration, 200 g dm⁻³; graphite sheets as electrodes. A cobalt/manganese catalyst, embedded into pyrolyzed soot in the cathode compartment. Supporting electrolyte 16.5 g dm⁻³ NaCl for both compartments. External ohmic resistance 10 ∧ (Fig. 7b).

Table 4. Comparison of the calculated by the Faraday's law and the determined by analysis oxidation rates with oxygen as oxidizer with Co-Mn catalyst in the cathode compartment, mg/h

Number of		1	2	4	6	8
exchanged						
electrons						
Analysis	8.8					
Faraday's		7.58	3.79	1.89	1.26	0.95
law, Eq.(1)						

4. Discussion

A comparison of the current and power densities determined for different electrodes and cathode processes are shown in Table 5.

Table 5. Comparison of the average current and power densities, obtained at different cathodes and cathode electrochemical reactions in sulfide-driven fuel cell.

	Curren t density, A/m ²	Power density, W/m ²
Titaniu m cathode	0.73 ± 0.35	0.12 ± 0.09
Co-Mn catalyst	1.95 ± 0.42	0.18 ± 0.07
Nitrate reduction	0.20 ±	0.60 ± 0.66

Control	0.03	0.006
experiment		

The current density when catalyst was used is superior to the rest ones. Good and stable results are obtained for the case.

The power density obtained when nitrate was used prevails the values determined when oxygen is used as electron acceptor although at very big data scatter. However, the high toxicity of nitrate and the resulting nitrite does not allow its use in the environmentally sensitive media like the marine water, Nitrate can be used as oxidizer when wastewater are treated with additional yield of energy.

The results obtained with titanium cathode show that the good electroconductivity of the metal cannot compensate the disadvantages of oxygen with its low solubility in water and low mass transfer rates.

The complicated and controversial results for the oxidation product in the anode compartment can be explained by the big variety of possible anode reactions of sulfide oxidation at its higher concentrations.

Our further efforts will be directed toward the use of gasdiffusion cathode with embedded catalyst within.

Acknowledgement. This work was supported by the Fund for Scientific Research, Bulgaria, project KP-06-H67/3.

REFERENCES

- [1] Midilli, A.; Ay, M.; Kale, A.; Nejat Veziroglu, T. A parametric investigation of hydrogen energy potential based on H2S in Black Sea deep waters. *Int. J. Hydrogen Energy* 2007, 32, pp. 117–124. [CrossRef]
- [2]. Neklyudov, I.K.; Bortz, B.V.; Polevich, O.W.; Tkachenko, V.I.; Shilyaev, B.A. Alternative hydrogen sulfide energetics in the Black Sea. Part I. State of the art, problems and perspectives (in Russian). *Int. Sci. J. Altern. Energy Ecol. (ISJAEE)* 2006, 12, pp. 23–30.
- [3]. Beschkov V., Razkazova-Velkova, E., Martinov, M.,Stefanov S., Electricity Production from Marine Water by Sulfide-Driven Fuel Cell, Appl. Sci. 2018, 8, 1926; doi:10.3390/app8101926
- [4]. Beschkov, V.; Hristov, V.; Petkov, P. Energy Yield from Sulfide Containing Marine Water. B.G. Patent No. 1775/25.11.2013, Ref. No. 2352/14.02.2013.
- [5]. Chuang, K.T.; Luo, J.; Sanger, A.R. Evolution of fuel cells powered by H2S-containing gases. Chem. Ind. Chem. Eng. Q. 2008, 14, pp. 69–76.
- [6]. Jucai Wei, Yun Liu, Xu Wu, Recycling sulfidic spent caustic streams using a sulfide/air fuel cell, Separation and Purification Technology, 2024, 329, 125234
- [7]. Kim, K.; Han, J.-I. Performance of direct alkaline sulfide fuel cell without sulfur deposition of anode. *Int. J. Hydrogen Energy* 2014, 39, pp. 7142–7146.
- [8]. Jucai Wei, Xu Wu, A sulfide self-driven fuel cell for H2O2 electrosynthesis and sulfur recycling, Journal of Water Process Engineering, 56, December 2023, 104505.
- [9]. O'Hayre, R.P.; Cha, S.-W.; Colella, W.G.; Prinz, F.B. Fuel Cell Fundamentals, 2nd ed.; John Wiley & Sons, Inc.: Hoboken, NJ, USA, 2009; pp. 59–64.
- [10]. Rabiee, H., Lei Ge, Xueqin Zhang, Shihu Hu, Mengran Li, andZhiguo Yuan, Gas diffusion electrodes (GDEs) for electrochemical reduction of carbon dioxide, carbon monoxide, and dinitrogen to value-added products: a review, Energy Environ. Sci., 2021,14, pp. 1959-2008.
- [11]. Ipsakis, D.; Kraia, T.; Konsolakis, M.; Marnellos, G. Remediation of Black Sea ecosystem and pure H2 generation via H2S-H2O co-electrolysis in a proton-

- conducting membrane cell stack reactor: A feasibility study of the integrated and autonomous approach. Renew. Energy $2018,\,125,\,pp.\,806-818.$
- [12]. Suhotin, A.M. Guidebook on Electrochemistry (in Russian); Himia: Leningrad, Russia, 1981.
- [13]. Kirk, T.J.; Winnick, J. A hydrogen sulfide solid-oxide fuel cell using ceria-based electrolytes. J. Electrochem. Soc. 1993, 140, 3494–3496.
- [14]. Goldman, E., Jacobs, R., Determination of nitrates by ultraviolet absorption, J. Am. Water Works Assoc. 1961, 53, pp. 187–191.

Institute of Catalysis and Inorganic Chemistry named after acad. M. Nagiyev Ministry of Science and Education of the Republic of Azerbaijan H.Javid ave., 113, AZ 1143, Baku, Azerbaijan

*E-mail: <u>vuska_80@mail.ru</u>

Abstract. The work is devoted to the electrochemical deposition of thin Fe-Se films and the study of some of their properties. An aqueous electrolyte was chosen to obtain thin films. Co-deposition on the Pt electrode occurs in a potential range of 0.65 - (-0.6) V. The effect of the concentration of the starting ions constituting the electrolyte on the electrochemical co-deposition process of Fe and Se was studied in the range of 0.025-0.055 M (For iron ions) and the range of 0.0005 - 0.0075 M (For selenite ions). The effect of the potential scanrate on the co-deposition process was studied in the range of 0.005 - 0.08 V/s. The thickness of the deposited thin layers is 4-6 μ m. According to the results of EDS (element composition) analysis, the composition of the coatings corresponds to stoichiometry and consists of 42.2% Fe, 57.8% Se.

ვ. მაჯიზადე, ს. ჯავადოვა, ს. ჯაფაროვა, ა. ალიევი, დ. ტაგიევი — Fe-Se თხელი ფენების ელექტროდეპონირება და ზოლის განსაზღვრა

რეზიუმე. ნაშრომი ეძღვნება Fe-Se თხელი ფენების ელექტროქიმიურ დალექვას და მათი ზოგიერთი თვისების შესწავლას. თხელი ფენების მისაღებად შეირჩა ელექტროლიტის წყალხსნარი. Pt ელექტროდზე თანადალექვა ხდება 0.65 - (-0.6) ვოლტის პოტენციურ დიაპაზონში. ელექტროლიტის შემადგენელი საწყისი იონების კონცენტრაციის გავლენა Fe-სა და Se-ს ელექტროქიმიური თანადალექვის პროცესზე შესწავლილი იქნა 0.025-0.055 მ დიაპაზონში (რკინის იონებისთვის) და 0.0005-0.0075 მ დიაპაზონში (სელენიტის იონებისთვის). პოტენციური გაწმენდის სიჩქარის გავლენა თანადალექვის პროცესზე შესწავლილი იქნა 0.005-0.08 ვ/წმ დიაპაზონში. დალექილი თხელი ფენების სისქეა 4-6 მკმ. EDS ანალიზის (ელემენტური შემადგენლობა) შედეგების მიხედვით, საფარის შემადგენლობა შეესაბამება სტექიომეტრიას და შედგება 42.2% Fe, 57.8% Se-სგან.

Keywords: Fe-Se thin films, electrodeposition, semiconductors, polarization curve.

Introduction

Recently, iron chalcogenides have received much attention due to their applications in magnetoelectronics, spintronics, and solar cells [1-3]. Iron diselenide (FeSe₂) is an active layer in solar photovoltaic and photoelectrochemical cells. It is a very promising but not widely studied semiconductor used as a semiconductor. This compound, which is of great interest for producing solar cells, is a p-type semiconductor with a band gap of 1.03 eV [3-5]. Recently, iron selenide has been studied for its unusual structure and electronic properties. has attracted widespread attention. Two homogeneous and stable phases exist in this system, α - FeSe and FeSe₂ [6, 7]. The α - FeSe phase crystallizes in tetragonal and hexagonal structures, while the FeSe₂ phase crystallizes in rhombic marcasite and cubic structures.

Iron monoselenide (FeSe) and diselenide (FeSe2) are considered as substitutes for platinum as auxiliary electrodes for sensitive solar cell crystals. They have catalytic activity and higher energy conversion efficiency than platinum. In addition to being effective, they are stable in highly corrosive environments [8-12]. Iron selenides can also be semiconductors with properties of ferro/ferrimagnetic metals or even superconductors, depending on their composition and structure [13-18]. Iron diselenide thin films can be obtained by various methods. knows: pyrolysis spraying, soft selenization of iron layers, flash evaporation, metal-organic chemical vapor deposition, solvothermal method, chemical vapor deposition. Polycrystalline iron diselenide layers, consisting of a mixture of FeSe and FeSe2, can be obtained by selenization of deposited sputtered iron thin films. In addition, various synthetic methods for the synthesis of iron selenide have been developed, including elementary reactions in high-temperature vacuum tubes, Aqueous solutions of metal salts and mechanical melting have been used by applying H₂Se gas.

Experimental part

Potentiodynamic studies were performed using IviumSoft - programmed and computer-equipped "IVIUMSTAT Electrochemical Interface" potentiostat. In this case, a three-electrode electrochemical cell with a volume of 100 ml was used. Pt wire with an area of 0.3 cm² and Ni plate with an area of 2 cm² were used as working electrodes. Saturated silver/silver chloride (Ag/AgCl/KCl) electrode was used as the reference electrode, and Pt plate with an area of 4 cm² was applied as the auxiliary electrode. Electrolyte solutions containing 0.035 M Fe(NO₃)₃ + 0.0025 M H₂SeO₃ were used during the experiments.

The surface of the Pt electrode has been cleaned as follows: the Pt electrode is kept for several minutes in pure H_2SO_4 at a potential of 1.2 V. At this potential, many organic substances are oxidized and desorbed from the electrode surface. The electrode is kept at a more negative potential from 0.0 V to reduce the adsorbed oxygen. The Pt electrode is kept at a potential of 0.3 V to remove the adsorbed hydrogen, and thus its surface is completely cleaned.

Before experiments, the surface of the Ni electrodes is mechanically polished, treated with concentrated HNO₃ acid for 30 s to remove oxide layers, immersed in alcohol or acetone, and finally washed with bidistilled water. Electrochemical polishing of Ni electrodes has been carried out in a solution consisting of 55 mL of H₂SO₄, 55 mL of H₃PO₄, 50 mL of H₂O (T=293–303 K, i=50A/dm², τ =180 s), and then washed with bidistilled water. The electrochemical deposition has also been accomplished in the potentiostatic mode.

Results and discussion

On the polarization curve of co-electrodeposition of iron with selenium on the surface of the Ni electrode at potential intervals of 0.0 - (-0.3) V, the reduction of selenite ions to selenium is noticeable (Fig. 1). Starting from a potential of -0.3 V to -0.4 V, selenium atoms are reduced to selenide ions. Further, after -0.4 V potential, the resulting selenide ions combine with iron

ions in the electrolyte, forming a thin layer of iron monoselenide. The co-deposition process has also been studied on the surface of a Pt electrode. Co-deposition on the Pt electrode occurs at a potential range of 0.65-(-0.6) V. Here the potential range of 0.65-(-0.38) V corresponds to the electroreduction of selenite ions. **Fig.**

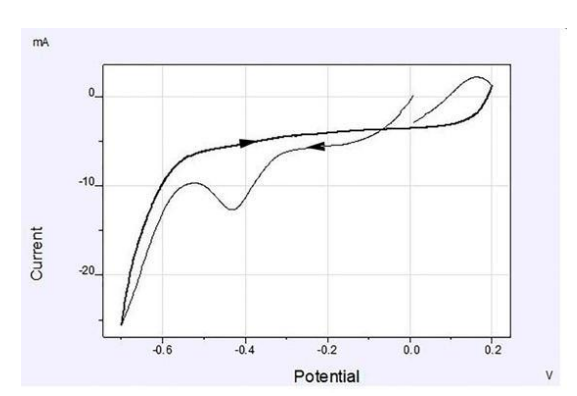
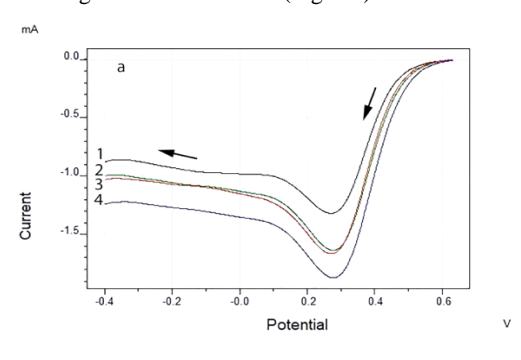


Fig. 1. Cyclic polarization curve of co-electrodeposition of Fe and Se from an aqueous electrolyte onto a Ni electrode

After selenide ions formed in the electrolyte interacted with iron ions, and were deposited in thin Fe-Se layers. The effect of the concentration of the starting ions constituting the electrolyte on the electrochemical co-deposition process of Fe and Se (Fig. 2 a, b) was studied by drawing linear polarization curves. When studying the effect of concentration, the concentration of selenite ions in the solution was initially kept constant. In contrast, the concentration of iron ions varied in the range of 0.025-0.055 M (Fig. 2 a).



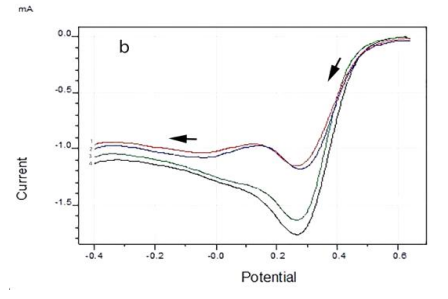
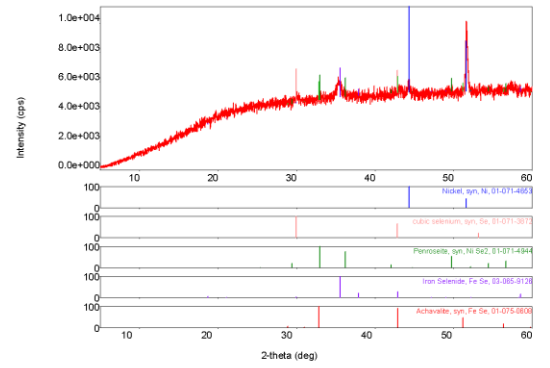


Fig. 2. Effect of concentration Fe and Se ions on the codeposition process of Fe-Se from aqueous electrolyte on the Pt electrode. Electrolyte (M): 1- 0.025; 2- 0.035; 3- 0.045; 4- 0.055 Fe(NO₃)₃ + 0.0025 M H₂SeO₃ (fig. 2a) 0.035 Fe(NO₃)₃+ 1- 0.0005; 2- 0.0025; 3- 0.005; 4- 0.0075 H₂SeO₃(fig. 2 b); E_V =0.02 V/s. T = 298 K.

Keeping the concentration of iron ions constant, the effect of the concentration of selenite ions was studied in the range of 0.0005 - 0.0075 M (Fig. 2 b). As seen from the figure, in both cases, a serious potential jump is not observed in the

electrochemical deposition process, only the current consumed in the process increases slightly (0.5 mA).





The effect of the potential scanrate on the co-deposition process was studied in the range of 0.005 – 0.08 V/s. As

seen from the figure, although the potential shift to the positive side is not observed during the study of the potential change rate, an increase in the current consumed for the electrodeposition process is noticeable. This increase is approximately 0.8 mA.

Iron monoselenide samples deposited on the Ni electrode surface by electrochemical deposition were also studied by X-ray and SEM analyses.

The results show that the intensities of the diffraction peaks of this sample are very weak. This is because the deposited iron monoselenide has an amorphous structure. To increase the crystallinity of the samples, they were thermally treated in an argon atmosphere at a temperature of 450° C for 0.5 - 1 hour (Fig. 4). The results of repeated X-ray phase analysis show that better crystals were observed in the sample thermally treated for 1 hour. The thickness of the deposited thin layers is 4-6 μ m. According to the results of EDS (element composition) analysis, the composition of the coatings corresponds to stoichiometry and consists of 42.2% Fe, 57.8% Se.

The phase composition of Fe-Se deposited on the surface of a Ni electrode by electrochemical method was studied by Raman spectroscopy.

According to literature data [19-22], three characteristic Raman spectral modes are observed for FeSe₂ samples at 179-182, 216-220, and 254-258 cm⁻¹. Here, the modes in the 179-182 and 254-258 cm⁻¹ wavenumber intervals correspond to the oscillation (libration is a type of mutual motion in which an object with a fixed orientation rotates back and forth a few times) and valence vibrations of the Se-Se bond. The noticeable modes at 216-220 cm⁻¹ are the stretching modes of Se-Se.

Conclusion

The preparation of thin films of the Fe-Se compound was confirmed using X-ray phase analysis and Raman spectroscopy.

In the Raman spectral modes in the 179-182 and 254-258 cm⁻¹ wavenumber intervals correspond to the oscillation and valence vibrations of the Se-Se bond. The noticeable modes at 216-220 cm⁻¹ are the stretching modes of Se-Se.

The band gap of Fe-Se thin films, calculated using the equation $\Delta E{=}2\kappa$ tga, is 1.26 eV.

REFERENCES

- [1] Thanikaikarasan S., Mahalingam T., Raja M., Kim T., Kim Y.D., "Characterization of electroplated FeSe thin films", *J. Mater. Sci. Mater. Electron.*, 2009, vol. 20. no. 8. pp. 727–734.
- [2] Prinz G.A., "Magnetoelectronics", *Science*, 1998, vol. 282. pp. 1660–1663.

- [3] Kwon H.J., Thanikaikarasan S., Mahalingam T., Park K.H., Sanjeeviraja C., Kim Y.D. "Characterization of electrosynthesized iron diselenide thin films", *J. Mater. Sci. Mater. Electron.*, 2008, vol. 19, pp. 1086–1091.
- [4] Mahalingam T., Thanikaikarasan S., Chandramohan R., Raja M., Sanjeeviraja C., Kim J.-H., Kim Y.D., "Effects of bath temperature in electrodeposited FeSe₂ thin films" *Mater. Chem. Phys.*, 2007, vol. 106. pp. 369–374.
- [5] Harada T., "Transport Properties of Iron Dichalcogenides FeX₂ (X=S, Se and Te)", *J. Phys. Soc. Jpn.*, 1998, vol. 67. pp. 1352–1358.
- [6] Kubaschewski O., Iron-Binary Phase Diagrams, Springer, Berlin, 1982, 113 p.
- [7] Hansen M., Andrenko K., Constitution of Binary Alloys, Geminuim Publishing Company, New York, 1985, 710 p.
- [8] Wang W., Pan X., Liu W., Zhang B., Chen H., Fang X., Yaob J., Dai S., "FeSe₂ films with controllable morphologies as efficient counter electrodes for dyesensitized solar cells", *Chem. Commun.*, 2014, vol. 50. pp. 2618-2620. https://doi.org/10.1039/C3CC49175G.
- [9] Duan Y., Tang Q., Liu J., He B., Yu L., "Transparent metal selenide alloy counter electrodes for high-efficiency bifacial dye-sensitized solar cells", *Angew. Chem., Int. Ed.* 2014, vol. 53. pp. 14569-14574. https://doi.org/10.1002/anie.201409422.
- [10] Liu J., Tang Q., He B., Yu L., "Cost-effective, transparent iron selenide nanoporous alloy counter electrode for bifacial dye-sensitized solar cell", *J. Power Sources*, 2015, vol. 282. pp. 79-86. https://doi.org/10.1016/j.jpowsour.2015.02.045
- [11] Huang S., He Q., Chen W., Qiao Q., Zai J., Qian X., "Ultrathin FeSe₂ Nanosheets: Controlled Synthesis and Application as a Heterogeneous Catalyst in Dye-Sensitized Solar Cells", *Chem.: Eur. J.*, 2015, vol. 21. pp. 4085-4091. https://doi.org/10.1002/chem.201406124.
- [12] Huang S., He Q., Chen W., Zai J., Qiao Q., Qian X., "3D hierarchical FeSe₂ microspheres: Controlled synthesis and applications in dye-sensitized solar cells", *Nano Energy*, 2015, vol. 15. pp. 205-215. https://doi.org/10.1016/j.nanoen.2015.04.027.
- [13] Wu X.J., Shen D.Z., Zhang Z.Z., Zhang J.Y., Liu K.W., Li B.H., Lu Y.M., Yao B., Zhao D.X., Li B.S., Shan C.X., Fan X.W., Liu H.J., Yang C.L., "Growth of FeSe on general substrates by metal-organic chemical vapor

- deposition and the application in magnet tunnel junction devices", *Appl. Phys. Lett.*, 2007, vol. 90. 112105.
- [14] Wu X.J., Zhang Z.Z., Zhang J.Y., Li B.H., Ju Z.G., Lu Y.M., Li B.S., Shen D.Z. "Two-carrier transport and ferromagnetism in FeSe thin films", J. Appl. Phys., 2008, vol. 103. 113501. https://doi.org/10.1063/1.2936977.
- [15] Hsu F.C., Luo J.Y., Yeh K.W., Chen T.K., Huang T.W., Wu P.M., Lee Y.C., Huang Y.L., Chu Y.Y., Yan D.C., Wu M.K. "Superconductivity in the PbO-type structure α-FeSe", *Proc. Natl. Acad. Sci. U.S.A.*, 2008, vol. 105. 14262. https://doi.org/10.1073/pnas.0807325105.
- [16] Pimentel J.L.P., Pureur P., Lopes C.S., Serbena Francisco Carlos, Foerster C.E., da Silva S.A., Jurelo A.R., Chinelatto A.L., "Mechanical properties of highly oriented FeSe_{0.5}Te_{0.5} superconductor", *Journal of Applied Physics*, 2012, vol. 111. 033908. https://doi.org/10.1063/1.3677948
- [17] Martínez-Piñeiro E., Escudero R. "Superconducting Properties of FeSe_{0.5}Te_{0.5} Under High Pressure", *J. Supercond. Nov. Magn.*, 2016, vol. 29, pp. 891–896. https://doi.org/10.1007/s10948-015-3363-4
- [18] Zeynalova A.O., Javadova S.P., Majidzade V.A., Aliyev A.Sh., "Electrochemical synthesis OF iron monoselenide thin films", *Chemical Problems*, 2021, vol. 19. no. 4. pp. 262-271 doi: 10.32737/2221-8688-2021-4-262-271
- [19] Yuan B., Hou X., Han Y., Luan W., Tu Sh., "Facile synthesis of flake-like FeSe₂ particles in open-air conditions", New J. Chem., 2012, vol. 36. pp. 2101–2105
- [20] Bastola E., Bhandari K.P., Matthews A.J., Shrestha N., Ellingson R.J., "Elemental Anion Thermal Injection Synthesis of Nanocrystalline Marcasite Iron Dichalcogenide FeSe₂ and FeTe₂", RSC Adv., 2016, no. 6. pp. 69708-69714
- [21] Yuan B., Luan W., Tu Sh., "One-step synthesis of cubic FeS₂ and flower-like FeSe₂ particles by a solvothermal reduction process", *Dalton Trans.*, 2012, vol. 41. pp. 772-776
- [22] Wei X., Tang C., An Q., Yan M., Wang X., Hu P., Cai X., Mai L., "FeSe2 clusters with excellent cyclability and rate capability for sodium-ion batteries", Nano Research, 2017, vol. 10. pp. 3202–3211

Selection of Starting Reagents, Reactor Material and Synthesis Method for Semi-Industrial Production of Promising Cathode Materials for Lithium-Ion Batteries

T. Paikidze*, Sh. Japaridze, G. Tatishvili, E. Kachibaia

R. Agladze Institute of Inorganic Chemistry and Electrochemistry Iv. Javakhishvili Tbilisi State University, 11, Mindeli str., Tbilisi, 0186, Georgia,

*E-mail: tamarpaikidze@gmail.com

Abstract. Type large-scale production of cathode materials based on lithium-manganese spinels for lithium-ion batteries by industrial and semi-industrial methods is associated with a noticeable decrease in their characteristics. To solve the problem, three methods for producing cathode material, various starting reagents, and three reactor materials were studied. The optimal synthesis method, temperature and duration, as well as starting reagents and reactor material were selected. X-ray phase and X-ray structural analysis of the obtained samples was carried out and their cyclic characteristics were studied using a half-cell of the 2023-coin type.

თ. პაიკიძე, შ. ჯაფარიძე, გ. ტატიშვილი, ე. ქაჩიბაია – ლითიუმ-იონური აკუმულატორებისთვის პერსპექტიული კათოდური მასალების ნახევრად ინდუსტრიული წარმოებისთვის საწყისი რეაგენტების, რეაქტორის მასალის და სინთეზის მეთოდის შერჩევა

რეზიუმე. სამრეწველო და ნახევრად სამრეწველო გზით ლითიუმ-იონური აკუმულატორებისათვის ლითიუმ-მანგანუმიანი შპინელების საფუძველზე საკატოდე მასალების მსხვილმასშტაბური მიღება დაკავშირებულია მათი მახასიათებლების აშკარა შემცირებასთან. პრობლემის აღმოსაფხვრელად შესწავლილია საკატოდე მასალის მიღების სამი მეთოდი, სხვადასხვა საწყისი რეაგენტი და რეაქტორის სამი მასალა. შერჩეულია სინთეზის ოპტიმალური მეთოდი, ტემპერატურა და ხანგრძლივობა, აგრეთვე, საწყისი რეაგენტები და რეაქტორის მასალა. ჩატარებულია მიღებული ნიმუშების რენტგენოფაზური და რენტგენოსტრუქტურული ანალიზი, შესწავლილია აგრეთვე მათი ციკლური მახასიათებლები 2023-ტიპის მონეტური ნახევარელემენტის მაკეტის გამოყენებით.

Keywords: cathode material, lithium-manganese spinels, lithium-ion batterie, semi-industrial method.

Introduction

Currently, among the many types of lithium batteries, Lithium-ion rechargeable batteries (LiA) have received much attention, which are widely used in military and space technology, consumer electronics (mobile phones, personal computers, laptops, portable medical equipment), electric vehicles, etc. The production technology of lithium-ion batteries is constantly being improved, technical characteristics are improved and production costs are reduced. The performance of these batteries, among other factors, strongly depends on the composition of the cathode materials, methods and conditions for their production. Currently, much attention is paid to promising lithiummanganese spinel - LiMn₂O₄, which is considered as a promising cathode material in the production of lithium-ion batteries. However, it is characterized by a sharp drop in capacity during cycling, which is mainly due to the reactions of spinel manganese with HF in the electrolyte and the oxidation of organic compounds during repeated cycling. Partial replacement of manganese with ions of various metals can be used as one of the ways to solve this problem. From this point of view, LiMn₂O₄ (lithium-manganese spinels) doped (substituted) with other transition metals - $LiMe_xMn_{2-x}O_4$ (where Me=Ni, Co, Cr, Al, and x=0÷0.5) are important.

These compounds are mainly characterized by a high theoretical discharge capacity and relative structural stability during cycling. It has been established that by replacing Mn ions with transition metal ions, it is possible to avoid the presence of impurities and stabilize the deformed structure of spinels.

Therefore, they have significantly better electrochemical properties than undoped ones. When choosing cathode materials, synthesis methods and firing temperature are of great importance, since it affects the final formation of the structure and, consequently, the properties of spinels, as well as the cost of the resulting materials.

Methodological part

The goal of this work is to develop nanosized, phase-pure, inexpensive and less toxic promising cathode materials for lithium-ion batteries. We synthesized the samples using different starting reagents, different methods and at different temperatures by doping lithium-manganese spinel with an element or pair of elements of transition valence.

The amount of cathode materials for lithium-ion batteries obtained in a corundum crucible is determined in grams. An analysis of the scientific literature also shows that the majority of the work results in cathode materials being produced in gram quantities. There is practically no work on

obtaining 1 kg or more of cathode materials and studying their characteristics. Technologists are aware of the problem of the transition to large-scale production, in particular, with an increase in the mass of the receiver material, their characteristics noticeably decrease. Therefore, the question arises about the need to improve methods for obtaining the cathode materials being developed. This means that it is necessary to choose one of various synthesis methods that provide large quantities (in an industrial or semi-industrial manner) of phase-pure, nano-sized, promising cathode materials with high characteristics. In addition, it is also necessary to select the material for the synthesis reactor. First, the synthesis of spinel-LiMn₂O₄ was carried out. As a result of X-ray diffraction and X-ray phase analysis, the starting reagents, synthesis method and reactor were established. LiMn₂O₄ samples were synthesized by three methods. In the first step, LiMn₂O₄ was synthesized using the above starting reagents, various reactors and methods. Xray phase and X-ray diffraction analysis of these samples showed the acceptability of using Li₂CO₃ as a lithiumcontaining starting reagent. In addition, it is not possible to use a titanium crucible because in all three cases it was coated with a white substance (probably an oxide layer) during the synthesis, so we did not use it after the first synthesis. Stainless steel was chosen as the reactor material. According to the X-ray phase and X-ray structural analysis of the synthesized samples using the following method - the double stirring method: the initial reagents were Li₂CO₃, Mn₂O₃, Ni₂O₃, Cr₂O₃ and Co₂O₃ (depending on the composition of the samples) were taken in the amount necessary to obtain the specified samples (for all three methods). This mixture was mixed well (ground) in a porcelain mortar, transferred to crucibles made of corundum, titanium and stainless steel and placed in a cold electric furnace. Upon reaching 830°C in the oven, the crucibles were taken out, cooled, mixed in a porcelain mortar, transferred back to the crucibles and again placed in the oven at 830°C for 1 hour. Then the above-mentioned cooling-stirring process was repeated again and put back in the oven at 830°C for 1 hour. Then they took it out and cooled it in air. After such processing, nano-sized phase-pure cubic spinel cathode materials are obtained.

The samples synthesized using the selected starting reagents, method and reactor were submitted for testing to determine their suitability as cathode materials and thus three samples were selected: LiNi_{0.5}Mn_{1.5}O₄, LiCo_{0.2}Ni_{0.3}Mn_{1.5}O₄ and LiCr_{0.3}Ni_{0.2}Mn_{1.5}O₄. Testing was carried out in a 2032 coin type half cell using lithium metal as anode and electrolyte - 1M LiPF₆ in EC/DEC/EMC (1/1/1).

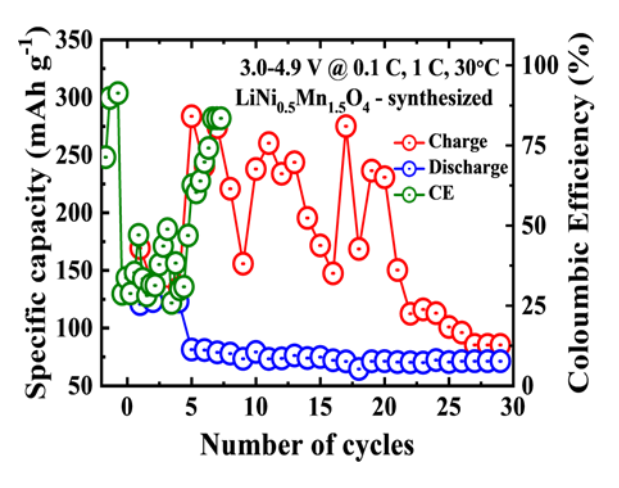


Fig. 1. Cyclic characteristics of synthesized LiNi_{0.5}Mn_{1.5}O₄ (LNMO).

As can be seen from the figure, the synthesized sample has a good capacity of 110÷120 mAh/g (theoretical capacity of commercial LNMO 130÷147 mAh/g), but also has accelerated power delivery and structural instability, which leads to degradation of the cathode material. There are many publications in the literature devoted to the mechanisms of LNMO degradation. The degradation of high voltage batteries is mainly due to electrolyte breakdown caused by high potential. Reduction and oxidation of the solvent are possible on the anodic and cathodic sides of the potential. Additional loss of capacity is associated with dissolution of the transition metal.

In the case of $LiCo_{0.2}Ni_{0.3}Mn_{1.5}O_4$, the initial capacity of the sample is lower (85 mAh/g) than that of the $LiNi_{0.5}Mn_{1.5}O_4$ we synthesized, although it is characterized by stable characteristics without degradation during cycling. (Fig. 2).

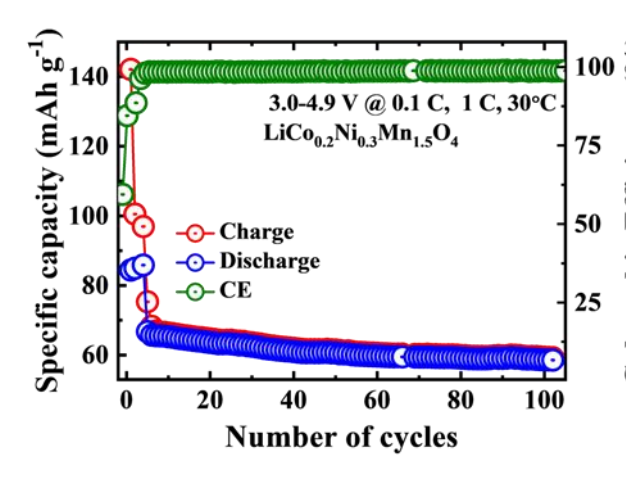


Fig 2. Characteristics of cyclization of synthesized $LiCo_{0.2}Ni_{0.3}Mn_{1.5}O_4$

The next sample we synthesized was LiCr $_{0.3}$ Ni $_{0.2}$ Mn $_{1.5}$ O₄. This active material has a higher initial capacity (95 mAh/g) than the cathode material LiCo $_{0.2}$ Ni $_{0.3}$ Mn $_{1.5}$ O₄ (Fig. 3). In

addition, no structural degradation is observed during testing and it is structurally stable. Capacity retention after 100 cycles is 97%.

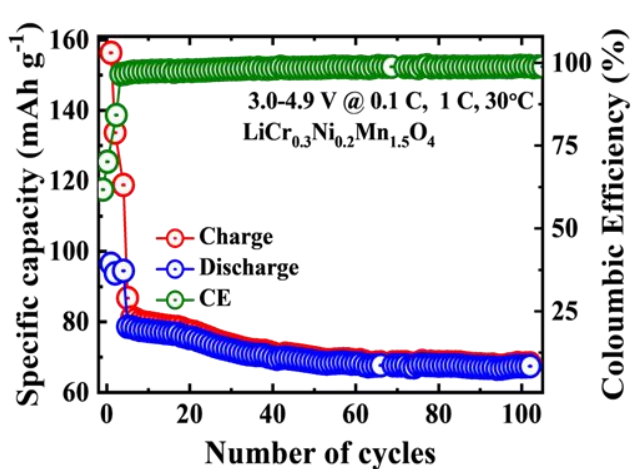


Fig. 3. Cyclic characteristics of the synthesized LiCr_{0.3}Ni_{0.2}Mn_{1.5}O₄

Having analyzed the test results, we can conclude that doping the starting material - LiNi_{0.5}Mn_{1.5}O₄ - contributes to the stability of the structure during cycling. Replacing some of the nickel atoms in LNMO -cathode materials with Co or Cr reduces degradation during cycling of cathode materials, which increases the possibility of its use in coin-type elements.

Table 1. Test results of the synthesized samples

Sample	Cell vo	ltage, V	Specific capacitan cemAh/g	Fast burst time	Load curr relation to C, A·ч			operating temperat ure
	max.	min			Constant	Pulse	Optima 1	range 🕵
LiNio3Mru3O4	4.9	3.0	77	24 min,20 sec	0.1C	1C	0.1 C	25-30
LiCro3Nio2Mro3O4	4.9	3.0	81	28 min,31 sec	0.1C	1 C	0.1 C	25-30
LiCon/Nin/Mrn.3O4	4.9	3.0	85	26 min,12sec	0.1C	1 C	0.1 C	25-30

As can be seen from the figures and the table of test results, the doped samples we synthesized, despite the low initial capacity, can be used in a coin-type element, since they maintain structural stability during cycling. The test results indicate that further work is needed to improve the electrochemical characteristics of the developed cathode materials to increase the initial capacity and eliminate the sharp drop in capacity during cycling. In addition, it is necessary to clarify the methodology for producing cathode materials using a semi-industrial method and accumulate them in case of demand for further sale.

References

Kachibaia, E.I., Paikidze, T.V., Imnadze, R.A., Japaridze, Sh.S. "Development of Promising Cathode Materials Based on Modified Spinels for Li-ion Batteries". Deuton-X Ltd./EuroChemBull. 2020, vol. 9, N12, pp. 401-402

Magnetic heat capacity anomalies of lanthanide-iron complex oxides

V. Varazashvili*, M. Tsarakhov, T. Mirianashvili, M. Khundadze, T. Machaladze

R. Agladze .Institute of Inorganic Chemistry and Electrochemistry, Iv. Javakhishvili Tbilisi State University (TSU), 11, Mindeli str., Tbilisi, 0186, Georgia,

*E-mail: v_varazi@yahoo.com

Abstract. Lanthanide iron mixed oxides because of their specific magnetic properties are widely applied in many fields of technology. In the work, the effect of magnetic anomalies on the thermal characteristics of garnet-type rare earth ferrites with the general formula $R_3Fe_5O_{12}$ (R is lanthanide ions from Sm to Lu) is reported. The study is based on the calorimetric investigation of heat capacity in the range of 20-1300K. The following heat capacity anomalies were revealed and characterized: 1. the "low-temperature" magnetic anomaly ($T_v<100K$), due to the magnetic disordering of lanthanide ions. 2. The lambda-type anomaly associated with ferromagnetic-paramagnetic phase transitions. 3. Schottky-type anomaly caused by the redistribution of the electrons over lanthanide ions Stark levels. The thermal characteristics associated with anomalies are reported: the Curie points, peaks of low-temperature anomalies; and the excess thermodynamic properties - heat capacity, entropy, and enthalpy of magnetic origin.

ვ. ვარაზაშვილი, მ. ცარახოვი, თ. მირიანაშვილი, მ. ხუნდაძე, თ. მაჩალაძე – ლანთანიდ-რკინის კომპლექსური ოქსიდების მაგნიტური სითბოტევადობის ანომალიები

რეზიუმე. ლანთანოიდებისა და რკინის რთული ოქსიდები, მათი განსაკუთრებული მაგნიტური თვისებების გამო, ფართოდ გამოიყენება თანამედროვე ტექნიკის სხვადასხვა სფეროში. სამუშაოში წარმოდგენილია გრანატის სტრუქტურის მქონე იშვიათ მიწა მეტალების ფერიტების - $R_3Fe_5O_{12}$ (R არის ლანთანოიბის იონი Sm-დან Sm-დანტრული კვლევის შედეგების ანალიზს (Sm-1300K). გამოვლენილია თბოტევადობის შემდეგი ანომალიები: Sm-დაბალტემპერატურული ანომალია" ((Sm-100K), რომელიც უკავშირდება ლანთანიოდის ქვეგისოსის განმაგნიტების პროცესს. Sm-დატემპერატური გარდაქმნის ლამდა-ტიპის ანომალია. Sm-დადგენილია ელექტრონების გადანაწილებით ლანთანოიდების იონების შტარკის ქვედონეებზე. დადგენილია ამ ანომალიების ტემპერატურული ზღვრები, კიურის წერტილები, აგრეთვე ანომალიებით გამოწვეული Sm-დაზის ტემპერატურული და მაგნიტური თავისებურებების გათვალისწინებით.

Keywords: Rare-earth garnets, calorimetry, phase transitions, thermodynamic properties

Introduction

Lanthanide iron mixed oxides form a large family of garnet-type compositions (RIG). Because of the specific magnetic properties of this group of insulators, they are widely applied in many fields of technology [1-3]. The new garnet materials with advanced magnetic properties can be elaborated and verified by compositional modification and special thermal treatment. This stipulates the study of the magnetic behavior of garners in the large temperature and compositional range, and the analysis of the impacts of these factors on energetic parameters. In the present work, we report the effect of magnetic anomalies on the thermal characteristics of the main group of garnet-type rare earth ferrites with the general formula R₃Fe₅O₁₂ (where R is lanthanide ions from Sm to Lu).

Neel's theory explains the specific magnetic properties of garnet-type ferrites based on their three-sublattice crystal structure [1]. The antiferromagnetic interactions between paramagnetic ions distributed over sublattices of three types (octahedral 2Fe⁺³-a, tetrahedral 3Fe⁺³-d, and dodecahedron $3R^{+3}$ - c) result in the magnetic moments as M=3Mc-[3Md-2Ma]. The disordering process of the cation magnetic interactions of a-and d iron sublattices, when heated, affects energetic parameters and creates excess cooperative magnetic contribution to the heat capacity $-C_F$. The other cooperative magnetic heat capacity component (C_l) may appear in some garnets at low temperatures due to destroying magnetic exchange a-c, b-c interactions with the participation of lanthanide ions [2]. Besides these two anomalies of cooperative nature, considering the electronic structure of lanthanides, we should expect the non-cooperative heat capacity anomaly (Csh) due to the redistribution of lanthanide f-electrons on exited Stark levels. So, we can present the heat capacity function of RIG as a complex quantity where besides the main regular lattice Creg part, there is an excess Cex component which represents the summary effect of cooperative and non-cooperative magnetic anomalies.

Separating and evaluating the excess magnetic heat capacity increments for lanthanide garnets is the main purpose of the presented work. The following data are evaluated and reported: the temperature limits of anomalies, the temperature of peaks (Curie point- T_c , the peaks of Low-temperature anomaly $-T_l$); The excess thermodynamic properties - heat capacity (C_{ex}), entropy (S_{ex}), enthalpy (H_{ex}) associated with anomalies of ferromagnetic origin.

Results and Discussion

The study is based on the analysis of the heat capacity versus temperature functions $C_p(T)$ in the range of 20-1300K, obtained by the following calorimetric methods: low-temperature adiabatic calorimetry for the temperature interval 20-320K, accuracy \pm 0.25%; DSC - 300-900K, \pm 1.5%; and high-temperature drop calorimeter 300-1200K, \pm 1.5%.

The one-phased garnet samples are synthesized by ceramic technology, which includes two stages of high-temperature sintering (at 1650K) of mixed starting oxides. Crystal parameters are in agreement with [1-3].

The combined heat capacity Cp(T) function for the temperature interval (20-1300K) is typical for all group members. Just one obvious λ -type anomaly area is detected on all Cp(T) curves which corresponds to the ferromagnetic-paramagnetic transformation with the peak at Curie point. Two other expected effects do not manifest the clear excess anomaly and therefore, special methods should be employed for their revealing.

The morphology of heat capacity functions of RIG, taking into account all expected excess components, can be presented as:

$$C_p(RIG) = C_{reg} + C_F + C_R + C_{Sh} \tag{1}$$

where C_{reg} is the main vibrational part of a crystal lattice, C_F – ferromagnetic contribution, C_R - the "low-temperature" anomaly caused by the magnetic disordering process of lanthanoid ions, C_{Sh} – Schottky anomaly due to redistributions of lanthanide f-electrons on Stark levels.

To determine the energetic impacts of all contributions, the main task is to separate them from the regular part and each other. The complex nature of the crystal and magnetic structure of garnets causes the anomaly regions, the temperature intervals of which overlap. This creates difficulties in the estimation of individual contributions and necessitates the use of non-standard methods.

FERROMAGNETIC TRANSITION

In the presented work, the main attention is directed to the energetic characterization of the ferromagnetic transformation of garnets. For this purpose, we applied the method previously offered by us in [4]. In Figure 1 the heat capacity curve for RIG, including the region of ferromagnetic transition (curve 1), is illustrated. The separated ferromagnetic component C_m is represented by curve 2. All other garnets have the same graphical form of $C_m(T)$. In Figure 2 the C_m and (C_m/T) are presented as the functions of reduced temperature (T/T_c) , and they were used for calculating of magnetic enthalpy (H_m) and magnetic entropy (S_m) of garnets, as:

$$H_m = \int C_m dT$$
; and $S_m = \int (C_m/T) dT$ (2)

We can see that Curie temperatures and other characteristics such as the summary entropy (S_{tr}) and enthalpy (H_{tr}) of ferromagnetic transition vary very slightly in the garnet series (Table 1).

The temperature function of the heat capacity being of λ -type is characteristic of ferromagnetic-paramagnetic transitions of the second kind. The magnetic disordering process covers a large area from ~250K to ~650K. The region up to T_c coincides with the process of a gradual decrease in the saturation magnetization of garnets [1-3]. It corresponds to the destruction of long-range exchange interactions between iron ions distributed in a and d sublattices, that form the ferrimagnetic behavior of garnets in a given temperature range. At Curie temperature T_c , the curve $C_m(T)$ has a sharp peak followed by abrupt drops and an asymptotic return to a normal paramagnetic course. The "tail" extends ~ 100K above T_c and corresponds to the influence of diminishing short-range exchange interactions between the nearest magnetic cations.

Analyzing the λ -type temperature function of heat capacity we evaluate the enthalpy and entropy associated with long – and short-magnetic interactions between iron ions distributed on octahedral and tetrahedral sites in the garnet lattice (Table 1). The enthalpy of short interactions accounts for about 20% of the total transformation enthalpy and therefore it should be taken into consideration when modeling ferromagnetic transitions.

The negligible difference in the energetic characteristics of ferromagnetic transformation for all members of the group is caused by the fact that the ferromagnetic behavior in this temperature region (above 250K) is formed by iron ions distributed in the octahedral and tetrahedral sublattices, which have identical structures for all garnets. The impact of lanthanide ions is manifested only in the low-temperature region T<150K, where influences of a and d iron sublattices are minimal. The difference in the corresponding thermal parameters of garnets at low temperatures is due to the variety of magnetic moments of lanthanide sublattices, and their exchange interactions are very weak and cannot affect the energetic parameters above ~ 150 K.

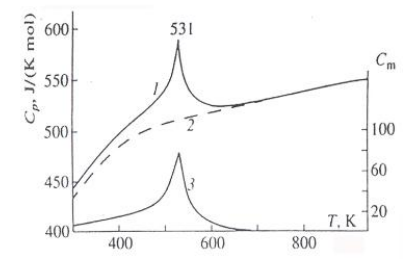


Fig. 1. Heat Capacity of Lu₃Fe₅O₁₂

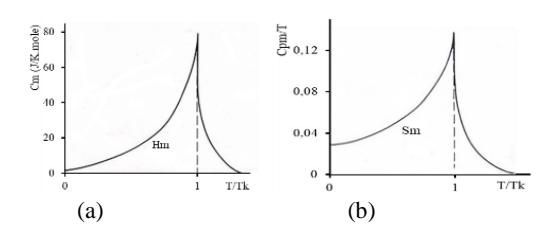


Fig. 2. The Curves for estimation enthalpy (a) and entropy (b) of the ferromagnetic disordering of rare-earth iron garnets

THE ANOMALIES AT LOW TEMPERATURES

The experimental heat capacity curve at low temperatures has no obvious anomaly. At the same time, the theoretical estimates presented in [2] indicate the possibility of revealing excess heat capacity components associated with the

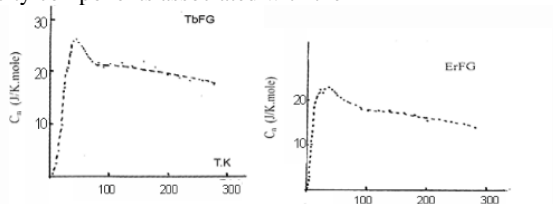


Fig. 3. The low-temperature anomalyof $Tb_3Fe_5O_{12}$ and $Er_3Fe_5O_{12}$

destruction of magneto-exchange interactions of rare-earth ions (a-c and d-c). Experimental confirmation of this fact for GdIG and DyIG was given in our previous papers [4-6]. It should be noted that this kind of anomaly is expected only for those members of the group of garnets that have anomalous magnetization functions with the compensation point, such as Gd, Dy, Tb, Ho, and Er IG. The excess heat capacity contribution of these ferrites was separated using LuIG as the isostructural baseline, since in the low-temperature region no magnetic anomaly is expected for compounds with Lu diamagnetic ions:

$$C(l.an) = Cp(RIG) - Cp(LuIR)$$
(3)

The separated anomaly area can be associated exactly with the "low temperature" effect for only GdIG because no Schottky anomaly is expected for Gd(III) ions in the S-type ground state. For the other ferrites with normal magnetization—temperature functions (DY, Tb, Ho, Er) IG [1] at the same temperatures, the Schottky anomaly overlaps the cooperative "low temperature" increment. So, for them, the excess component represents the joined effect $C_{ex} = C_l + C_{sh}$, which is demonstrated in Figure 4. For Sm and Eu ferrites with normal Weis-type magnetization functions, and therefore having no low-temperature anomaly, the excess heat capacity C_{ex} corresponds to Schottky anomaly (Figure 4).

It is shown (Table 1), that in the garnet series, the low-temperature point and $\,$ Curie temperature tend to linear decrease depending on decreasing the lattice parameter - a. $H_{\rm m}$

of SmIG and EuIG slightly exceed the values of these parameters for the group of garnets from Gd to Lu.

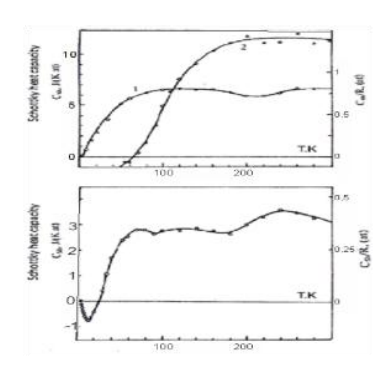


Fig. 4. Schottky heat capacity anomalies for SmIG(1), EuIG(2), and Dy(3) garnets

Table 1 (annex) presents all energetic parameters of the ferromagnetic-paramagnetic transformations of RIG, exactly: Curie point $-T_c$; enthalpy- H_m and entropy $-S_m$ of ferromagnetic transition; enthalpy- H_l , H_{sh} , and entropy $-S_l$, S_{sh} of long and short exchange interactions; excess heat capacity at Cutie temperature $-\Delta C(T_c)$.

Conclusion

The thermodynamic properties of rare earth iron garnets are affected by the anomalies of cooperative and noncooperative magnetic origin. By calorimetric study in the temperature range 20-1300K of the series of garnets $R_3Fe_5O_{12}$ (where R is lanthanide ions from Sm to Lu), the following anomalous regions on heat capacity Cp(T) function were detected: the "low-temperature" magnetic anomaly (T₁<100K), due to the magnetic disordering process of lanthanide sublattices; the lambda-type anomaly associated with ferromagneticparamagnetic phase transitions; Schottky-type anomaly caused by the redistribution of the f-electrons over lanthanide ions Stark levels. The thermal characteristics associated with anomalies are reported: the Curie points, peaks of lowtemperature anomalies; and the excess thermodynamic properties - heat capacity, entropy, and enthalpy of magnetic origin. The results are considered in connection with the magnetic and crystal structure of garnets. In the garnet series, the low-temperature point and Curie temperature tend to decrease depending on decreasing the lattice parameter.

	SmIG	EuIG	GdIG	TbIG	DyIG	HoIG	ErIG	TmIG	LuIG
Crys. a, nm	1.2530	1.2490	1.2450	1.2420	1.2390	1.2370	1.2330	1.2310	1.2270
Тс,К	565	563	560	556	553	547	543	539	531.5
T(l.t).K	-	-	45-50	40-45	45	40	35	-	-
H _m ,J/mol	8000	7700	7350	7400	7300	7500	7000	7200	7100
H _{short} ,J/mol	1420	1330	1150	1160	1400	1160	1400	1500	1550
S _m ,J/K.mol	16.5	16.5	15,1	15.2	15.2	15,5	14.5	15.2	14/8
S _{short} J/K.mol	2.3	2.1	1.9	1,9	2.3	2.0	2.3	2.5	2.5
ΔC(T _c J/K.mol	85.0	76.0	82.0	82.0	78.0	84.0	78.0	78.0	30.0

REFERENCES

- Krupicka, S."Physik der Ferrite und der Verwandten Magnetischen Oxides", Academia, Prague, 1973.pp, 5-250
- [2] Belov, K.P. Rare-earth magnetics and their application, "Nauka", Moskow, 1980. pp 3-50
- [3] Parada, S.C., Rakshit, S.K., Ziley Singh, J. Solid State Chemistry, 181 2008, pp. 101-121
- [4] Varazashvili, V.S., Tsarakhov, M.S., Mirianashvili, T.B., PavleniSvili, T.A. J. of Inorganic Chemistry (Russian), 1997, vol. 42, no. 4, pp. 597-599
- [5] Lahoubi, M., Younsi, W., Soltani, M.L., Voiron, J., Schmitt, D. J. of Physics: Conference Series, 2009, p.042108
- [6] Boutaba, Assia, Lahoubi, Mahieddine, Varazashvili, Vera Shengli Pu, J. Magnetism and Magnetic Materials, 2018

A Comparative Study of Synthesis from Solution-Melts with Thermal Synthesis for Obtention of Condensed Phosphates

M. Avaliani*, V. Chagelishvili, E. Shapakidze, G. Todradze, N. Barnovi, K. Chikovani

- ¹ R. Agladze Institute of Inorganic Chemistry and Electrochemistry I. Javakhishvili Tbilisi State University,
- 11, Mindeli str., Tbilisi, 0186, Georgia
- ²A. Tvalchrelidze Caucasian Institute of Mineral Resources, I. Javakhishvili Tbilisi State University, 11, Mindeli str., Tbilisi, 0186, Georgia
 - *E-mail: avaliani21@hotmail.com; marine.avaliani@tsu.ge

Abstract. By crystallization from solution-melts of polyphosphoric acids at the temperature range 120-600°C we have synthesized for the first time more than 85 new double condensed phosphates of monovalent and trivalent metals. All compounds were identified by roentgen phase analysis and investigated by thermo-gravimetric analysis, X-ray structural techniques, IR spectroscopy. The physicochemical properties of various di- and triphosphates, cyclotetraphosphates, cyclooctaphosphates, cyclododecaphosphates, long-chain polyphosphates and ultraphosphates are evaluated. A detailed comparative study of the thermal synthesis of previously unknown condensed phosphates versus crystallization from solution-melts of polyphosphoric acids was carried out to obtain new inorganic materials with predetermined valuable properties. During interaction in the polycomponent system, the formation of the acidic triphosphates (forms I and II) and their crystallization areas were determined. It has been established and confirmed by experts that acidic triphosphate form I is the best ion exchanger and indeed could be used in the future.

მ. ავალიანი, ვ. ჩაგელიშვილი, ე. შაფაქიძე, გ. თოდრაძე, ნ. ბარნოვი, ქ. ჩიქოვანი – კონდენსირებული ფოსფატების მისაღებად ბსნარიდან ნალექების სინთეზის შედარებითი კვლევა თერმული სინთეზით

რეზიუმე. პოლიფოსფორმჟავათა ხსნარ-ნალღობებიდან 120-600°C ტემპერატურულ ინტერვალში კრისტალიზაციით პირველად არის სინთეზირებული 85-ზე მეტი ერთ- და სამვალენტიანი ლითონების ორმაგი კონდენსირებული ფოსფატი. ყველა ნაერთი იდენტიფიცირებულია რებნტგენოფაზური ანალიზით, შესწავლილია ინფრაწითელი სპექტროსკოპიის მეთოდით და თერმოგრავიმეტრული ანალიზით, ხოლო ზოგიერთი-სტრუქტურული ანალიზის მეშვეობით. შეფასებულია ჩვენს მიერ მიღებული დი- და ტრიფოსფატების, ციკლოტეტრაფოსფატების, ციკლოოქტაფოსფატების, ციკლოდოდეკაფოსფატების, გრმელჯაჭვიანი პოლიფოსფატების და ულტრაფოსფატების ფიზიკო-ქიმიური თვისებები. ჩატარდა მანამდე უცნობი კონდენსირებული ფოსფატების თერმული სინთეზის და ხსნარ-ნალღობებიდან ანალოგიური ნაერთების სინთეზის დეტალური შედარებითი კვლევა წინასწარ განსაზღვრული ღირებული თვისებების მქონე ახალი არაორგანული მასალების მისაღებად. პოლიკომპონენტურ სისტემაში ურთიერთქმედებისას მიღებულია მჟავა ტრიფოსფატები (I და II ფორმის სახით) და დადგენილია მათი საკრისტალიზაციო არეები. ექსპერტებმის მიერ დაადასტურებულია, რომ მჟავა ტრიფოსფატის ფორმა I საუკეთესო იონ-მიმომცვლელია და შესაძლოა მისი ამ მიზნით გამოყენება სამომავლოდ.

Keywords: Condensed compound, Cyclophosphate, Inorganic polymer, Phosphoric acid, Synthesis, Ultraphosphate.

Introduction

Since the 21st century, the domain of condensed compounds has become a trend in polymer chemistry due to their wide application in modern technologies. The field of phosphate chemistry, in particular that of condensed compounds of rare earth metals, has attracted the interest of scientists from all over the world. The German school of chemistry has been very forceful and dynamic in the domain of condensed phosphates. Starting from the pioneer works of French and German scientists a lot of number of condensed compounds - inorganic polymers were synthesized, and a great number of innovative researches in the XX Century were really valuable and appreciated [1-9]. Midst a diversity of methods of condensation of phosphoric anions, one of them leads to the predetermination of oligomeric, cyclic, or polymeric structures of condensed phosphates [1-2, 6, 10-15].

The major cause of the development of the mentioned domain was the advance of innovative methods of analysis and the important application of phosphate materials in several technical domains, including nanotechnologies. The chemistry of inorganic compounds of phosphorous has developed intensively also for the purpose that condensed compounds of phosphorus are greatest relevant, useful, and convenient for promoting the development

of the chemistry of inorganic polymers, materials used in engineering, construction, and other areas. They are the best fertilizers, detergents, and raw complexes for the creation of phosphate glasses, thermo-resistant agents, effective applying nourishments, cleaners, cement substances, ion-exchange ingredients, and also catalytic agents [16-27]. The thermal, vibrational, and luminescent properties of condensed compounds determine their use in quantum electronics, nanotechnologies, etc.

Experimental

The presented work is a review article and concern condensed forms of phosphorus and its various inorganic compounds, namely primarily synthesized by us numerous condensed composites. Our method for the production of condensed compounds is based on high-temperature synthesis (100-600 $^{\circ}$ C) in multi-component systems $M^{1}\!\!_{2}O\!\!_{3}\!\!_{2}P_{2}$ Os-H2O (where $M^{I}\!\!_{1}$ monovalent alkali metals and Ag and M^{III} – Ga, In, Sc, etc.) for the purpose to receive new condensed compounds - inorganic polymers. The technology is founded on the creation of new condensed forms - double inorganic oligomers, and/or cyclic compounds, and long-chain polymeric composites via condensation of polyphosphosphoric acids [12, 15, 18, 19-20].

The subject that is solved through this work is the synthesis of a new, yet unknown double-condensed oligo-, poly-, and cyclophosphates, analyzing their structural composition, and the examination of general properties. Over the last few decades, numerous researchers have been paying thoughtful attention to the synthesis and investigation of condensed phosphates – so-called inorganic polymers. This was possible afterward the notable advance of different fields of new technologies, as well as expanding the research area of nanotechnology and fundamental general research [21, 24-26, 28-30].

By examining the crystallization conditions and general properties of polymeric compounds, the targeted synthesis of new inorganic polymers with predictable properties will be possible, as well as the choice and management of the optimal regimes for the formation of monocrystals and in some cases — nanocomposites.

Another way for obtainment condensed oligomers and/or polymeric composites is thermal synthesis (in other words the thermal decomposition) of already synthesized double acidic phosphates. To determine the composition of synthesized double condensed compounds, a chemical analysis of these compounds has been conducted.

The abovementioned analysis has been compared to the existing methods of research, and the optimal methods for determining phosphorus, mono- and trivalent metals in condensed compounds.

In our work over the last few decades, we have reported on studies in the open systems $M_2^IOM_2^IO_2M_2^{III}O_3M_2^{III}O_3.P_2O_5$ $P_2O_5.H_2OH_2O$ between temperature range 130^0 - 550° C°C , where $M_2^IOM_2^IO$ are oxides of alkali metals and also Silver's oxide, and $M_2^{III}O_3M_2^{III}O_3$ — oxides of gallium, indium and scandium [12,15,18-20,24-25]. Various experiments revealed that by crystallization from melts of polyphosphoric acids were obtained the following double condensed compounds — namely a series of an formerly new class of inorganic polymers: double condensed di- and triphosphates, cyclotetraphosphates, cyclooctaphosphates, cyclododecaphosphates, at the molar ratio

 $_{\rm n=}M_2^IO/M_2^IO/$ $M_2^{III}O_3M_2^{III}O_{3}$ =2,5:1,0; 5:1,0; 7,5:1,0; 10:1,0 and 3,5:1,5; 5:1,5; 6:1,5; 7,5:1,5; 8,5:1,5; 12:1,5. Attained condensed phosphates were detailed examined by thermogravimetric analysis TGA, X-Ray diffraction analysis, some compounds were examined by paper chromatography and other methods [30].

Results and discussion

The Preparation of double oligo phosphates of some alcali metals with trivalent metals and determination of optimal crystallization conditions.

Analyzing the series of experiments carried out [12.15, 18, 19-20. 24-25, 30] and comparing them with literary data [1-2, 6-10, 31-38] demonstrated that there is a certain isomorphism between compounds of Ga and In. Targeted condensed cyclic phosphates were obtained for other alkali metals and also for Ag. By analyzing systems that contain gallium, indium, aluminum, or scandium as a trivalent metal, the following regularity is observed: the diffractograms show a small and monotonous shift of the lines, sometimes variation of intensities and splitting of some reflexes, indicating a slight distortion of the network, although the structural type remains unchanged. In general, in the structure of highly condensed double compounds of various monovalent and multivalent metals, the monovalent metal has less influence on the structural characteristics of the composite, than the trivalent metal. In the case of Ga and In, there is complete isomorphism between the respective classes of compounds. In the case of aluminum and scandium, we can speak either of isomorphism or of structural analogy, with a certain variation of the lattice [2, 39-41].

Various classes of newly synthesized double condensed phosphates are presented in the Table 1. Long-chain polyphosphates of gallium, indium and scandium $(M^{III}PO_3)$ were synthesized also, at the molar ration of initial components $n = P/M^I/M^{III}P/M^I/M^{III} = 15/2,5/1$

initial components n= P/M / M = 15/2,5/1 and temperature of synthesis approximately 250-550 °C [39-44].

Table 1. Newly synthesized condensed phosphates [44].

M ^I M ^{III} (H ₂ P ₂ O ₇) ₂ Double acidic diphosphates	M ^I M ^{III} P ₂ O Double diphosphate s	M ^I M ^{III} HP ₃ O ₁₀ Double acidic triphosphates	M ₂ ^I M ^{III} P ₃ O ₁₀ Double triphosphates	M ^I M ^{III} (PO ₃) ₄ Long chain polyphosphate (a), ultraphosphate (b), cycloocta-phosphate (c), cyclotetra-phosphate (e), cyclododecaphosphate (d)
$LiSc(H_2P_2O_7)_2$	$LiScP_2O_7$	$LiScHP_3O_{10}$	$Li_2ScP_3O_{10}$	$\{LiSc(PO_3)_4\}_{x(a)}$
$NaSc(H_2P_2O_7)_2$	$NaScP_2O_7$	$NaScHP_3O_{10}$	$Na_2ScP_3O_{10}$	Na ₃ ScP ₈ O _{23 (b)}
$KSc(H_2P_2O_7)_2$	$KScP_2O_7$	$KScHP_3O_{10}$	$K_2ScP_3O_{10}$	$K_2 S c_2 P_8 O_{24 (c)}$
$RbSc(H_2P_2O_7)_2$ $RbSc(H_2P_2O_7)_2$	$RbScP_2O_7$	RbScHP ₃ O ₁₀	$Rb_2ScP_3O_{10}$	Rb ₂ Sc ₂ P ₈ O _{24 (c)}
$CsSc(H_2P_2O_7)_2$	$CsScP_2O_7$	$CsScHP_3O_{10}$	$Cs_2ScP_3O_{10}$	$Cs_3Sc_3P_{12}O_{36}$ (d)
$Ag(H_2P_2O_7)_2$ $Ag(H_2P_2O_7)_{2+}$	$AgScP_2O_7$	$AgHScP_3O_{10}$		$Ag_3Sc_3P_{12}O_{36}$ (d)
AgHScP ₃ O ₁₀ AgHScP ₃ O ₁₀ Mix phases				
$AgSc(H_2P_2O_7)_2:H_2O$				AgScP ₄ O _{12 (e)}

		$AgGaP_4O_{12 \text{ (e)}}$
		$AgInP_4O_{12 (e)}$

Table 2. The formation of solid phases in the system, containing Na and Sc as a function of temperature and molar ratio of initial components

<u>t</u> , ℃	<u>n</u> =5	<u>n</u> =10
150	((
175	NaSc(H2P2O7)2	NaSc(H ₂ P ₂ O ₇) ₂
200		_
250	(r
280	NaScHP3O10	Na ₂ ScP ₃ O ₁₀ +NaScP ₂ O ₇
300		,
350	(ſ
400	Na ₃ ScP ₈ O ₂₃	Na ₃ ScP ₈ O ₂₃
410		`

Table 3 shows the correlation between the composition of condensed forms from temperature T and the initial molar ratio of the oxides of silver and scandium.

Table 3. Reliance of composition from synthesis temperature T and molar ratio $n = M^I/M^{III}M^I/M^{III}$ [30]

			-	[1
T, °C	<i>n</i> = 1.5–2.5	n=3.5-5.0	n=6.0-7.5	n=8.0-10.0
130 – 150	Sc(PO ₃) ₃ -C	AgScHP ₃ O ₁₀	AgSc(H ₂ P ₂ O ₇) ₂	AgSc(H ₂ P ₂ O ₇) ₂
180 – 200	<u>Sc(</u> PO ₃) ₃ –C	$AgScHP_{3}O_{10} \\$	AgScHP ₃ O ₁₀	AgScHP ₃ O ₁₀
220 – 240	<u>Sc(</u> PO ₃) ₃ –C	$AgScP_4O_{12}$	AgScP ₄ O ₁₂	AgScP ₄ O ₁₂
310 – 335	Sc(PO ₃) ₃ -C ^I	$AgScP_4O_{12}$,	AgScP ₄ O ₁₂	AgScP ₄ O ₁₂
		$AgScHP_{3}O_{10} \\$		
340 – 355	Sc(PO ₃) ₃ -C ^I	$AgScP_4O_{12}$	$AgScP_4O_{12}+$	AgScP ₄ O ₁₂
			$Ag_3Ga_3P_{12}O_{36}$	
400 – 450	Sc(PO ₃) ₃ -C ^I	$AgScHP_{3}O_{10} \\$	AgScHP ₃ O ₁₀	$Ag_2ScP_3O_{10}$
500 - 550	Sc(PO ₃) ₃ -C ^I	Ag ₂ ScP ₃ O ₁₀	AgScHP3O10,	AgScP ₂ O ₇
565			Ag ₂ ScP ₃ O ₁₀	AgScP ₂ O ₇

Having carried out the regio-controlled synthesis of condensed oligo-, poly- and/or cyclo-phosphates, and after their solid-state properties' characterization, we can make some suggestions and inferences. The analyze of the investigational data has shown that we obtained the following condensed phosphates: acidic di- and triphosphates of Ga, In and Sc with Ag, such as: $AgSc(H_2P_2O_7)_2AgSc(H_2P_2O_7)_2$

 $\begin{array}{lll} AgScHP_3O_{10} & AgScHP_3O_{10} & AgGaHP_3O_{10} \\ AgGaHP_3O_{10} & \text{and double cyclic tetra-phosphates} \\ AgGaP_4O_{12}AgGaP_4O_{12}, AgScP_4O_{12} \end{array}$

AgScP₄O_{12, AgInP₄O₁₂, and also somewhat earlier, similar} compounds with all alkali metals [30, 42-44]. All these compounds have been obtained for the first time. We have discovered and clearly defined crystallization regions and optimal conditions for these phosphates. It was found that condensed compounds of scandium-silver, according to their composition and structure, correspond with phosphates of sodium-gallium and sodium-scandium and sometimes with Cs-Ga and Cs-Sc. In addition, we can determine: that attained phosphates are not analogous to corresponding compounds of rare earth elements [24-25, 30, 39-44]. Furthermore, the influence of molar ratio is nevertheless very important. For example, in the case of molar ratio n=5 at temperature 335-340 °C and duration of experiment two weeks is obtained cyclic dodecaphosphate of Ag-Ga, and at molar ratio 7.5 on the same temperature and similar synthesis conditions the basic phase is

tetraphosphate. Sodium did not form a similar compound with gallium and indium, although in general the corresponding condensed compounds of Ga, In and Sc are either isomorphic or very similar.

Conclusions

Our study of the investigation of polycomponent systems containing mono- and trivalent metals and phosphoric acid has revealed the reliance of composition versus temperature & molar ratio of the initial components. The dependence of structural forms of compounds from duration of synthesis and radius of the interrelated cations has been discovered.

It has been experimentally proven that at a relatively low temperatures it is more feasible to produce double acidic diphosphates and triphosphates. With increasing temperature the tetra-phosphates of gallium-silver and scandium-silver are formed. The tetraphosphates of silver are isomorphs among themselves and are iso-structural with the sodium-gallium and sodium-indium tetra-phosphates.

Optimal conditions for the synthesis of cyclophosphates with great cyclic anions is the correlation of the big monovalent cations versus trivalent metals with a small ionic radius.

Concerning the series of structures $[M^IM^{III}(PO_3)_4]_x$ we can underline: that if the radius of trivalent metals' decreases, the identity period of the polyphosphate chain increases, due to the complication of its form factors. The cycles regularly appear, and the number of structural types increases caused by the correlation of middling distances between the trivalent metal, and oxygen atoms (M III $^-$ O), and the monovalent metal-oxygen atoms relatively (M I $^-$ O). The lesser is the correlation (molar ratio), the likelihood of a big cycle formation increases. The lower the correlation (molar ratio), the greater the probability of a large cycle forming.

Acknowledgement

We would like to express our sincerest gratitude to the esteemed scientists, Academician Ivan Tananaev and Professor André Durif (France), for their invaluable advice and guidance, provided years ago, which has undoubtedly motivated us to persist in our work and research in the field of inorganic polymers- condensed phosphates.

References

- [1]Tananaev I.V. Less-Common Element Chemistry. Rare-Earth Element Chemistry. Silicates, Germinates, Phosphates, Arsenates, Vanadates, 2nd ed., IUPAC, Amsterdam, 1991, 289 p.
- [2]Durif A.. Crystal Chemistry of Condensed Phosphates. Plenum Press, 2nd edition, Springer/Business media, 2013, 424 p.
- [3] Byrappa K., Keerthiraj N., Byrappa Sh. M. "Hydrothermal Growth of Crystals-Design and Processing" in *Handbook of Crystal Growth*, 2nd Ed. (Eds. Rudolph P.), Elsevier, 2015, pp. 535-575

- [4] Ribero D. Kriven W.M. "Synthesis of LiFePO4 powder by the organic-inorganic steric entrapment method". *J.Mater. Res.*, 2015, vol. 30, n°14, pp. 2133-2143. https://doi.org/10.1557/jmr.2015.181
- [5] Kozlovska J., Kaczmarkiewicz A., Stachowiak N., Sionkowska A."Preparation of new materials based on the incorporation of micropractiles into collagen matrices", 6th ICSP&AM6, Batumi, Georgia, pp. 61-62, 2019
- [6] Murashova E.V., Chudinova N.N. "Double condensed phosphates of caesium-indium", *J. Inorg. Mater.*, 2001, vol. 37, n° 12, pp. 1521-1524.
- [7] Komissarova L.N. Inorganic and analytical chemistry of Scandium, Editorial URSS, Moscow, 2011, 510 p.
- [8] Vassel N.P, Vassel S.S., Pavlova I.V., Kaklyugin A.V. "Thermal study of systems involving the metaphosphates of trivalent metals and silver". *Proc. Inst. High. Educ.*, *Phys.*, 2011, vol. 1-2, pp. 121-124.
- [9] Strutinska N.Y., Zatovsky I., Ogorodnyk O.V., Slobodyannik N. "Rietveld refinement of AgCa₁₀(PO₄)₇ from X-ray powder data", *Acta Crystallogr. Sect. E Struct Rep Online*, 2013, 69:23, pp. 23-24.
- [10] Suthanthiraraj S.A., Sarumathi R., « A new silver ion conducting SbI₃--Ag₄P₂O₇ nano composite solid electrolyte", *J. Appl. Nanosci.*, 2013, vol. 3, pp. 501-508.
- [11] Grunze, I., Palkina, K.K., Chudinova, N.N., Guzeeva, L.S., Avaliani M.A., Maksimova, S.I. "Structure and thermal transitions of double cesium calcium phosphates", *Inorg. Mater. (Engl. Transl.)*, United States, 2009, vol. 23, n°4, pp. 539-544.
- [12] Avaliani M.A., Tananaev I.V., Gvelesiani M.K., "Synthesis and investigation of double condensed phosphates of Scandium and akali metals", Abstracts for Synthesis Chemists, FIZ CHEMIE Berlin, J. Phosphorus, Sulfur Silicon Relat. Elem.publ.online 2009, vol.51, n° 1-4, p. 453.
- [13] Tananaev I.V., Grunze X., Chudinova N.N. "Prior directions and results in the domain on condensed phosphates' chemistry", J. Neorg. Mater., 1984, vol. 20, n°6, pp. 887-900.
- [14] Avaliani M. "Investigation and thermal behavior of double condensed phosphates of gallium, scandium and silver". (RN:52072881). Intern. Atomic En. Agency Bull./ International Nuclear Information System: INIS-IAEA bulletin, 2021, vol. 52(1), n°31, p. 560.
- [15] Avaliani M., Gvelesiani M., Barnovi N., Purtseladze B., Dzanashvili D., "New investigations of poly-component systems in aims for synthesis of new group of inorganic polymers-condensed phosphates", *J. Proc. Georgian Acad. Sci. Chem. Ser.* 2016, vol. 42, pp. n° 3,308-311.
- [16] Marsh T.P., "Studies into the ion exchange and intercalation properties of AlH₂P₃O₁₀•2H₂O", Ph.D. diss. School of Chem. Coll. of Engineer. Physical Sci. Univ. of Birmingham, United Kingdom, 2011.
- [17] Yokoi T., Kawashita M., Kawachi G., K. Kikuta K., Ohtsuki Ch. "Synthesis of calcium phosphate crystals in a silica hydrogel containing phosphate ions." *J. Mater. Res.*, 2011, vol. 24, n°6, pp.2154-2160. https://doi.org/10.1557/jmr.2009.0242.
- [18] Avaliani M., Shapakidze E., Chagelishvili V., Gvelesiani M., Barnovi N., Vibliani M., Chikovani K. "Properties of the synthesized inorganic polymeric phosphate materials and the possibilities for production of new environmentally friendly and economically viable supplies from local industrial waste." *Nano Studies*, vol.1, n°20, pp. 65-70.
- [19] Avaliani M., Dzanashvili D., Gvelesiani M., Barnovi N., Shapakidze E. "About New Inorganic Polymers-Double Condensed Phosphates of Silver and Trivalent Metals", J. Chem. Chem. Eng. USA, 2017, vol. 11, pp. 60-64.

- [20] Avaliani M. "Investigation and thermal behaviour of double condensed compounds of Gallium, Scandium and Silver". *J. Nano Studies*, 2018, n°17/18, pp. 21-24.
- [21] Dersch R., Steinhart M., Boudriot U., Greiner A., Wendorff J.H. "Polymers for Advanced Technologies, Nanoprocessing of polymers: applications in medicine, sensors, catalysis, photonics", 7th Intern. Symp.on Polymers for Adv. Techn., Fort Lauderdale, Florida, USA, 16 (2-3): 276-282, 2005.
- [22] Suzuki Sh., Whittaker M.R, Grøndahl L., Monteiro J., Wentrup-Byrne E. "Synthesis of Soluble Phosphate Polymers by RAFT and Their in Vitro Mineralization", *J. Biomacromolecules*, 2006, vol.7, n°11, pp. 3178-3187.
- [23] Zanello P., Chains, Clusters, Inclusion Compounds, Paramagnetic Labels. 2nd ed., Elsevier, Siena (Italy) 2012, 661p.
- [24] Avaliani M., Purtseladze B., Shohiashvili E., Barnovi N. "Apropos of inorganic polymers-condensed phosphates and spheres of their applications". *J. Proc. Georgian Acad. Sci. Chem. Ser.*, 2015, vol. 41, n°3, pp. 227-231.
- [25] Avaliani M., Barnovi N., Gvelesiani M., Esakia N. "Topics in double condensed phosphates' chemistry of mono- and trivalent metals", *Georg. Chem. J.*, 2017, n°1, pp. 23-27.
- [26] Avaliani M., "Main Types of condensed phosphates synthesized in open systems from solution-melts of phosphoric acids", *Proc. of 4th Int. Conf. NANO-2016*, GTU, Tbilisi, Georgia, 2016, vol.1, p. 51.
- [27] Brostow W., Hagg Lobland H.E., Materials: Introduction and Applications, John Wiley & Sons, New Jersey, 2017, 480p.
- [28] Mark J.E., Allcock H.R., West R. Inorganic polymers, 2nd ed., Oxford University Press, United Kingdom, 2005, 352p.
- [29] Avaliani M., Shapakidze E., Barnovi N., Dznashvili D., Todradze G., Kveselava V., Gongadze N., "Regiocontrolled Synthesis of Double Condensed Oligo-, Polyand Cyclo-Phosphates, Their Characterization and Possibilities of Applications, Due to their Solid-State Properties", Nano Studies, 2019, vol.2, n°19, pp. 273-284.
- [30] Avaliani M., Chagelishvili V., Shapakidze E., Gvelesiani M., Barnovi N., Kveselava V., Esakia N., "Crystallization fields of Condensed Scandium-Silver and Gallium-Silver Phosphates". *EuroChemBull.*, 2019, vol. 8, n°5, pp. 164-170, DOI: http://dx.doi.org/10.17628/ecb.2019.8.164-170
- [31] Palkina K.K., Maksimova S.L., Chibiskova N.T., "Structure of crystals LiGa(PO₃)₄". *Izv. AN SSSR, J. Neorg. Mater.* 1981, vol. 17, n°1, 95-98.
- [32] Janssen T. "Icosahedral Crystals, Quasi-Crystals: New Forms of Incommensurate Crystal Phases", *J. Phys. Colloques.47*, 1986, vol.C3, pp.C3-85-C3-94, DOI: 10.1051/jphyscol:1986308.
- [33] Averbuch–Pouchot M.-Th., Durif A. Topics in Phosphate Chemistry, World Sci., Singapore, 1996, 404 p.
- [34] Bandurkin, G. A., Chudinova, N. N., Lysanova, G. V. Krut'ko, V. A., Palkina, K. K., Komova, M. G. "Heavy lanthanide phosphates: nanostructuring during their solid-phase synthesis", *Russ. J. Inorg. Chem.*, 2006, vol. 51, n°9, pp. 1473-1482. DOI: 10.1134/S0036023606090117
- [35] Chudinova, N.N., Murashova, E. V. Yluikhin. A. B., "Double cyclohexaphosphates of cesium and divalent metals", *Inorg. Mater.*, 2003, vol. 39, n°12, pp.1298-1302.
- [36] Hore K., "The Investigation of Condensed Phosphates of Alkaline Earth Metals for Use as Biomaterials". Ph.D. diss. School of Chem. Coll. of Engineer. Physical Sci. Univ. of Birmingham, United Kingdom, 2011.
- [37] Kulakovskaya T. V., Vagabov V. M., Kulaev I. S., "Inorganic polyphosphate in industry, agriculture, and medicine: Modern state and outlook", *Process Biochem.*, 2012, vol. 47, n°1, pp. 1-10.

- [38] Oudahmane, D. Avignant, D. Zambon, «Dipotassium dialuminium cyclo¬octa¬phosphate», *Acta Crystallogr. Sect E Struct. Rep. Online*, 2010, 1, 66(Pt 7), pp. i49–i50. doi: 10.1107/S1600536810020751.
- [39] Avaliani M. "General Overview of Synthesis and Properties of a New Group of Inorganic Polymers-Condensed Phosphates", Intern. Confer. Advanced Materials and Technologies-2015, in Proceed. Advanced Materials and Technologies; Tbilisi, Georgia, pp. 200-245, 2015. https://doi.org/10.52340/ns.2020.09
- [40] Avaliani M., Chagelishvili V., Shapakidze E., Todradze G. "Condensation process in solutions of polyphosphoric acids-expectations and surprises on obtaining cyclo- and polyphosphates", *Nano Studies*, 2023, N23 (to be published- in process).
- [41] Avaliani M., Chagelishvili V., Shapakidze E., Barnovi N., Chiqovani K., Vibliani M. "Expanding the horizons for creating new inorganic cyclic and polymeric compounds in the promising trend of synthetic chemistry", in Proceed. of Intern.Sci.Conf. dedicated to 90th Ann. of acad. G. Tsintsadze «Chemistry-achievements & perspectives», GTU, Tbilisi, Georgia, 11, 2023.

- [42] Avaliani M., Shapakidze E., Chagelishvili V., Todradze G. "Variants of the Thermal Decomposition of Condensed Phosphates as an Opportunity to Obtain New Cyclic or Polymeric Compounds", *in Proceed. 8th ICSP&AM-8*, TSU, Tbilisi, Georgia, p. 3, 2023.
- [43] Avaliani M., Shapakidze E., Chagelishvili V. "Newfangled dimension of scientists' responsibility: solutions in the context of sustainable development & evolution of chemical processes for clean environmental management", in book Environmental Technology and Sustainability: Physical. Chemical and Biological Technologies for Environmental Protection, (eds. Tatrishvili T, Abraham A.R, Haghi A.K.), Apple Acad. Press/Taylor & Francis Group, Palm Bay, Florida USA, ch.9, 2024.
- [44] Avaliani M. "Recapitulation of Earlier and Recent Studies Carried Out in Open Multi-Component Systems Focused on the Synthesis of Condensed Phosphates", in book Advanced Polymer Structure. Chemistry for engineering application Part II: Materials and Properties, (eds. Mukbaniani O., Tatrishvili T, Abadie J.M.), Apple Academic Press /Taylor & Francis Group, Palm Bay, Florida USA, 2024, ch. 6, pp. 67-82.

Features of the Synthesis of Metakaolin Based on Calcined Shales

E. Shapakidze*, M. Avaliani, M. Nadirashvili, V. Maisuradze, I. Gejadze, T. Petriashvili

Abstract. The cement industry is known to be one of the largest carbon dioxide polluters in the air, so efforts are underway throughout the scientific world to replace Ordinary Portland Cement (OPC) with clinker-free cementitious materials. Replacing OPC with geopolymer material (GPM) is one of the most realistic strategies to reduce environmental impact. One of the main components for the production of GPM is a synthetic mineral metakaolin, which is obtained by heat treatment of the kaolin mineral or kaolin clays. The amount of these materials in the world is limited, so the production of metakaolin from shale is of particular interest, which is the purpose of this work. Clay shales from the banks of the Duruji River, near the city of Kvareli, were selected as the object under study. The data obtained confirmed the ability of calcined shale to react with granulated slag in an alkaline environment and form GPM.

ე. შაფაქიძე, მ. ავალიანი, მ. ნადირაშვილი, ვ. მაისურაძე, ი. გეჯაძე, თ. პეტრიაშვილი – კალცინირეზული ფიქლების საფუძველზე მეტაკაოლინის სინთეზის თავისებურებები

რეზიუმე. ცნობილია, რომ ცემენტის მრეწველობა ჰაერის ნახშირორჟანგის აირით ერთ-ერთი ყველაზე ძლიერი დამაზინძურებელი წარმოებაა. ამის გამო მთელ მსოფლიოში მიმდინარეობს ძიებები პორტლანდცემენტის (OPC) შესაცვლელად უკლინკერო მჭიდა მასალებით. OPC-ს ჩანაცვლება გეოპოლიმერული მასალებით (GPM) ითვლება გარემოზე ზემოქმედების ერთ-ერთ ყველაზე რეალურ სტრატეგიულ მიმართულებად. GPM-ის საწარმოებლად ერთ-ერთ მთავარ კომპონენტად ითვლება სინთეზური მინერალი მეტაკაოლინი, რომელიც მიიღება მინერალ კაოლინის ან კაოლინური თიხების თერმული დამუშავებით. ამ მასალების მარაგები მსოფლიოში შეზღუდულია, ამის გამო განსაკუთრებულ ინტერესს იწვევს მეტაკაოლინის მიღება თიხური ფიქლებისგან, რაც წინამდებარე სამუშაოს მიზანს წარმოადგენს. მიღებულმა შედეგებმა დაადასტურეს კალცინირებული თიხური ფიქლების ტუტე გარემოში გრანულირებულ წიდასთან რეაქციაში შესვლის შესაძლებლობა და GPM-ის წარმოქმნა.

Keywords: Ordinary Portland Cement (OPC), Geopolymer material (GPM), Clay shales.

Introduction

Ordinary Portland cement (OPC) is typically made by heating a mixture of raw materials in a rotary kiln to approximately 1450 °C, cooling this semi-molten material to form a solid clinker, and then grinding it with calcium sulfate to produce a fine powder. The main raw material used is limestone (mainly CaCO₃), which is mixed with materials such as shale or clay to produce the required alumina and silica. The clinker is predominantly calcium silicate, which is rapidly cooled to stabilize a mixture of alite (3CaO·SiO₂) and belite

completely replacing cement, for example, with geopolymers [4, 5].

Geopolymers are considered environmentally friendly materials due to their lower CO2 emissions compared to their Portland cement counterparts. Geopolymer concrete appears to have been an ancient form of concrete, rediscovered in the second half of the 20th century by Joseph Davidovits [6]. The concept of geopolymerization was first described by him in his numerous papers and patents on the subject and provided new insight into this class of inorganic polymers. Davidovits developed the concept of a geopolymer (an inorganic polymer of Si/Al) to better explain these chemical processes and the resulting material properties. In parallel, during this period, many large infrastructure projects were built in Ukraine using [7, These geopolymer cements contain large amounts of calcium derived from blast furnace slag used as a (2CaO·SiO₂) with small (but important) CaO-rich aluminate and aluminoferrite phases. However, when limestone is heated in a kiln, it decomposes in a reaction releasing 0.78 tons of CO₂ per ton of CaO produced [1].

 $CaCO_3 \rightarrow CaO + CO_2$

To overcome the environmental crisis associated with the production of Portland cement, over the past few decades there has been a significant increase in the tendency to search for new environmentally friendly building materials, either by partially replacing cement with materials with pozzolanic properties [2,3] or "alkali cements" [8]. binder. The projects included multi-storey residential

buildings in Kyiv, which are now about 57 years old.

The slow transition from conventional Portland cements (calcium silicate-based cements) to geopolymer cements (aluminosilicate-based cements) in the building and construction industry holds great promise for the environment around the world. The global cement industry currently contributes between 7 and 10% of global carbon dioxide emissions through the necessary calcination of limestone during the cement production process. This releases approximately 1 t. of CO2 for every t. of Portland cement produced. The cement industry is rightly trying to reduce this figure by improving combustion methods and diluting raw OPC with additional cementitious materials such as fly ash and granulated blast furnace slag. However, since the reaction phase in any binder combination must be a continuous phase, there is a limit to substitution with inert or

¹ Ivane Javakhishvili Tbilisi State University, Alexander Tvalchrelidze Caucasian Institute of Mineral Resources; 11 Mindeli Street, 0186 Tbilisi, Georgia;

² R. Agladze Institute of Inorganic Chemistry and Electrochemistry, Ivane Javakhishvili Tbilisi State University,

¹¹ Mindeli Street, 0186, Tbilisi, Georgia *E-mail: elena.shapakidze@tsu.ge.

slow-reacting additives. Geopolymer cements offer a low carbon alternative (typically around 80% lower) and given that geopolymer concretes are generally stronger and more durable, they offer a longer design and service life, reducing the need for raw materials in the future. Given the conservative nature of the global cement industry, the need for industry standards, and the general dependence on ambient temperature curing, this transition will take time [9]. Geopolymers are a class of inorganic polymers formed by the reaction between an alkaline solution and an aluminosilicate source or feedstock. The hardened material has an amorphous three-dimensional structure similar to the structure of aluminosilicate glass. However, unlike glass, these materials are formed at low temperatures and as a result can incorporate an aggregate frame and reinforcement system, if necessary, during the forming process.

One of the main components for the production of GPM is a synthetic mineral—metakaolin, which is obtained by heat treatment of the kaolin mineral or kaolin clays at 500–800 °C. The amount of these materials in the world is limited, so the production of metakaolin from shale (a widely distributed raw material) is of particular interest, which is the purpose of this work.

In our experiments to receive metakaolin were used alluvium shales, formed as a result of mud flows. The optimal mode of heat treatment of shales has been elaborated, which ensures maximal presence of metakaolin.

Results and discussion

The mineral composition of the shales is a mixture of hydromica, muscovite, biotite, pyrite, limonite, quartz, augite, sericite, calcite, plagioclase, orthoclase, chlorite and aggregates of shales.

The chemical composition of shales is (wt.%): L.O.I.- 4.50, $SiO_2 - 59.95$, $Al_2O_3 - 17.30$, $Fe_2O_3 - 3.45$, FeO - 3.65, CaO - 1.53, MgO - 2.43, $SO_3 - 0.3$, $Na_2O - 2.20$, $K_2O - 2.20$.

According to the differential-thermal analysis data (Fig. 1) the endothermic effect within the temperature range 100-150 °C corresponds to the removal of the absorption water. In the temperature range 440-680 °C loss of weight about 4 % takes place. This is obviously due to the loss of constitutional water, and at 560-650 °C temperature the exothermic effect is observed, which corresponds to burning out of organic inclusions and oxidizing of iron. In the temperature range 680-730 °C there is noted an endothermic effect, which is evidently the result of destruction of the crystalline lattice of shales and their active amorphization.

Differential thermal analysis showed that during heating of clay shales, the active temperature region is the temperature range of 600–800 °C. Based on this, for further research, the clay shales were subjected to temperature treatment at 600, 700 and 800 °C with exposure for 2 and 3 hours.

X-ray phase analysis has fixed phase transformations of clay shales during heat treatment (Fig. 2). On the diffractogram of natural shale No.1 is noted: quartz (4.25, 3.34, 2.454, 2.285, 2.238, 2.128, 2.000, 1.985, 1.817 Å); clay mineral chlorite (14.14, 7.08, 4.73, 3.54, 2.88, 2.383 Å); mica (9.96, 4.96, 2.564, 2.000 Å); Ca-Na feldspar (4.03, 3.78, 3.67, 3.20, 2.954, 3.000, 2.9300, 2.395 Å). On diffractogram No.2 and No.3 (heat-treated shales at a temperature of 600 °C), the amount of chlorite and mica decreases and an x-ray amorphous phase is formed - the x-ray acquires a convex shape. On the diffractogram No.4 and No.5 (heat - treated shales at a temperature of 700 °C) clay minerals completely disappear, the amount of mica is further reduced, and the amount of the amorphous phase is growing. Diffractogram No.6 and No.7 (heat-treated shale at 800 °C) are identical to diffractogram No.4 and No.5.

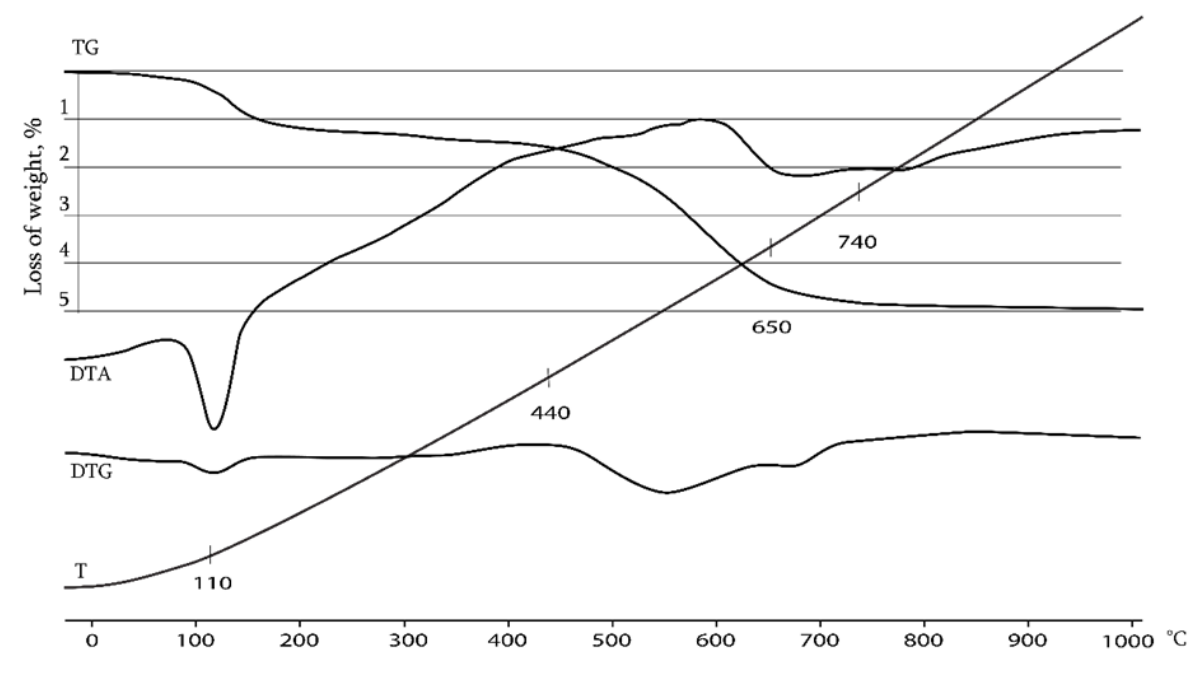


Fig. 1. Differential-thermal pattern of shales

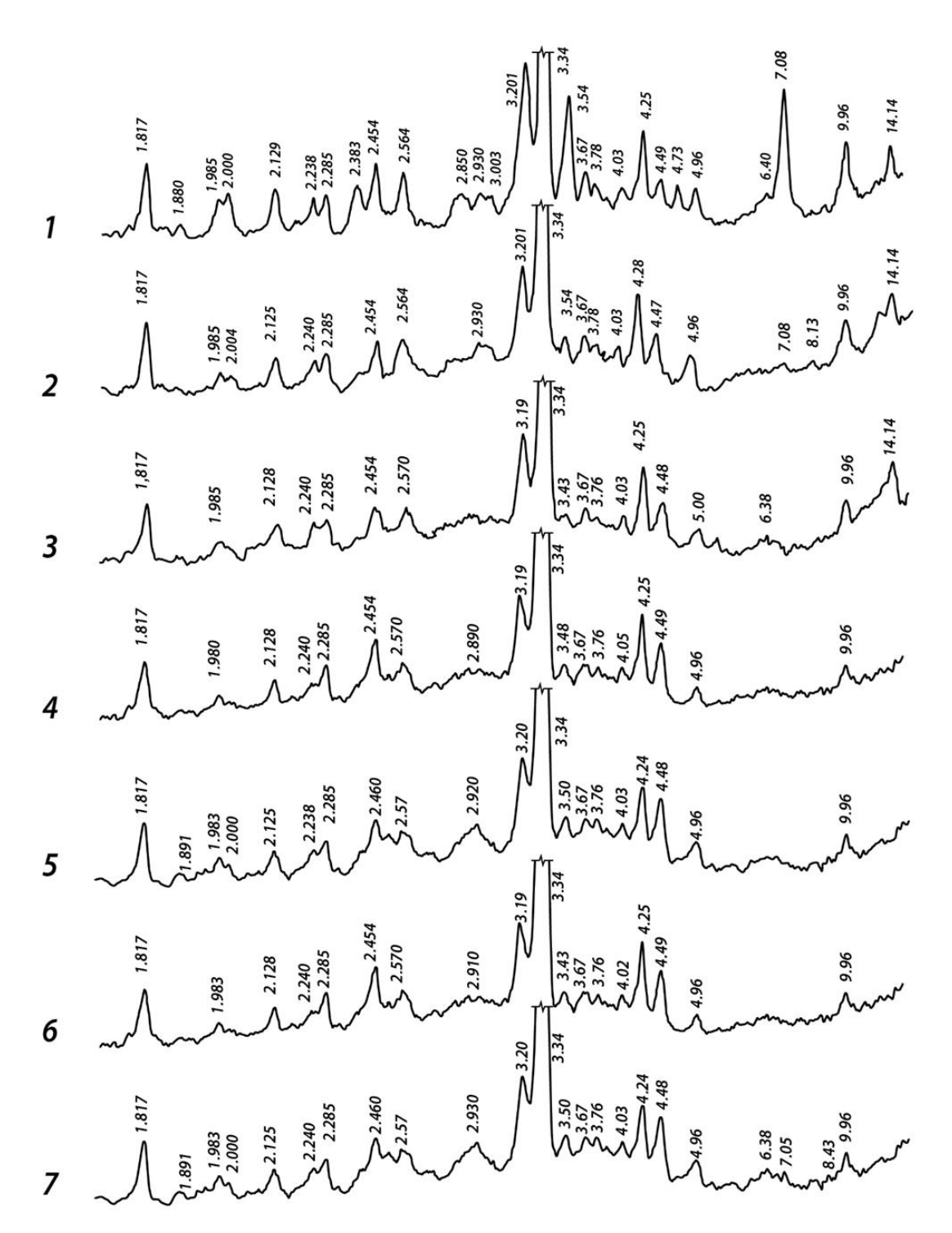


Fig 2. Diffraction patterns of shales: No.1- natural (untreated shale); **No.2** - heat-treated at 600 °C, 2 hours exposure; **No.3** - heat-treated at 600 °C, 3 hours exposure; **No.4** - heat-treated at 700 °C, 2 hours exposure; **No.5** - heat-treated at 700 °C, 3 hours exposure; **No.6** - heat-treated at 800 °C, 2 hours exposure; **No.7** - heat-treated at 800 °C, 3 hours exposure.

Calcination of shales was carried out at 600, 700 and 800 °C with different times of exposure at the maximum temperature. After this the optimal regime for the synthesis of metakaolin was established.

With X-ray phase analysis, it is impossible to fix the appearance of metakaolin because of its amorphous structure, but it is quite possible to determine the

amount of active SiO_2 and the kinetics of its growth by the method of chemical analysis [10] (Table 1).

Table 1. Kinetics of growth of active SiO_2 with increasing temperature and exposure time

No.	Treatment temperature, °C	Exposure, hour	Amount of active SiO ₂ , % by mass
1	Untreated	=	10.21
2	600	2	16.88
3	600	3	20.64
4	700	2	26.77
5	700	3	21.00
6	800	2	26.93
7	800	3	19.56

According to Table 1, the maximum amount of active ${\rm SiO_2}$ is formed in the temperature range of $700{\rm -}800^{\circ}{\rm C}$. In this case, the exposure time is also important; Two hours can be considered as optimal, because with 3-hour exposure, obviously, the compaction of the formed metakaolin occurs and it becomes less reactive. Thus, the optimal temperature treatment of clay shales was found—it is from 700 to 800 °C with exposure time of 2 hours.

For the manufacture of GPM, the following were used: granulated metallurgical slag, calcined shale (processed at 800°C for 2 hours) and an alkaline activator-3% NaOH solution.

The following compositions were selected:

No. 1—slag (100 %);

No. 2—slag (50 %) + untreated shale (50 %);

No. 3—slag (75 %) + calcined shale (25 %);

No. 4—slag (50 %) + calcined shale (50 %);

No. 5—slag (25 %) + calcined shale (75 %).

Test results are presented in Table 3.

The data in Table 2 shows that when calcined shale is added to granular metallurgical slag, the strength of the geopolymer binder increases. As expected, under different hardening conditions the strength of the binder changes: under air hardening conditions it is higher, under air-humid conditions it is lower, and even lower when hardening in water. But in all cases, the developed calcination regime for clay shales increases the physical and mechanical parameters of GPM. We have developed different GPM compositions using calcined clay rocks of Georgia and studied their physical and mechanical properties and resistance in an aggressive environment [11–15].

Table 2. Results of physical and mechanical testing CPM

No.	Compressive strength after 28 days according to hardening conditions, MPa					
	On air	In water	In	an	air-humid	
	environment					
1	55.0	35.0	40.0			
2	22.8	17.0	18.5			
3	56.0	36.0	37.6		_	
4	64.0	44.0	47.5			

|--|

CONCLUSION

The experimental results showed that calcined shales actively interact with granulated metallurgical slag and an alkaline activator to form GPM, which is due to the formation of metakaolin in the shales. At the same time, the optimal amount of metakaolin is formed during temperature treatment of clay shales at 800°C with exposure for 2 hours.

ACKNOLEDGMENTS

The authors of the article express their gratitude to the organizers of the 2nd International Scientific Conference: "Science, Education, Innovations and Chemical Technologies – From Idea to Implementation 2023"

REFERENCES

- [1] Provis J. L., Duxson P., Kavalerova E., Krivenko P.V., Pan Zh., Puertas F., van Deventer J. S. J. Alkali Activated Materials. State-of-the-Art. Report, RILEM TC 224-AAM. Chapter 2. Historical Aspects and Overview, 2014, 11-56.
- [2] Scrivener, K.L., Kirkpatrick, R.J. Innovation in use and research on cementitious material. Cem. Concr. Res. 38. 2008, 128-136.
- [3] Taylor, M., Tam, C., Gielen, D.: Energy efficiency and CO₂ emissions from the global cement industry. International Energy Agency, 2006.
- [4] Gartner, E.: Industrially interesting approaches to "low-CO2" cements. Cem. Concr. Res. 34 (9), 2004, 1489–1498.
- [5] Damtoft, J.S., Lukasik, J., Herfort, D., Sorrentino, D., Gartner, E.: Sustainable development and climate change initiatives. Cem. Concr. Res. 38 (2), 2008, 115–127.
- [6] Davidovits, J. Global warming impacts on the cement and aggregate industries. World Resource Review 1994, Vol 6, p 263, 2017, 263 p.
- [7] Krivenko, P.K., Alkaline Cements., in Proceedings of the First International Conference on Alkaline Cements and Concrete, VIPOL Stock Company, Kiev, Ukraine, Vol. 1, 1994, 11-129.
- [8] Palomo, A.; Krivenko, P.; Garcia-Lodeiro, I.; Kavalerova, E.; Maltseva, O.; Fernández-Jiménez, A. A review on alkaline activation: new analytical perspectives. Materiales de Construcción, Vol 64, 2014, 315 p.
- [9]Gourley J. T. Geopolymer Cement; Environmental Considerations. Geopolymer Alliance. ResearchGate. 2020.
- [10] Shapakidze E., Nadirashvili M., Maisuradze V., Gejadze I., Avaliani M., Todradze G. Elaboration of the Optimal Mode for Heat Treatment of Shales for Obtaining Metakaolin. Eur. Chem. Bull., 8(1), 2019, 31–33;
- [11] Shapakidze E., Avaliani M., Nadirashvili M., Maisuradze V., Gejadze I., Petriashvili T. Obtaining of Geopolymer Binders Based on Thermally Modified Clay Rocks of Georgia. Nano Studies/Eur. Chem. Bull.

No.20, 1, 2020, 43-52.

- [12] Shapakidze E., Avaliani M., Nadirashvili M., Maisuradze V., Gejadze I., Petriashvili T. Geopolymers Based on Local Rocks as A Future Alternative to Portland Cement. Apple Academic Press, USA. Chapter in Book. 2020. 351–358.
- [13] Shapakidze E., Avaliani M., Nadirashvili M., Maisuradze V., Gejadze I., Petriashvili T. Obtaining and Studying the Properties of New Geopolymer Binders Based on Calcined Clay Rocks and Local Industrial Waste. Eur. Chem. Bull. 11(6), 2022, 67–73.
- [14] Shapakidze E., Avaliani M., Nadirashvili M., Maisuradze V., Gejadze I., Petriashvili T. Study of corrosion resistance of geopolymers obtained on the basis of local raw materials. Annals of Agrarian Sciences. Vol.20, No.2, 2022. 84-90.
- [15] Shapakidze E., Avaliani M., Nadirashvili M., Maisuradze V., Gejadze I., Petriashvili T. Investigation of the Durability of geopolymer materials obtained using thermally modified clay rocks. Nano Studies No.21-22. 2022. 129-136.

PECULIARITIES OF GLAZE PRODUCTION USING TECHNOGENIC RAW MATERIALS

M. Kapanadze*, M. Mshvildadze, N. Kebadze, T. Loladze Georgian Technical University, 77 Kostava Str. Tbilisi, 0160, Georgia E-mail: m.kapanadze@gtu.ge

Abstract: The issue of using artificial raw materials in the production of various types of ceramic products, for example, glazes, is becoming increasingly relevant. This is due to the fact that quite expensive and scarce materials included in the final composition will be saved and by introducing technogenic materials into the final composition, the quality of the end product can be improved. This work proposes a method for producing a low-melting glaze using residues of Chiatura manganese enrichment waste, a typical technogenic raw material, containing following oxides (wt.%): SiO₂-54,25; MnO₂ – 7,86; TiO₂-0,27; P₂O₅-0,35; Al₂O₃-7,73; Fe₂O₃-2,88; FeO-0,23; MnO-6,30; CaO-3,76; MgO-1,27; BaO-0,69; K₂O-1,82; Na₂O-1,02; CO₂-3,59; SO₃-0,63. Oxides in the raw materials are represented by quartz and hydrous SiO₂, anhydrous and hydrous aluminosilicates, complex and anhydrous manganese-containing oxides, carbonates and impurity minerals. The article also discusses the features of physical and chemical processes when cooking glaze. The studies have shown that it is possible to obtain general purpose glazes with colour from black to brownish, various technological and operational properties for different application, and reduced preparation time.

მ. კაპანაძე, მ. მშვილდაძე, წ. ქებაძე, თ. ლოლაძე – ტექნოლოგიური ნედლეულის გამოყენებით მინანქრის წარმოების თავისებურებები

რეზიუმე. სხვადასხვა სახის კერამიკული ნაწარმის, მაგალითად, ჭიქურების მიღების სფეროში ტექნოგენური ნედლეულის გამოყენების საკითხს სულ უფრო დიდი მნიშვნელობა ენიჭება, რაც განპირობებულია იმით, რომ, ერთი მხრივ, იზოგება გამოსავალ კომპოზიციაში შემავალი საკმაოდ ძვირადღირებული და არცთუ იშვიათად, დეფიციტური მასალები, მეორე მხრივ კი - ტექნოგენური მასალების შეყვანით გამოსავალ კომპოზიციაში შეიძლება გაუმჯობესდეს მისაღები პროდუქტის ხარისხი. წინამდებარე ნაშრომში შემოთავაზებულია ადვილდნობადი ჭიქურის მიღება ჭიათურის მანგანუმის მადნის გამდიდრების ნარჩენების გამოყენებით, რომელიც ტექნოგენური ნედლეულის ტიპური წარმომადგენელია და შედგება შემდეგი ოქსიდებისაგან (მას %) SiO₂-54,25; MnO₂ - 7,86; TiO₂-0,27; P₂O₅-0,35; Al₂O₃-7,73; Fe₂O₃-2,88; FeO-0,23; MnO-6,30; CaO-3,76; MgO-1,27; BaO-0.69; $K_2O-1.82$; $Na_2O-1.02$; $CO_2-3.59$; $SO_3-0.63$; ოქსიდეზი ნედლეულში წარმოდგენილია კვარცისა და წყალშემცველი SiO_2 -ით, უწყლო და წყლიანი ალუმინსილიკატებით, მანგანუმის შემცველი რთული და უწყლო ოქსიდებით, კარბონატებითა და მინარევი (აქცესორული) მინერალებით. ნაშრომში აგრეთვე განხილულია ჭიქურის ხარშვისას მიმდინარე ფიზიკურ-ქიმიური პროცესების თავისებურებები. ჩატარებულმა კვლევებმა გვიჩვენა, რომ შესაძლებელია მივიღოთ ფართო დანიშნულების ჭიქურები, რომლებსაც გარკვეული ტექნოლოგიური და საექსპლუატაციო თვისებების დაკმაყოფილების გარდა მოეთხოვება შავსა და მოყავისფროს შორის შეფერილობის უზრუნველყოფა; სხვადასხვა სახის და დანიშნულების კერამიკისათის ტექნოლოგიური და ექსპლუატაციური თვისებების რეგულირება; ჭიქურის ხარშვის ხანგრძლივობის შემცირება.

Keywords: technogenic raw materials, fritted glass, manganese-containing compounds.

Introduction

From the end of the 20th century and the beginning of the 21st century, more and more importance has been given to the issue of using man-made raw materials in the field of making various types of ceramic products, for example, glazes. [1] This is due to the fact that, on the one hand, rather expensive and often scarce materials included in the output composition are saved, and on the other hand, it is possible to improve the ecological issues of the "storage"

location of waste from various enterprises. By introducing man-made materials into the end composition, the technical-economic indicators of the acceptable product can be improved. [2-3]

Results and Discussion

Based on ongoing research, conducted at GTU since 1966, in the field of manganite glasses certain conclusions have been made about the role of manganese in the formation of

the reception, structure and properties of glass materials. According to one of the conclusions, manganese-free compositions can be used to obtain vitreous coatings and also frittable glazes of certain types and purposes. On the one hand, this is indicated by the temperature limits of the glass formation areas in the R₂O-RO-MnO-B₂O₂-SiO₂ system and the properties of the obtained glasses. On the other hand, we can assume that by combining different types of divalent ions, it is possible to create compositions that allow obtaining glazes with appropriate properties by varying the amount of these cations.

Based on these prerequisites, we have established a group of compositions. Their composition varied in the following ranges of basic oxides (mass%) SiO₂ 33-45; Al₂O₃ 3-8; BO)₃ 10-20; MnO 3-18; RO 5-12; R₂O 6-12 and provided easy-to-obtain coatings with some adjustment of composition.

In the present paper, it is proposed to obtain a low-melting glaze within the framework of the above-mentioned composition using the residues of Chiatura manganese ore enrichment, which is a typical representative of technogenic raw materials and consists of the following oxides (mass %) SiO₂-54,25; MnO₂ – 7,86; TiO₂-0,27; P₂O₅-0,35; Al₂O₃-7,73; Fe₂O₃-2,88; FeO-0,23; MnO-6,30; CaO-3,76; MgO-1,27; BaO-0,69; K₂O-1,82; Na₂O-1,02; CO₂-3,59; SO₃-0,63; Raw materials are represented by quartz and hydrous SiO₂, anhydrous and hydrous aluminosilicates, complex and anhydrous manganese-containing oxides, carbonates and impurity (accessory) minerals. The peculiarities of the physico-chemical processes during glaze production are also discussed.

The composition of the received glazes showed that by using composite materials it is possible to obtain wide-purpose glazes, which, in addition to meeting certain technological and operational properties, are required to provide a color between black and brownish. It is possible to adjust the technological and operational properties of ceramics of different types and purposes. It is possible to vary the amount of composite material in the composition in a wide range, starting from 30% and ending with the use of only composite material as the main raw material through the introduction of a number of corrective additives. The results of the calculated composition of one of the wide ranges of glaze compositions are given. The composition indicated in the table is prepared at a rather low temperature (up to 1250°C) and then it is kept at the maximum temperature for several tens of minutes, which, in our opinion, is due to use of technogenic raw materials.

As it was mentioned, the composite material is a typical multi-mineral system, which is characterized by the coexistence of different types of natural minerals obtained during processing and interaction with the environment in the tailing dump. Most of them are silicate, which reduces the energy expenditure required for their formation in the composition. On the other hand, hydrous aluminosilicates undergo structural destruction during the stepwise decomposition of structural water, which promotes active interaction with other components of their system. Besides, the addition of preservatives such as boric acid, sodium carbonate, and fluoride should help reduce boiling and roasting temperatures.

When recalculating the blend composition on minerals, it is established that the composition actually contains not five, but many more components. The calculation shows that within 5% of the composition, there are at least 5 types of impurity minerals (apatite, rutile, barium sulfate, iron sulfide and geotite) and up to 20% are hydrous aluminosilicates (muscovite, kaolinite, chlorides, the three main minerals of feldspars — orthoclase, albite, anorthite). The dominant component of the composite material is quartz, the content of which is 39%. A certain part of it should be represented by water-bearing SiO₂. In addition to the minerals listed above, boric acid (20%), sodium carbonate (9%) and titanium and zinc oxides (4%) are included in the composition.

Based on the above, it is clear how difficult it is to track the physico-chemical processes during heating in such a multimineral system and to accurately establish the sequence of these processes and the number of products obtained. Therefore, the opinions listed by us below, which are based on the thermodynamic-petrochemical method of the mentioned processes and predictions and the data obtained by derivatography, diffractography, infrared spectroscopy, crystallographic research, should be perceived more as an assumption than a statement of reality. However, it must be noted that the basic findings satisfactorily explain the lowering of boiling and roasting temperatures.

In our opinion, the scheme of glass formation processes from the given composition should correspond to the one below. $20\text{-}120^{\circ}\text{C}$ - removal of hygroscopic water;130-150°C - the beginning of the removal of constitutive water from boric acid with the formation of HBO₂. Water begins to separate from the geotite and upper magnetite to form hepatite and manganese oxides.

150 -180°C - the first areas of liquefied gas are formed due to eutectics and their fusion between H₃BO₃ and HBO₂. In the same interval, the formation of borates and the oxidation-reduction process of the received oxides begin. [4]

 $180\text{-}500^{0}\text{C}$ - the formation of borates and silicates ends; Reactions involving Na_2 CO_3 , as well as other carbonates, are mostly complete. The amount of the liquid phase increases mainly with the participation of Na_2O and B_2O_3 and the formation of eutectics. It is also possible to form eutectics of three-component silicates with other silicates and quartz. From about 700^{0}C the active participation of SiO_2 begins with the formation of the first boronatrosilicates, which also contributes to the increase in the amount of the liquid phase. At 800^{0}C , the amount of liquid phase reaches about 30-35%.

At $800\text{-}1000^{0}\text{C}$ the products present in the composition and obtained as a result of dehydration of water-containing aluminum silicates take place in the solid phase reactions. In the same interval, a number of silicates begin to melt and form eutectics. The mass is cakey and bubbly. The amount of liquid phase is 70-75%.

At 1000-1100°C, the mass is almost completely amorphous, although non-uniform. Crystalline inclusions that are mostly non-silicate (magnetite, hausmannite) are visible. In the microscope, the presence of liquid phases with different colors is clearly visible, which seem to differ in the degree of uneven distribution of manganese ions. [5-6]

At 1110 - 1250°C the boundary between liquid phases with different colors gradually disappears. Refractory compounds are dissolved. A highly mobile liquid phase is obtained, however, drop-like inclusions different from the main mass are observed in it, which decrease in size with the increasing temperature. The mass is ready for frying. [7]

Conclusion

Thus, at low boiling temperatures, boron and silicon act independently with other constituents of the system, and noticeable interaction between them starts only from 700-800 °C. At different temperature stages of the boiling process, feldspars, quartz, rhodenite, a number of borates, hypoxene group minerals were clearly fixed. It was difficult to experimentally determine the presence of other compounds due to their abundance and the approximate values of their characteristics. We discussed the possibility of their formation by evaluating the results of thermodynamic-technochemical calculations.

Finally, it should be noted that the obtained glazes, apparently, cannot be attributed to completely homogeneous ones. They are heterogeneous, but do not exhibit liquefaction-induced phenomena after application onto ceramics.

References:

[1] Minco M.I. et al. Glazes based on crystalline slates

- // Glass and ceramics. 1990, No. 9, p. 2-3.
- [2] Mukhamedzhanov N. G. Irkakhodzhaeva A. P. Synthesis of colored and jade glazes based on mining waste // Glass and ceramics. 1991, No. 7, p. 6-7.
- [3] Levitsky I. A. Jade glazes using galvanic slags // Glass and ceramics. 1993, No. 8, p. 2-4.
- [4] Lemeshev V. G. et al. Recycling of coal mining waste in the production technology of ceramic materials // Glass and ceramics. 2004, No. 9, p. 30-32.
- [5] Sarukhanishvili A.V. Polymanganese borate and silicate glasses. Tbilisi: ed. Tbilisi State University, 1989. - p. 160.
- [6] Cheishvili T. Sh. Glasses of three-component systems containing d-elements. (Obtaining, structure, properties) // Tbilisi State, University, 2003. p. 36.
- [7] Steinberg Yu. G. Turn E. Yu. Vitreous coatings for ceramics // L. Stroyizdat, 1989. p. 193.

ON THE ISSUE OF SAFE RECYCLING OF AMORTIZED LEAD BATTERIES

L. Bagaturia*, T. Chakhunashvili

¹ Ivane Javakhishvili Tbilisi State University, Alexander Tvalchrelidze Caucasian Institute of Mineral Resources; 11 Mindeli Street, 0186 Tbilisi, Georgia;

*E-mail: lamzirabagaturia@mail.ru

Abstract. The article discusses the advantages and disadvantages of existing technological options for processing amortized lead batteries. A reasonable conclusion is made that none of them provides maximum environmental safety and economic efficiency of production. The advantage and prospects of the technology developed by the authors in comparison with existing methods are considered. These advantages are due to the following circumstances:

- 1. The technological scheme is locked and (practically) environmentally safe;
- 2. The utilization of all components of monoblocks is envisaged by obtaining a marketable product;
- 3. In the main operations, cheap and affordable secondary raw materials are used instead of expensive reagents and materials:
- 4. The volume of production wastewater is minimized at the expense of recirculation.

ლ. ბაღათურია, თ. ჩახნაშვილი – ამორტიზებული ტყვიის აკუმულატორების უსაფრთხო გადამუშავების საკითხზე

რეზიუმე. განხილულია ამორტიზებული ტყვიის სასტარტერო აკუმულატორების გადამუშავების არსებული ტექნოლოგიური ვარიანტების ღირსებები და ნაკლოვანებები. გაკეთებულია დასაბუთებული დასკვნა, რომ ვერც ერთი მათგანი ვერ უზრუნველყოფს წარმოების მაქსიმალურ ეკოლოგიურ უსაფრთხოებასა და ეკონომიკურ ეფექტურობას. განხილულია ლაბორატორიულ დონეზე ავტორების მიერ დამუშავებული ტექნოლოგიის უპირატესობა და პერსპექტიულობა არსებულ მეთოდებთან შედარებით. ეს უპირატესობა განპირობებულია შემდეგი გარემოებებით: 1. ტექნოლოგიური სქემა ჩაკეტილია და პრაქტიკულად ეკოლოგიურად უსაფრთხო; 2. გათვალისწინებულია მონობლოკების ყველა კომპონენტის უტილიზაცია სასაქონლო პროდუქტის მიღებით; 3. საკვანძო ოპერაციაში ძვირადღირებული რეაგენტებისა და მასალების ნაცვლად გამოიყენება იაფი და ხელმისაწვდომი მეორადი ნედლეულის გარკვეული სახეობები; 4. რეცირკულაციის ხარჯზე მინიმუმამდეა შემცირებული საწარმოო ჩამდინარე წყლების მოცულობა; მოწყობილობა-დანადგარების ძირითადი ნაწილი არასტანდარტულია და შესაძლებელია მათი ადგილზე დამზადება, რაც განაპირობებს მინიმალურ საწარმოო კაპიტალდაბანდებას.

Keywords: technological scheme, amortized lead batteries, affordable secondary raw materials, waste.

Introduction

The need to dispose of amortized lead batteries is due to two main reasons:

- 1. The reserves of natural resources of lead are almost exhausted. Therefore, more than 70% of lead is produced by recycling waste batteries [1]. 81-82% of lead produced in the USA is obtained from recycled materials. At the same time, 86% of recycled lead is used for the production of new batteries [2]. The consumption of used secondary lead in Russia is gradually growing and currently accounts for 88% of all lead produced, the share of lead obtained from battery recycling is 70% [3].
- 2. Lead and its compounds, which are particularly dangerous substances, belong to the first class of toxic substances, and their maximum permissible concentration (mpc) in the air is 0.01 mg/m³. For comparison, the maximum permissible concentration of mercury is 0.05 mg/m³, and the MPC of such harmful toxic substances as sulfur dioxide and nitrogen oxides, 1000 and 500 times higher than the same indicator. Consequently, the disposal of worn-out lead batteries, in addition to economic importance, is to some extent connected with the solution of environmental and social problems. Lead deficiency is also reflected in the social

sphere. Timely isolation of radiation sources detected on the territory of Georgia requires the creation of a reserve of lead. Amortized lead batteries, due to their complex composition, belong to a certain type of secondary raw materials, which determines the need to develop a technological scheme for their processing that would ensure maximum environmental safety and economic efficiency. It depends on factors such as: the amount of raw materials, territorial distribution, availability of energy, market demand for related products that are obtained in the production process, etc.

Worldwide, according to recent years, primary lead is produced in 68 plants, and secondary lead is produced in 190 [4]. A decisive role in the disposal of lead batteries in developed countries is played by international and national acts in this area, environmental awareness of the population, an effective system for the collection and disposal of scrap metal, etc. collecting worn-out lead batteries is the first stage of their disposal, for the solution of which it is necessary to carry out the following measures [5]:

- State regulation by special acts and norms;
 - Expansion of the collection network of battery scrap metal by involving organizations selling batteries and vehicle service stations in this process;

 Discount when buying a new one in case of delivery of an old battery.

From the collection point of worn-out batteries to the recycling plant, they must necessarily be transported with electrolyte, unloading from the electrolyte without emptying must be carried out at the factory, where an appropriate place with proper technical equipment must be allocated. In America, for this purpose, there is an infrastructure that fully controls the entire process of collecting, transporting and recycling scrap metal from lead batteries.

Equally important is the issue of licensing in the field of collection and processing of secondary raw materials containing ferrous and non-ferrous metals. The licensing problem, as the authors rightly point out [6-7], should be divided into two stages: 1. The granting of authority (permission) to carry out a particular activity; 2. The "Licensor" must have the technical capabilities to carry out this activity in environmentally friendly conditions.

After the geopolitical changes in the post-Soviet republics, including Georgia, spontaneously and non-transparently appeared enterprises where battery scrap metal is processed. Most of these enterprises do not comply with environmental standards, are not equipped with gas- and dust-proof, as well as wastewater treatment systems, the rules of storage and isolation of industrial waste are not observed, the collection and disposal of electrolyte is not carried out.

The choice of a waste disposal scheme for battery scrap is especially important. Due to the specifics of this raw material (a complex system of monoblocks - housing, electrolyte, metal electrodes, lead oxides, lead sulfate), it is almost impossible to choose one universal scheme of its processing for different countries and regions. In developing countries, where raw materials reserves are small (small population, low level of automation), it is impractical to use technologies used in developed industrial countries for the following reasons:

- They are selected and processed for large-scale production (with an annual capacity of 5000 tons of lead /year or more):
- 2. Differ in the high cost of equipment and technologies in general;

In order to avoid the release of gases and dust in large quantities into the environment, due to intractable problems and the high price of metallurgical coke, the use of mine furnaces has lost its importance. In the EU countries, the use of mine furnaces has been prohibited since 2002 [9].

Modification of the technology using other types of furnaces in the process of recycling spent batteries partially solved the environmental problems of the enterprise and increased economic performance [10]. In Europe, it is still considered a widespread technology (after disassembly and fractionation of monoblocks) to restore the lead-containing fraction in a rotating furnace operating in a periodic mode [10-12], however, due to the formation of a large amount of slag (5-10% of raw materials), the isolation, burial or disinfection of which creates certain problems, many of them were closed. In the second half of the XX century, the use of electrothermal furnaces in the production of secondary lead reduced the volume of process gases, significantly reduced the cost of carbon-containing, expensive reducing agents,

improved the sanitary and hygienic operating conditions of the enterprise [8]. The processing of secondary leadcontaining raw materials in furnaces of any type is necessarily associated with the combustion of process gases, which is carried out in order to reduce the content of harmful furans and dioxins in them. This, in turn, is associated with serious technical difficulties and, accordingly, significant investments.

It should also be noted that the choice of the lead extraction scheme from amortized lead batteries is due to the production capacity (e.g., the use of reflective furnaces in the USA), the availability of energy carriers, the volume and location of raw materials sources. The organization of low-tonnage enterprises (500-1500 tons of lead per year) should be considered as the most acceptable for raw materials located on a large territory. In this case, it is relatively easy to take preventive measures to solve environmental problems, mechanization and automation of operations. It should also be noted that relatively promising are the processes that are carried out using electrothermal furnaces.

As can be seen from the table, the advantages of electrothermal processing of lead batteries are noticeable from the point of view of environmental safety. In this case, the lead content in the slag is low. However, with long-term operation of the furnace, the use of lead-containing slag still becomes problematic. In addition, the temperature of the process is high, so this method cannot be considered ideal from an environmental and economic point of view.

Currently, there are two main alternative schemes for the disposal of used batteries:

- 1. Melting of monoblocks purified from sulfuric acid in the presence of a reducing agent in furnaces of various types. At this time, the organic mass is burned in air or in technical oxygen;
- 2. Preliminary mechanical disassembly of monoblocks and subsequent processing of the obtained semi-finished products pyrometallurgical, hydrometallurgical hydroelectrometallurgical methods. Each of these methods has both advantages and disadvantages [11]. Environmental measures and methods related to pyrometallurgical operations, as already mentioned, are extremely complex, require high costs of electricity, water and appropriate reagents and are characterized by low efficiency. Some modern operating or proposed technological schemes provide for preliminary fractionation of battery monoblocks [12]. At this time, three main types of semi-finished products are obtained: organic (polyvinyl chloride - PVC, polypropylene, polyethylene), metallic (Pb - Sb) and oxide-sulfate (PbO, PbO₂, PbSO₄). The organic fraction is removed before carrying out metallurgical transformations using hydrostatic and hydrodynamic operations.
- 3. The metal fraction is a semi-finished product, which, after melting and proper correction by refining in ionic melts, can be used in the production of new batteries.

Table 1. The advantages of electrothermal processing of lead batteries

Parameter	Technological scheme	Degree of lead extraction	Temperature, °C	Conditional fuel consumptio n, kg/t Pb	Cyclic process	Amoun t of slag, %	Lead content in slag, %
Mine furnace of the company "VARTA"	Discharge of electrolyte from batteries, melting, air purification	95-98	1100-1200	215	Continu ous	5-8,5	0,9-2,0
Reflective Furnace RSR corporation USA	Battery disassembly, charge preparation, drying, melting, air purification	70-80	950-1050	152	Continu	8-10	1,5-3,0
rotary kiln "Egitec impianti" Italy	Battery disassembly, desulfatization, flow mixing, melting, air purification	97	1000-1100	148	Continu	11-12	5-10
Electric furnace riaztsvetmet, Russia	Battery disassembly, drying, melting, air cleaning	98-99	1100-1150	151	Continu ous	1,6-2,5	1,2-1,7

Processing of the oxide-sulfate fraction, in turn, can be carried out according to two schemes:

- 1. By converting the entire fraction into sulfate and then producing lead by hydro-electrometallurgical method. This process has significant drawbacks: a) lead dioxide needs to be converted to lead monoxide insoluble in acid, which is technically difficult to implement. b) according to the scheme, there is a need to use water-soluble toxic inorganic compounds, which, in turn, have a negative impact on the environmental situation. Consequently, there is a need for the availability of sewage treatment plants and equipment for wastewater treatment, which significantly increases capital investments in production.

 3.
- 2. Hydrochemical desulfatization of the fraction by conversion to lead hydroxide. During the heat treatment of lead hydroxide, lead oxide is obtained, and then lead is obtained by its chemical or electrochemical reduction. After fractionation, the sulfate-oxide mixture is directly reduce using a solid, liquid or gaseous reducing agent. The sam environmental problems manifest themselves here as during the restoration of entire monoblocks.

In the works of the leading scientists of our institute [13], priority is given to a scheme that provides for the complete conversion of the oxide-sulfate fraction into oxide with further production and refining of lead based on molten electrolytes. A closed and waste-free production scheme for the processing of scrap metal of lead batteries is proposed, which completely eliminates environmental problems and is economically promising due to extremely simple hydro- and pyrometallurgical operations. The technological scheme consists of the following operations:

 $\label{eq:continuous} Utilization of the electrolyte (using industrial waste) to obtain a marketable product CaSO_4^2H_2O.$

Mechanical disassembly of mono-blocks, removal and fragmentation of electrodes.

Hydro-separation in hydrostatic or hydrodynamic mode.

The use of organic fraction for the manufacture of household goods (sewer pipes).

Desulfatization of the lead-containing mass by converting lead into hydroxide and regeneration of the primary solution. Thermal decomposition of hydroxide.

At the final stage – the recovery of lead in the molten electrolyte environment using certain types of household polymer waste.

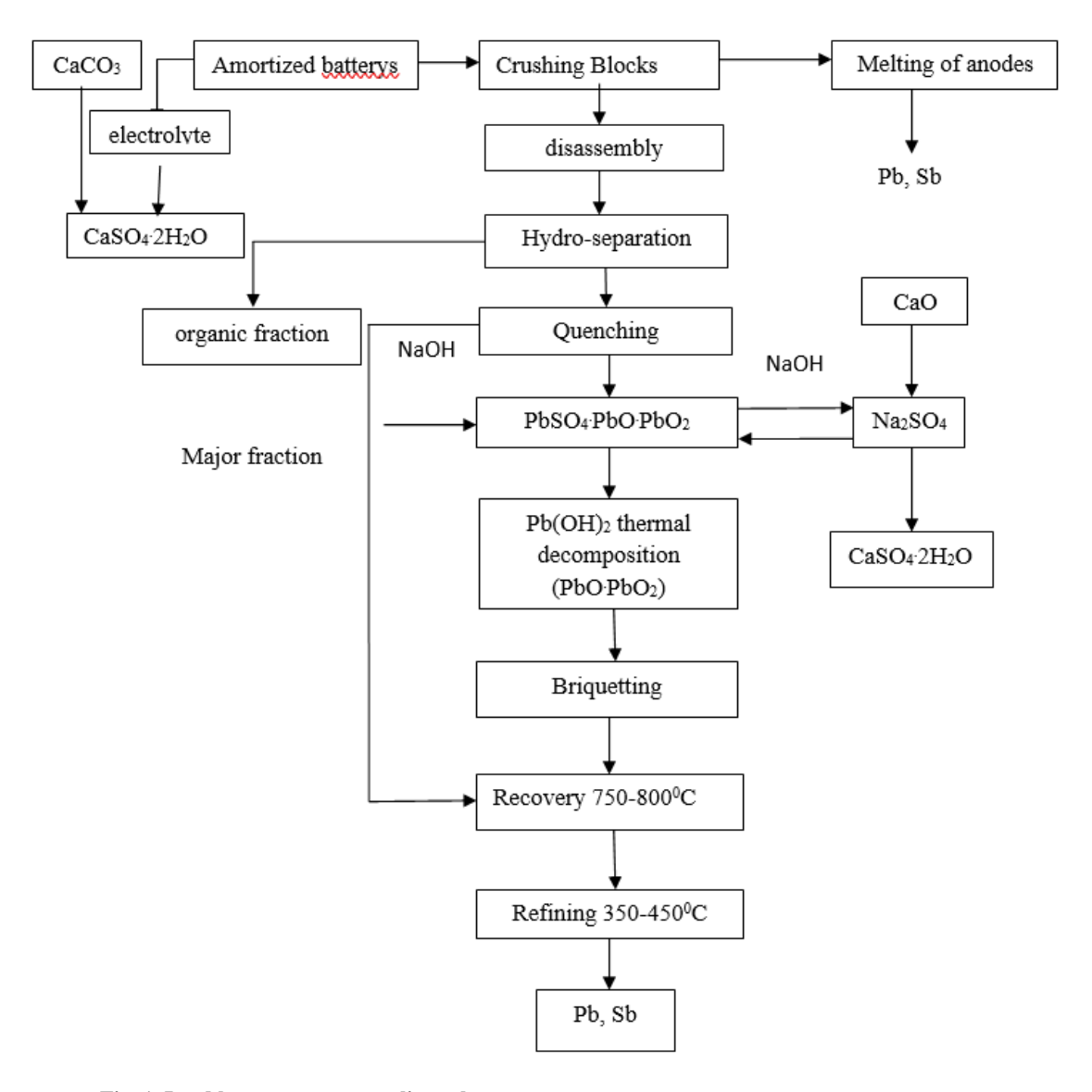


Fig. 1. Lead battery scrap recycling scheme

The expediency of using ion melts at the final stage is due to the fact that the melting layer protects the metal from oxidation, eliminates the possibility of lead and its compounds entering the environment, promotes the reunification and precipitation of lead vapors into droplets. The whole process can be carried out in a closed technological cycle, and, consequently, the absence of industrial wastewater ensures maximum environmental safety and, therefore, requires minimal capital investment in production.

Thus, instead of expensive reducing agents (C, CH₄) in the recycling process, we offer household polymer waste as a REFERENCES

- [1]. Lead and Zinc Statistics. Monthly bulletin of the ILZSG 2004. v. 44, 2005.
- [2]. Бессер А. Д. Вторичные ресурсы 2001, № 5-6,45, с.33-55.
- [3]. Lead and Zinc in Batteries, ILZSG, London, 2003.
- [4]. World Directory 2003; Primary and Secondary Lead Plants ILZSG
- [5]. Кошелев, В. А., Аксельрод Ф. Р., Рыбочук Н.Т. Цветная металлургия 1999, № 2-3, с. 36-40
- [6]. Сурык В.В. Цветная металлургия 2001, №7, с. 24-27.

reducing agent, the issue of disposal of which, in turn, is on the agenda.

The technological scheme developed by us for the disposal of used batteries not only solves the problem of environmental pollution with lead, but also helps to clean the environment from the above-mentioned waste, and therefore is environmentally safe and at the same time economically profitable.

This technology should be considered acceptable for low-tonnage enterprises (500-1500 tons of lead per year) it can also be offered to small republics of the post-Soviet space.

- [7]. Сурык В.В. Цветная металлургия 2001, №6, с. 21-25
- [8]. Манцевич, Н. М., Бессер А.Д., Гнатовский Е.С., Пащенко Г.Г. Цветные металлы, 1995, №11, с. 21-25.
- [9].Солдатенко В. А. Сбор и переработка лома свинцовокислотных аккумуляторов в России. Действительность и перспективы 2003-2006 гг. 2004, №2, с.22-27.
- [10]. Терасов А.В., Бессер А.Д., Малцев В.И., Сорокин В.С. Металлургическая переработка вторичного свинцового сырья. Под ред. А.В. Терасова.- М.: Гинцветмет, 2003

- [11]. Моречевский, А.Г. Переработка вторичного свинцового сырья. С-ПБ. 2003, с.173.
- [12]. Morean G.Y. Power Sources 42 (1-2), 1993, pp. 283-290
- [13]. Tziklauri, O., Marsagishvili, T., Chakhunashvili, T. The optimum circuit of processing of amortized leaden accumulators for small tonnage enterprises. *Georgian Chemical journal*, Vol.2, n°3, 2002, pp. 249-253

Heat-Acid Treatment of Natural Georgian Heulandite

V. Tsitsishvili*, N. Dolaberidze, N. Mirdzveli, M. Nijaradze, Z. Amiridze, B. Khutsishvilili

- ¹ Georgian National Academy of Sciences, 52 Rustaveli Av., Tbilisi 0108, Georgia
- ² Petre Melikishvili Institute of Physical and Organic Chemistry, Tbilisi State University,
- 31 A.Politkovskaia Str., Tbilisi 0186, Georgia

Abstract. The article considers the processes leading to a change in the structure and properties as a result of calcination followed by acid treatment of heulandite-containing tuff from the Georgian Dzegvi-Tedzami deposit. t has been established that preliminary heat treatment reduces the loss of mass and the degree of dealumination and decationization during subsequent acid treatment; with an increase in the preheating temperature, the leaching of sodium ions slows down, while that of potassium ions increases, and after annealing at 800 °C, compensating cations are not leached. Heulandite crystalline structure is partially preserved up to 400-450 °C and subsequent acid treatment. After heating to 500 °C and higher temperatures, the acid-treated samples transform into an amorphous state with crystalline inclusions of chabazite, α -quartz and albite. The volume of pores and hydrophobicity of the surface decrease with increasing calcination temperature; subsequent acid treatment has little effect on pore and surface characteristics.

ვ. ციციშვილი, ნ. დოლაბერიძე, ნ. მირძველი, მ. ნიჟარაძე, ზ. ამირიძე, ბ. ხუციშვილი – ბუნებრივი ქართული ჰეულანდიტის თერმული მჟავით დამუშავება

რეზიუმე. სტატიაში განხილულია პროცესები, რომლებიც იწვევს აღმოსავლეთ საქართველოში მდებარე ძეგვი-ტეძამის საბადოზე მოპოვებული ჰეილანდიტის შემცველი ტუფის სტრუქტურისა და თვისებების შეცვლას ჯერ სითბური, შემდეგ კი მჟავური დამუშავების შედეგად. დადგინდა, რომ წინასწარი სითბური დამუშავება ამცირებს როგორც მასის დანაკარგს, ისე დეალუმინირებისა და დეკატიონირების ხარისხს შემდგომი მჟავური დამუშავების დროს; სითბური დამუშავების ტემპერატურის მატებასთან ერთად, ნატრიუმის იონების გამორეცხვა ნელდება, ხოლო კალიუმის იონების იზრდება, ამავე დროს 800 °C ტემპერატურაზე დამუშავების შემდეგ, მაკომპენსირებელი კატიონები არ გამოირეცხება. წინასწარი სითბური დამუშავება ზრდის ნიმუშის მჟავამედეგობას: ჰეილანდიტის კრისტალური სტრუქტურა ნაწილობრივ შენარჩუნებულია 400-450 °C-მდე, 500 °C-ზე და უფრო მაღალ ტემპერატურამდე გათბობის შემდეგ, მჟავა დამუშავებული ნიმუშები გარდაიქმნება ამორფულ მდგომარეობაში, შაბაზიტის, α-კვარცისა და მინდვრის შპატის ალბიტის კრისტალური ჩანართებით. ფორების მოცულობა და ზედაპირის ჰიდროფობიურობა მცირდება სითბური დამუშავების ტემპერატურის მატებასთან ერთად; შემდგომ მჟავურ დამუშავება მცირე გავლენას ახდენს ფორების და ზედაპირის მახასიათებლებზე.

$\label{lem:Keywords:morphization} \textbf{Keywords: amorphization, dealumination, decationization, dehydration, heulandite.}$

Introduction

The zeolite-bearing tuff from the Rkoni plot of the Dzegvi-Tedzami deposit (Eastern Georgia) has been selected for the creation of new bactericidal zeolite filter materials for purification and desinfection of water from various sources [1]. According to the data of chemical analysis and X-ray data, the sample from the Rkoni plot is characterized by empirical formula |Na_{1.96}K_{0.47}Ca_{1.49}Mg_{1.17}|[Al_{7.8}Si_{28.2}O₇₂]· 23.4H₂O and contains ≈90% of zeolite phase which is a high-silica heulandite mixed with chabazite (crystal chemical data $|Ca_6(H_2O)_{40}|[Al_{12}Si_{24}O_{72}]$ -**CHA** according to [2, p. 96-97]) in a molar ratio of 8:1. The specific pore volume in heulandite-containing tuff is 89.5 mm 3 /g, of which \approx 54 mm³/g (≈60%) are micropores accessible to small polar water molecules, the remaining volume (≈40%) is mesopores with a diameter of up to 120 nm. Since the micropores of heulandite and chabazite have small "entrance windows", only a small part of the

micropore volume (\approx 6% mm³/g) is accessible to larger nonpolar nitrogen molecules [1].

The study of the thermal stability [3,4] and acid resistance [4,5] of heulandite-bearing tuff showed that under the influence of heat and an acidic environment the composition, structure and properties of the material change. Thus, acid treatment leads to significant dealumination and decationization of tuff with preservation of the crystalline structure, while the effective adsorbing surface area and the volume of micropores available for large molecules sharply increase. In addition, the acidic environment causes changes in the mesoporous system, leading to the predominance of nano-sized pores with a diameter of up to 4 nm. Heating the sample causes a process of dehydration (removal of water molecules from the crystal lattice, weight loss up to ≈15%), which continues stepwise up to a temperature of 800 °C, as well as amorphization, starting at 200 °C; at temperatures 500 °C, analcime-like mineral wairakite (Ca(Al₂Si₄O₁₂)·2H₂O) and quartz are formed, at higher temperatures peaks of albite feldspar in the X-ray diffraction pattern appear. Amorphization leads to a decrease in the adsorption volume of micropores, but does not cause a significant change in the mesopore system [4].

^{*}E-mail v.tsitsishvili@gmail.com

The chemical composition of samples calcined and then treated with hydrochloric acid solutions was also determined, and it was noted that such pre-heat treatment significantly reduced the degree of dealumination, especially for samples amorphized by high-temperature calcination [4]. Preliminary results from a study of heat-acid-treated heulandite samples were recently published [6].

The purpose of this work is a detailed examination of the influence of heat-acid treatment on the composition, structure and properties of the studied heulandite-bearing tuff.

Experimental

Materials. Samples of tuff containing up to $\approx 90\%$ of zeolite phase (high-silica heulandite mixed with chabazite in a ratio of 8:1) were collected in the southern section of the Tedzami-Dzegvi deposit, Eastern Georgia. Preparation of samples included crushing of tuff on a cone crusher, fractionation to a particle size of 1-1.4 mm (14-16 mesh), washing with distilled water to remove clay impurities, and drying at a temperature of 95-100 °C.

Treatment. Calcination of samples prepared and dehydrated at 180-200 °C for 2 hours, placed in heat-resistant round-bottomed cups, was carried out in a B400/410 muffle furnace (Naberthem, Carl Stuart Group) in the temperature range 400-800 °C under static conditions for 1 hour; the samples were cooled in a desiccator with calcined CaCl₂ and weighed on an FA 2204N electronic analytical balance (Joan lab, China) to determine the weight loss.

Acid treatment of heated samples was carried out in 0.5, 1.0, and 2.0 mol/L solutions of hydrochloric acid in a OLS26 Aqua Pro shaking water bath (Grant Instruments, US) operating in linear mode at 75 °C in three stages (1, 2 and 3 hours), after each step samples were washed, dried and weighed to determine the weight loss.

Characterization. Chemical composition of samples was calculated from the X-ray energy dispersive (XR-ED) spectra obtained from a JSM-6490LV scanning electron microscope (Jeol, Japan) equipped with an INCA Energy 350 XRED analyzer (Oxford, UK). Powder X-ray diffraction (XRD) patterns were obtained from a D8 Endeavor diffractometer (Bruker, Germany) and modernized Dron-4 diffractometer (USSR) both employing the Cu-K_{α} line ($\lambda = 0.154056$ nm); the samples were scanned in the 20 range of 5° to 68° with a 0.02° step at a scanning speed of 1°/min. The adsorption capacity for water and benzene vapors was measured under static conditions at room temperature; samples calcined at 260-280 °C and then weighed were placed in a desiccator and kept for 96 hours at a constant pressure of water vapor (relative pressure p/p₀=0.4 and saturated vapor pressure $p/p_0=1.0$) and benzene ($p/p_0=1.0$) and then the samples that absorbed the vapors were weighed again.

Results and Discussion

Weight loss. The weight loss during calcination of dehydrated samples averaged $12\pm1\%$, increasing slightly with increasing calcination temperature. Dehydration of the samples was carried out to remove adsorbed water molecules at a relatively low temperature (<200 °C), so as not to cause amorphization of the aluminosilicate crystal lattice, which

begins at temperatures above 200 °C. Under these conditions, with relatively slow heating rate (10 °C/min), approximately 40% of the "zeolite" water molecules (about 6% of the sample mass) are removed, so there is every reason to believe that the observed weight loss is associated with the gradual removal of the remaining "zeolite" molecules (3H₂O per Al atom in original sample).

The weight loss of calcined samples during a three-stage acid treatment depends on both the heat treatment temperature and the characteristics of the acid treatment (stage, concentration); these dependencies are shown in Figures 1-2.

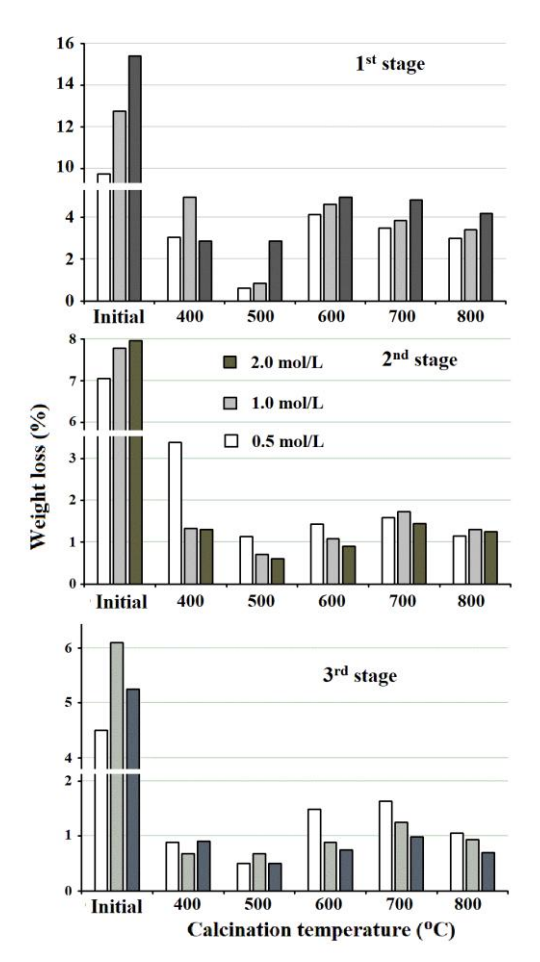


Fig. 1. Weight loss from the 1st, 2nd and 3rd stages of acid treatment of initial and calcined heulandites.

The weight loss of the initial sample at the first and second stages of acid treatment increases with increasing concentration of the hydrochloric acid solution; for calcined samples, especially at the second stage, this pattern is violated. Thus, the greatest weight loss of a sample calcined at 400 °C at the second stage of processing was recorded in a "diluted" solution of hydrochloric acid (0.5 mol/L), its value is almost three times greater than the weight loss in solutions of higher concentrations. At the third stage of processing, the greatest weight loss of the initial sample occurs in a solution of "intermediate" concentration (1 mol/L), but for calcined samples, with the exception of those heated to 500 °C, the greatest weight loss occurs in a "diluted" solution.

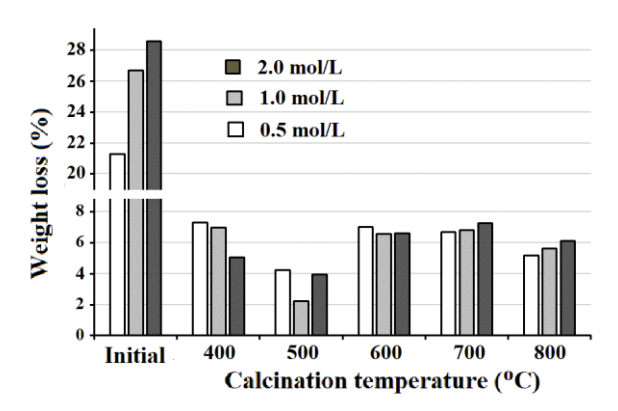


Fig. 2. Total weight loss from three stages of acid treatment of initial and calcined heulandites.

It should be noted that for the sample calcined at 500 °C, when the main heulandite phase is completely amorphized, the least weight loss is observed at all three stages of acid treatment.

In general, the calcined samples experienced at least three times less weight loss compared to the original sample, indicating a higher acid resistance of the amorphous phase.

Chemical composition. The results for chemical composition of the heat-acid-treated samples calculated for 72 oxygen atoms in the unit cell are given in Tables 1a and 1b in terms of averaged empirical formulas of dehydrated zeolites.

As the results obtained show, with increasing calcination temperature, the aluminum content in the unit cell increases compared to the content in samples subjected only to acid treatment. The change in the silicate modulus, expressed by the atomic ratio Si/Al, is shown in Fig. 3. For the initial sample, Si/Al increases almost threefold, while after calcination at 400 °C the modulus increases only by 50%, after calcination at 500 °C it remains constant, and after annealing at higher temperatures increases by only 20%. Such effects once again indicate that in an acidic environment the leaching of aluminum from an amorphous aluminosilicate is more difficult compared to the state when it forms a microporous crystalline structure.

Table 1b shows the change in cationic composition as a result of heating and subsequent acid treatment. In the initial sample, with increasing acid concentration, the total positive charge of alkaline and alkaline—earth compensating ions monotonically decreases from ≈ 1 to ≈ 0.68 ; in this case, the content of Na⁺ ions decreases by ≈ 9 times, the content of Mg²⁺ ions decreases by ≈ 2 times, the content of Ca²⁺ ions changes slightly (-7%), and the content of K⁺ ions increases non-monotonically.

For heat-treated samples, with increasing calcination temperature, the decrease in the relative specific content of sodium ions (Na/Al) slows down, and after high-temperature annealing (700-800 °C), on the contrary, Na/Al even increases (see Fig. 4). Thus, calcination promotes the retention of sodium cations in the zeolite framework..

Table 1a. Composition of aluminosilicate framework of initial (100) and heat-acid-treated samples.

Calcination	Concentration of Ho			
temperature (°C)	0	0.5	1.0	2.0
100	$Al_{7.8}Si_{28.2}O_{72}$	Al _{4.59} Si _{31.4} O ₇₂	Al _{4.26} Si _{31.7} O ₇₂	Al _{3.43} Si _{32.6} O ₇₂
400	Al _{7.63} Si _{28.4} O ₇₂	Al _{6.05} Si _{30.0} O ₇₂	Al _{6.29} Si _{29.7} O ₇₂	Al _{5.65} Si _{30.4} O ₇₂
500	Al _{6.84} Si _{29.2} O ₇₂	Al _{6.59} Si _{29.4} O ₇₂	Al _{6.52} Si _{29.5} O ₇₂	Al _{6.82} Si _{29.2} O ₇₂
600	Al _{7.55} Si _{28.5} O ₇₂	Al _{7.09} Si _{28.9} O ₇₂	Al _{6.79} Si _{29.2} O ₇₂	Al _{6.69} Si _{29.3} O ₇₂
700	Al _{7.71} Si _{28.3} O ₇₂	Al _{6.99} Si _{29.0} O ₇₂	Al _{7.68} Si _{28.3} O ₇₂	Al _{6.62} Si _{29.4} O ₇₂
800	Al7.63Si28.4O72	Al6.9Si29.1O72	Al7.38Si28.6O72	Al6.74Si29.3O72

Table 1b. Cationic composition of unit cell in initial (100) and heat-acid-treated samples.

Calcination	Concentration of HCl	solution (mol/L)		
temperature (°C)	0	0.5	1.0	2.0
100	$Na_{1.96}K_{0.47}Ca_{1.49}Mg_{1.17}$	$Na_{0.62}K_{0.67}Ca_{0.71}Mg_{0.47}$	$Na_{0.47}K_{0.40}Ca_{0.65}Mg_{0.46}$	$Na_{0.096}K_{0.50}Ca_{0.61}Mg_{0.26}$
400	$Na_{1.98}K_{0.46}Ca_{1.45}Mg_{1.14}$	$Na_{0.80}K_{0.56}Ca_{1.03}Mg_{0.79}$	$Na_{0.63}K_{0.52}Ca_{1.38}Mg_{0.52}$	$Na_{0.69}K_{0.46}Ca_{0.92}Mg_{0.54}$
500	$Na_{1.78}K_{0.48}Ca_{1.33}Mg_{1.06}$	Na _{1.06} K _{0.57} Ca _{1.58} Mg _{0.61}	Na _{1.22} K _{0.50} Ca _{1.30} Mg _{0.53}	Na _{1.25} K _{0.46} Ca _{1.34} Mg _{0.46}
600	$Na_{2.04}K_{0.53}Ca_{1.51}Mg_{1.13}$	$Na_{1.50}K_{0.48}Ca_{1.82}Mg_{0.81}$	$Na_{1.72}K_{0.46}Ca_{1.59}Mg_{0.33}$	$Na_{1.69}K_{0.40}Ca_{1.47}Mg_{0.38}$
700	$Na_{2.00}K_{0.46}Ca_{1.46}Mg_{1.08}$	$Na_{1.67}K_{0.46}Ca_{1.73}Mg_{0.75}$	$Na_{2.3}$ - $K_{0.53}Ca_{2.02}Mg_{0.38}$	$Na_{1.64}K_{0.44}Ca_{1.615}Mg_{0.35}$
800	Na _{1.91} K _{0.53} Ca _{1.45} Mg _{1.14}	Na _{1.50} K _{0.34} Ca _{1.88} Mg _{0.65}	Na _{2.10} K _{0.44} Ca _{1.94} Mg _{0.44}	Na _{1.57} K _{0.52} Ca _{1.72} Mg _{0.46}

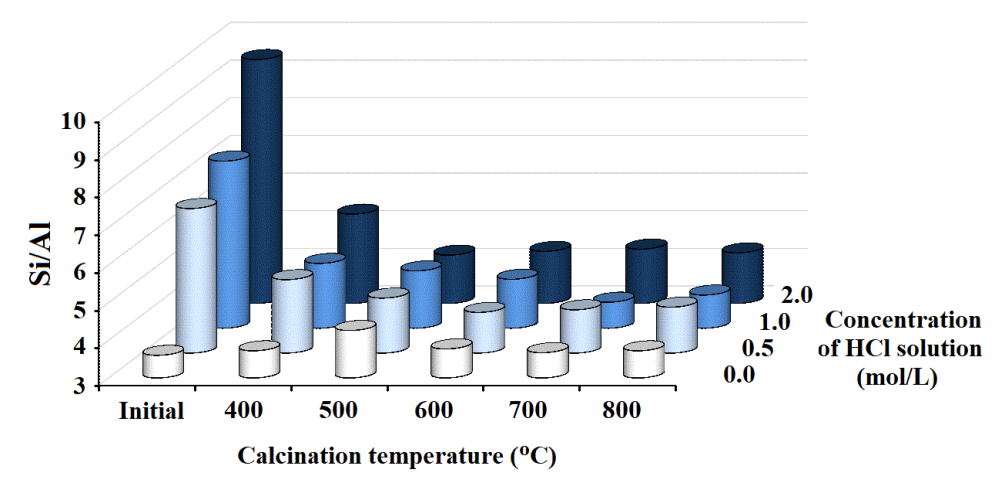


Fig. 3. The Si/Al atomic ratio calculated from XR-ED spectra in samples calcined at different temperatures and treated with HCl solutions of various concentrations.

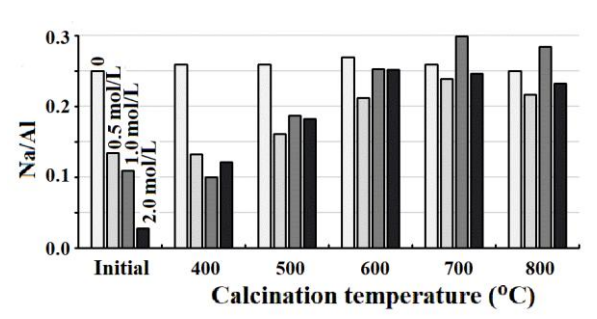


Fig. 4. Dependence of the content of sodium ions relative to aluminum atoms on the calcination temperature and the concentration of hydrochloric acid.

In the original sample, which was not subjected to heat treatment, potassium cations were practically not washed out under the action of hydrochloric acid, and the relative K/Al content increased; this growth, although to a lesser extent, continued in samples calcined at not very high temperatures (up to 600 °C), but after high-temperature annealing, K/Al decreases (see Fig. 5). Apparently, heating the zeolite promotes the involvement of potassium ions in the decationization process.

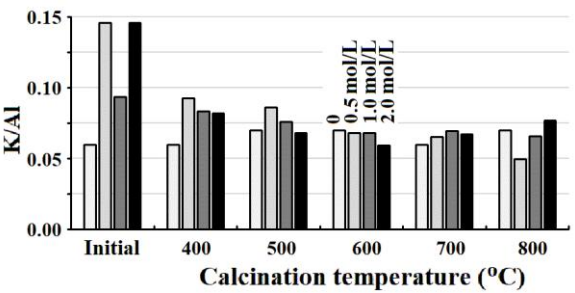


Fig. 5. Dependence of the content of potassium ions relative to aluminum atoms on the calcination temperature and the concentration of hydrochloric acid.

During acid treatment of the initial sample that was not calcined, magnesium cations were washed out to a lesser extent compared to sodium cations; after heat treatment, a more significant decrease in the relative Mg/Al content is

observed, especially in concentrated solutions and with increasing calcination temperature (see Fig. 6, top), which indicates an increasing role of magnesium ions in the decationization process.

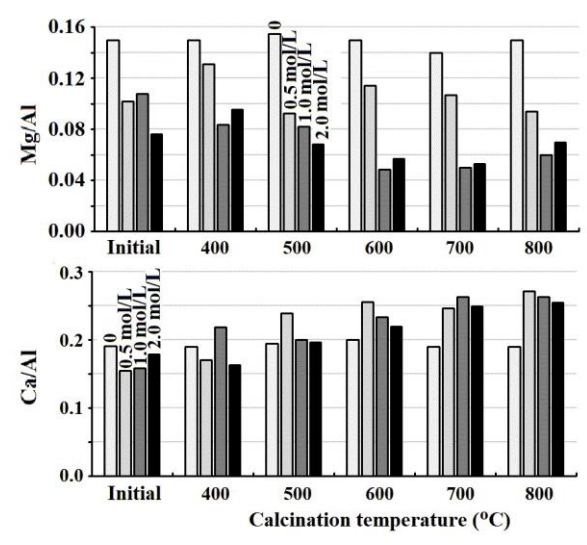


Fig. 6. Dependence of the content of magnesium (top) and calcium (bottom) ions relative to aluminum atoms on the calcination temperature and the concentration of hydrochloric acid.

During acid treatment of the initial sample, the relative content of calcium cations decreased slightly, but after heat treatment, on the contrary, Ca/Al increases with increasing calcination temperature (see Fig. 6, bottom), that is, heating the zeolite promotes the fixation of calcium ions in the crystal framework.

The change in the total charge of the compensating cations depending on the calcination temperature and the concentration of hydrochloric acid is shown in Fig. 7, from which it can be seen that preheating the zeolite reduces the degree of decationization.

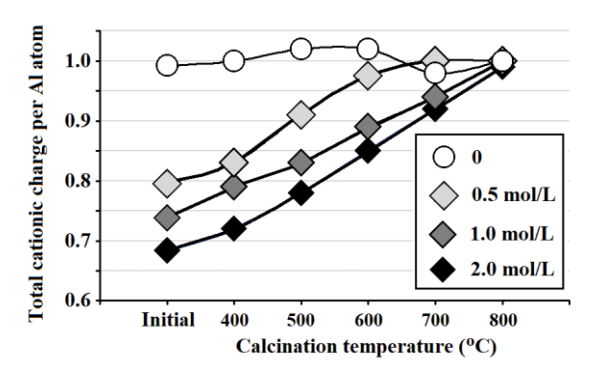


Fig. 7. Total cationic charge per Al atom in calcined initial (0) and acid-treated samples.

Changes in the cationic composition as a result of thermoacid treatment are reflected in X-ray diffraction patterns.

XRD patterns. Analysis of the XRD pattern of the original heulandite-bearing tuff is given in [5], the assignment of peaks to the main heulandite phase and the admixture chabazite phase was carried out on the basis of the simulated XRD patterns from [7]. The measured peak positions (Bragg's angles 2Θ) coincide with the simulated ones, but the peak intensities in the experimental and calculated XRD patterns differ. Thus, in the simulated XRD pattern, the peak at $\approx 9.9^{\circ}$, corresponding to the reflection of the (020) plane, has the highest

intensity (relative intensity I/Io=100%), while in the experimental XRD pattern the maximum intensity of the peaks is observed in the range of $22^{\circ} < 2\Theta < 23^{\circ}$, corresponding to reflections (131), (400), (330), (-421) and (240) with calculated relative intensities of 60.2, 34.7, 53.8, 21.9 and 29.4%, respectively. This discrepancy can be explained by the fact that the calculation of the powder XRD pattern was carried out from crystal data for the potassium form of low-silica heulandite with the empirical formula $|K_{8.48}(H_2O)_{18}|$ [Al9.36Si26.64O72] [8].

It was previously shown [6] that XRD pattern of the initial sample do not change after heating to 200 °C, but at higher calcination temperatures, the peaks of the heulandite phase begin to broaden and their intensity decreases compared to the narrow peaks of the chabazite phase; at temperatures above 500 °C, both a wide band of the amorphous phase and a sharp peak of quartz ($2\Theta = 26.6^{\circ}$) appear; after annealing the sample at 800 °C, the XRD pattern represents a wide band of the amorphous heulandite phase with an overlay of broadened chabazite peaks, as well as narrow peaks of such thermally stable minerals as quartz, the quartz polymorph cristobalite, and albite feldspar. Treatment in acidic solutions does not affect the position of the peaks in the XRD patterns, but the intensity of the peaks changes significantly [5,6]. Despite the formation of an amorphous phase, all intense peaks (I/I_o>10%) of heulandite remain in the XRD patterns when heated up to 400 °C and the peak positions are quite consistent with the simulated spectrum of heulandite [7], but after acid treatment the intensity of most peaks changes (see

Table 2. X-ray data of simulated pattern [7] and relative intensities of intense peaks in XRD patterns of initial, acid-treated and heat(400 °C)-acid-treated samples.

X-ray da	ata from ['	7]		Relative	intensity ((%)					
Miller	d	2Θ	I/I (0/)	Initial	Acid-treated samples			Heat-acid-treated samples			
index	(Å)	(°)	$I/I_o(\%)$	Illitiai	0.5	1.0	2.0	0.5	1.0	2.0	
020	8.979	9.85	100	100	100	100	100	100	100	100	
200	7.989	11.07	64.0	46.6	29.0	34.4	30.8	41	47	38	
-201	6.792	13.03	17.2	30.0	23.7	28.1	26.9	46	67	46	
220	5.969	14.84	12.9	4.9	<8	<8	<8	12.5	<12	<12	
-311	5.258	16.86	11.3	30.0	21.0	31.2	30.7	46	60	42	
111	5.157	17.19	32.0	37.9	25.0	34.3	32.7	50	73	48	
-131	4.661	19.04	20.3	31.1	22.4	31.3	30.8	20	20	19	
{131- 240}*	4.003- 3.914	22.21- 22.72	60.2	115	89.5	131	108	132	186	146	
-312	3.563	24.99	29.4	23.3	19.7	<10	<10	29	50	35	
-222	3.433	25.96	50.8	46.6	38.2	46.9	50.0	46	67	58	
-422	3.176	28.09	45.1	54.4	<i>EE</i> 2	01.2	102	9.6	120	110	
-441	3.132	28.49	34.1	23.3	- 55.3	81.2	182	86	120	112	
{151- 112}**	2.988- 2.975	29.90- 30.03	41.6	59.2	47.4	62.5	52.0	55	93	58	
530	2.819	31.74	43.6	39.8	26.3	35.9	30.8	25	40	31	

^{* –} peaks from (131), (400), (330), (-421) and (240).

XRD patterns of only acid-treated and only calcined heulandite samples are shown in publications [5,6], Table 2 shows the relative intensities of strong peaks (I/I_o>10% in low-angle range and I/I_o>20% for 2Θ >23°) in the XRD patterns of the original sample, acid-treated samples, as well as samples calcined at 400 °C and then treated with acid in comparison with the X-ray data of simulated pattern [7]; as

in the simulated XRD pattern, 100% relative intensity is assigned to the peak from the 020 plane.

The above-mentioned increase in the intensity of the peaks in the region of 22-23° for the original sample is leveled out after treatment in a "diluted" solution (0.5 mol/L), but occurs again after treatment in "concentrated" solutions. Probably, this effect can be associated with the change in the content of potassium ions that occurs during dealumination and decationization. Be that as it may, preliminary calcination at

^{** -} peaks from (151), (350) and (112) with relative intensities of 41.6, 27.8 and 12.7%, respectively.

 $400\,^{\circ}\text{C}$ leads to an even greater increase in the relative intensity of the peaks in the region of $22\text{-}23\,^{\circ}$.

In acid-treated samples, the peaks from the -422 and -441 planes merge and the intensity increases sharply with increasing acid concentration; in heat-acid-treated samples this effect also manifests itself, but not monotonously and not to the same extent. However, changes in the intensity of most peaks are non-monotonic and cannot be interpreted.

XRD patterns of samples pre-calcined at 500 °C and higher temperatures, followed by acid treatment in solutions of any concentration, represent a wide band of the amorphous phase with superimposed narrow peaks of quartz and albite, as well as broadened peaks of thermostable chabazite (the temperature of the collapse of the crystalline structure is over 900 °C); peaks of wairakite (Ca(Al₂Si₄O₁₂)·2H₂O), formed simultaneously with quartz, could not be identified.

Adsorption of water and benzene. Water vapor adsorption has been used since the early 1960s to determine pore volume of high-aluminum zeolites. Due to their small size, water molecules pass freely through the entrance windows into micropores and channels of heulandite crystal structure, and the amount of adsorption depends on the number of partially ionic hydrophilic centers associated with tetrahedrally coordinated aluminum (AlO₄)-. Adsorption isotherms of water vapor and other gases are described in different ways, the simplest of which is the Langmuir equation, the most commonly used is the Brunauer-Emmett-Teller (BET) model. According to the Brunauer-Deming-Deming-Teller classification adopted by IUPAC, the adsorption-desorption isotherms of water vapor on natural zeolites belong to type IV, and at low relative pressure (p/po<0.4) the isotherms reflect the complete filling of micropores, while at saturated vapor pressure (p/p₀=1) show the total volume of all pores. Benzene is a non-polar molecule used as a probe for studying hydrophobic adsorbents such as activated carbon and other carbon materials. The size of the benzene molecule (kinetic diameter of 0.585 nm) does not allow it to penetrate into the micropores and channels of heulandite; adsorption occurs on the surface and reflects its hydrophobicity.

According to the results obtained in previous studies [4-6], for untreated Georgian heulandite, the volume of micropores accessible for water molecules (5.3 mmol/g) is about twothirds of the total pore volume (8 mmol/g); adsorption in micropores practically does not change as a result of acid treatment, and the total adsorption in all pores slightly increases. Regarding the thermal effect, the adsorption capacity of micropores decreases with an increase in the calcination temperature, reaching very low values (<0.3 mmol/g) at temperatures above 500 °C, the adsorption capacity of all pores decreases monotonically with an increase in the calcination temperature; the difference between these two indicators, apores - amicropores, proportional to the volume of mesopores, before the onset of amorphization increases from 2.66 to 3.33 mmol/g, and then decreases to 2.2 mmol/g, which indicates the effect of heat treatment on the mesopore system as well. The change in benzene adsorption in the etched samples is insignificant, but heat treatment significantly reduces the hydrophobicity of the surface.

Results of measurements on heulandite calcined at different temperatures and then subjected to acid treatment in solutions with different concentrations of hydrochloric acid are given in Fig. 8.

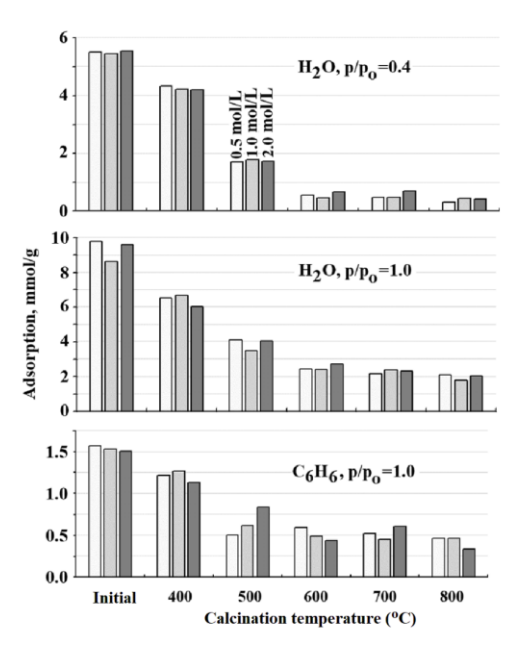


Fig. 8. Water vapor and benzene adsorption capacity of heat-acid-treated samples.

As would be expected, the decrease in adsorption of water molecules in micropores and in all pores, as well as the decrease in surface hydrophobicity demonstrated by benzene adsorption, are mainly determined by the calcination temperature, with subsequent acid treatment having little significance.

Conclusion

Preliminary thermal treatment of heulandite-containing tuff from the Tedzami-Dzegvi deposit, Eastern Georgia, reduces weight loss and the degree of dealumination during subsequent acid treatment, and also affects the decationization process: with increasing preheating temperature, the participation of sodium ions in the process slows down, while the participation of potassium ions increases, the overall degree of decationization decreases, and after annealing at 800 °C, the replacement of compensating cations with H+ ions and their leaching does not occur. Despite the amorphization that occurs at temperatures above 200 °C, the crystalline structure of heulandite is preserved even after heating to 400-450 °C and subsequent acid treatment, as evidenced by the preservation of the peak positions in the XRD patterns; the change in peak intensity depends on the acid concentration in the processing solution and is associated with changes in the content and distribution of cations. After heating to 500 °C and higher temperatures, the acid-treated samples transform into an amorphous state with crystalline inclusions of fine chabazite, α-quartz and albite feldspar; the presence of wairakite could not be confirmed. The adsorption of water molecules in micropores and in all pores, as well as the adsorption of benzene, reflecting the hydrophobicity of the surface, decrease with increasing calcination temperature; subsequent acid treatment is of little importance.

Acknowledgement

The authors express their gratitude to the International Science and Technology Center (ISTC) supported this work under the project GE-2506 "Scientific substantiation of the

possibility of creating new bactericidal zeolite filter materials for purification-decontamination of water from various sources".

REFERENCES

- [1] Tsitsishvili V., Panayotova M., Miyamoto M., Dolaberidze N., Mirdzveli N., Nijaradze M., Amiridze Z., Klarjeishvili N., Khutsishvili B., Dzhakipbekova N., Harutyunyan L. "Characterization of Georgian, Kazakh and Armenian natural heulandite-clinoptilolites". *Bull. Georg. Natl Acad. Sci.*, 2022, vol. 16, no 4, pp. 115-122.
- [2] Baerlocher Ch., McCusker L.B., Olson D.H. Atlas of Zeolite Framework Types, 6th Revised Edition, Elsevier: Amsterdam, 2007, 398 p.
- [3] Tsitsishvili V., Machaladze T., Dolaberidze N., Nijaradze M., Mirdzveli N., Djakipbekova N., Harutyunyan L. "Dehydration and structural transformations during thermal treatment of Georgian, Kazakhstani and Armenian natural heulandite-clinoptilolites". Scientific collection "InterConf", 2022, vol. 136, pp. 356-364.
- [4] Tsitsishvili V.G., Dolaberidze N.M., Nijaradze M.O., Mirdzveli N.A., Amiridze Z.S., Khutsishvili B.T. "Acid and thermal treatment of natural heulandite". *Chemistry*, *Physics and Technology of Surface*, 2023, vol. 14, no 4, pp. 519-533. DOI: 10.15407/hftp14.04.519

- [5] Tsitsishvili V., Panayotova M., Mirdzveli N., Dzhakipbekova N., Panayotov V., Dolaberidze N., Nijaradze M. "Acid resistance and ion-exchange capacity of natural mixtures of heulandite and chabazite". *Minerals*, 2023, vol. 13, # 364, 15 p. DOI: 10.3390/min13030364
- [6] Tsitsishvili V., Dolaberidze N., Dzhakipbekova N., Mirdzveli N., Nijaradze M., Amiridze Z., Khutsishvili B. "Heat-acid treatment of Georgian and Kazakhstani natural heulandite-chabazites". Scientific collection «InterConf+», 2024, vol. 43, pp. 461-476. DOI: 10.51582/interconf.19-20.03.2024.045
- [7] Treacy M.M.J., Higgins J.B. Collection of Simulated XRD Powder Patterns for Zeolites, Fifth Revised Edition, Elsevier: Amsterdam, 2007, 586 p.
- [8] Galli E., Gottardi G., Mayer H., Preisinger A., Passaglia E. "The structure of potassium-exchanged heulandite at 293, 373 and 593 K". *Acta Crystallographica Section B*, 1983, vol. 39, pp. **39**: 189-197.

DOI: 10.1107/S010876818300227X.

Coordination Capabilities of Olanzapine: A Semi-Empirical Approach

N . Gabitashvili¹, M. Tsintsadze^{1,2*}, N. Gegeshidze^{1,2}, N. Kilasonia^{1,2}, T. Tsintsadze^{1,2}, D. Lochoshvili²

E-mail: m.tsintsadze@gtu.ge

Abstract. The influence of various solvents on the metal ion complexation ability of the olanzapine molecule was investigated using the quantum chemical semi-empirical MP3 method. The study involved the calculation of energetic, electronic, and structural parameters of the molecule in the gas phase and in a series of solvents with different dielectric constants. The results enabled the identification of potential coordination centers within the olanzapine structure, determination of the most favorable conditions for the synthesis of its coordination compounds, and a preliminary assessment of their potential biological activity

ნ. გაზიტაშვილი, მ. ცინცამე, ნ. გეგეშიმე, ნ. კილასონია, თ. ცინცამე, დ. ლოჩოშვილი - ოლანზაპინის კოორდინაციული შესამლებლობები: ნახევრად ემპირიული მიდგომა

რეზიუმე. ნახევრადემპირიული PM3 მეთოდით დეტალურად შესწავლილია ოლანზაპინის მოლეკულის ელექტრონული სტრუქტურა და დადგენილია სხვადასხვა გამხსნელის გავლენა კომპლექსწარმოქმნის უნარზე. სავარაუდოდ, დონორია აზოტის ატომი N(9), რომელიც ლითონებთან კოვალენტური ბმების წარმოქმნის უნარს ავლენს ყველა შესწავლილ გარემოში. მაღალი დიელექტრიკული შღწევადობის მქონე გამხსნელები, როგორიცაა წყალი და მეთანოლი, ხელს უწყობენ მოლეკულის სტაბილიზაციას და შეიძლება რეკომენდებული იყოს ოლანზაპინის კომპლექსური ნაერთების სინთეზისთვის. კვანტური ქიმიური მიდგომა შესაძლებელს ხდის წინასწარ განისაზღვროს მოლეკულის კომპლექსწარმოქმნის უნარი სხვადასხვა პირობებში, ხელს უწყობს სინთეზის პირობების შერჩევას და ექსპერიმენტული მონაცემების ინტერპრეტაციას, მათ შორის ინფრაწითელ სპექტროსკოპიას და რთული ნაერთების სტრუქტურულ ანალიზს.

$Keywords: Olanzapine, quantum \ chemical \ calculations, MP3 \ method, complexation, donor \ atoms, solvents, electronic structure$

Introduction

The complexation of pharmaceutical compounds with metal ions represents a significant area of interest in medicinal chemistry, pharmacology, and materials science. Of particular interest is olanzapine, a psychotropic drug whose molecular structure suggests potential as a ligand. The aim of the present study is to identify the structural and electronic factors influencing the complexation ability of olanzapine in various environments.

Methodology

Quantum chemical calculations were carried out using the semi-empirical MP3 method. The solvents used in the study included water, ethanol, methanol, acetone, dimethyl sulfoxide (DMSO), chloroform, hexane, and citric acid. For the olanzapine molecule, the following parameters were calculated [1-5]:

- heat of formation;
- total formation energy;
- ionization potential;
- dipole moment;
- interatomic distances;
- bond angles and bond lengths;
- effective atomic charges;
- electron density distribution and atomic orbital populations.

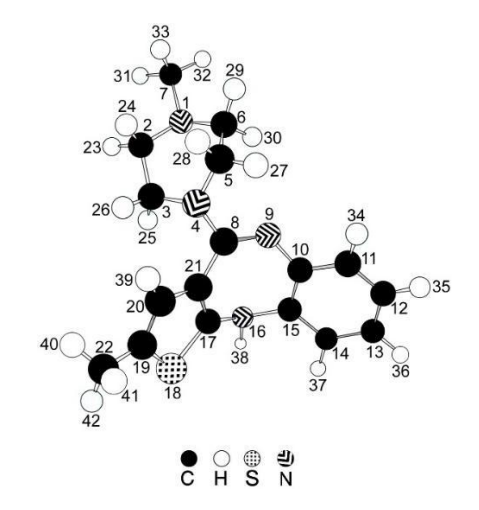


Fig. 1. OlanzapineMolecule

The results obtained in various solvents were compared with the parameters calculated for the gas phase.

Results and Discussion

Energetic and Electronic Stability. The calculations revealed that the heat of formation of the olanzapine molecule is lower in solvents than in the gas phase, indicating greater molecular stability in the condensed phase. The most

¹ Georgian Technical University, 77 Kostava Str. Tbilisi, 0160, Georgia

² I. Javakhishvili Tbilisi State University R.Agladze Institute of Inorganic Chemistry and Electrochemistry 11 MIndeli str, Tbilisi, 0186, Georgia

significant decrease in the heat of formation was observed in solvents with high dielectric constants and strong dipole moments (e.g., water — $\mu = 2.423$; ethanol — $\mu = 2.638$). This suggests that polar solvents stabilize the olanzapine molecule more effectively than nonpolar ones [6-10].

Table 1. Values of Heat of Formation (ΔH) and Dipole

Moments (µ) of the Olanzapine Molecule

111	ments (µ) of the Of		
N	Solvent	Heat of formation, kJ/mol	Dipole moment, Debye
1	gas	332.646	2.631
2	H ₂ O, water	295.377	2.423
3	C ₂ H ₆ SO,dimethyl sulfoxide (DMSO)	295.510	2.378
4	CH ₃ OH, methanol	296.476	2.392
5	C ₂ H ₅ OH, ethanol	298.242	2.638
6	(CH ₃) ₂ CO, acetone	296.569	2.327
7	CHCl ₃ , chloroform	309.968	2.388
8	C ₆ H ₁₂ , hexane	324.601	1.922
9	C ₆ H ₈ O ₇ , citric acid	296.046	2.360

Geometric Parameters. The bond lengths in the olanzapine molecule range from 1.402 to 1.494 Å, consistent with typical values for bonds involving atoms with sp² hybridization. The bond orders vary between 0.976 and 1.378, which also falls within the acceptable range for organic compounds. The valence angles between atoms, particularly those involving N(1), N(4), N(9), N(16), and S(18), further confirm the sp² hybridization of the respective atoms.

Electronic Characteristics and Donor centers. Orbital analysis showed that while N(1) contains an unpaired electron pair on a σ-orbital, the second pair is located on a 2pz orbital, which is suitable only for π -interactions. This limits its ability to form a σ-coordination bond with metal ions.

Table 2. Atomic charge, Electron density on the atom and Electron distribution in orbitals of the Olanzapine Molecule

Solvent		Atomic	Electron density on		Electron distribution in orbitals				
Solvent	Atom	charge	the atom	n	nS	nP_x	nPy	nPz	
Gas	N(1)	-0.080	5.080	2	1.510	1.022	0.963	1.586	
Water	N(1)	-0.091	5.091	2	1.512	1.033	1.045	0.091	
DMSO	N(1)	-0.094	5.094	2	1.513	1.035	1.039	1.507	
Methanol	N(1)	-0.091	5.091	2	1.513	1.035	1.060	1.484	
Ethanol	N(1)	-0.096	5.096	2	1.519	1.042	1.103	1.432	
Acetone	N(1)	-0.096	5.096	2	1.514	1.035	1.031	1.516	
Chloroform	N(1)	-0.094	5.094	2	1.518	1.040	1.093	1.443	
Hexane	N(1)	-0.070	5.070	2	1.503	1.025	1.071	1.470	
Citric acid	N(1)	-0.093	5.093	2	1.514	1.035	1.044	1.501	

A similar analysis for the N(4) atom reveals an unpaired electron pair on a σ -orbital and a second pair on a 2px orbital. However, the spatial arrangement and the charge (which is close to zero in most cases) make this atom an unlikely participant in complexation.

Solvent	Atom	Atomic	Electron density on the	n	Electron distribution in orbitals				
Solvein	Atom	charge	atom	n	nS	nP_x	nPy	nP_z	
Gas	N(4)	-0.009	5.009	2	1.451	1.174	1.057	1.327	
Water	N(4)	-0.045	5.045	2	1.476	1.142	1.410	1.017	
DMSO	N(4)	-0.044	5.044	2	1.475	1.136	1.421	1.012	
Methanol	N(4)	-0.043	5.043	2	1.475	1.141	1.404	1.023	
Ethanol	N(4)	-0.037	5.037	2	1.479	1.142	1.349	1.066	
Acetone	N(4)	-0.042	5.042	2	1.474	1.132	1.429	1.006	
Chloroform	N(4)	-0.028	5.028	2	1.471	1.140	1.307	1.111	
Hexane	N(4)	-0.018	5.018	2	1.464	1.138	1.376	1.040	
Citric acid	N(4)	-0.044	5.044	2	1.475	1.134	1.423	1.012	

The N(9) atom exhibits high electron density and stable occupation of the sp^2 orbital with an S-component. All parameters indicate its ability to form a covalent bond with a metal atom, making N(9) the most likely donor center.

Solvent	Atom	Atomic	Electron density on the		Elec	tron distri	bution in orl	oitals
Sorveill	Atom	charge	atom	n	nS	nP_x	nPy	nP_z
Gas	N(9)	-0.113	5.113	2	1.581	1.144	1.098	1.290
Water	N(9)	-0.113	5.113	2	1.581	1.144	1.098	1.290
DMSO	N(9)	-0.112	5.112	2	1.583	1.179	1.365	0.985
Methanol	N(9)	-0.113	5.113	2	1.583	1.179	1.377	0.975
Ethanol	N(9)	-0.124	4.124	2	1.585	1.195	1.389	0.955
Acetone	N(9)	-0.112	4.112	2	1.583	1.180	1.356	0.993
Chloroform	N(9)	-0.120	4.120	2	1.586	1.184	1.401	0.950
Hexane	N(9)	-0.092	4.092	2	1.577	1.164	1.390	0.962
Citric acid	N(9)	-0.111	4.111	2	1.583	1.180	1.364	0.985

Quantum chemical calculations performed using the semiempirical AM1 method revealed that the analysis of the effective charges of the nitrogen atom N(16), electron density on the atoms, and electron distribution across orbitals in the olanzapine molecule yielded the following: In three solvents—water, methanol, and acetone—the nitrogen atom N(16) can exhibit donor properties because one electron pair resides on a 2s orbital, while the other is located on a 2px orbital. This enables the atom to form a chemical bond with the metal complexing agent [11-13].

For the other solvents—DMSO, ethanol, chloroform, and hexane—the electron pair of the nitrogen atom N(16) is not

located on the 2px orbital but rather on the 2py and 2pz orbitals, which can participate in the formation of π -bonds, rather than σ -bonds.

Further quantum chemical calculations using the semiempirical MP3 method showed that, despite the presence of electron pairs, the coordination ability of the N(16) atom varies depending on the solvent. Only in water and methanol does it possess a negative charge and appropriate electron density distribution (2s and 2px orbitals), which can provide σ -donor ability. In other solvents, the electron pair is localized on π -orbitals (2py, 2pz), thus excluding the possibility of forming a σ -bond.

Solvent	Atom	Atomic Electron density on the			Electron distribution in orbitals				
Solvent	Atom	charge	atom	n	nS	nP_x	nPy	nP_z	
Gas	N(16)	0.164	4.836	2	1.382	1.005	1.466	0.983	
Water	N(16)	-0.113	5.113	2	1.583	1.177	1.372	0.980	
DMSO	N(16)	0.113	4.887	2	1.404	1.346	1.037	1.100	
Methanol	N(16)	-0.113	5.113	2	1.583	1.179	1.377	0.975	
Ethanol	N(16)	0.113	4.887	2	1.406	1.360	1.082	1.039	
Acetone	N(16)	0.117	4.883	2	1.403	1.335	1.025	1.013	
Chloroform	N(16)	0.126	4.874	2	1.402	1.300	1.130	1.042	
Hexane	N(16)	0.146	4.854	2	1.389	1.364	1.057	1.044	
Citric acid	N(16)	0.114	4.886	2	1.404	1.345	1.033	1.103	

Despite the high electron density, the positive effective charge on the sulfur atom S(18) under all conditions excludes its donor properties in coordination with metals.

Solvent	Atom	Atomic Electron density on the			Electron distribution in orbitals				
Solvent	Atom	charge	atom	n	nS	nP_x	nPy	nPz	
Gas	S(18)	0.284	5.716	3	1.876	1.225	1.548	1.068	
Water	S(18)	0.264	5.736	3	1.876	1.560	1.100	1.199	
DMSO	S(18)	0.263	5.737	3	1.876	1.527	1.107	1.226	
Methanol	S(18)	0.264	5.736	3	1.876	1.552	1.107	1.201	
Ethanol	S(18)	0.267	5.733	3	1.876	1.506	1.115	0.898	
Acetone	S(18)	0.264	5.736	3	1.876	1.508	1.111	1.241	
Chloroform	S(18)	0.269	5.731	3	1.876	1.469	1.102	1.284	
Hexane	S(18)	0.273	5727	3	1.876	1.555	1.104	1.192	
Citric acid	S(18)	0.264	5.736	3	1.876	1.523	1.109	1.227	

Conclusion

The MP3 method allowed for a detailed study of the electronic structure of the olanzapine molecule and the investigation of the influence of various solvents on its complexation ability.

The most likely donor atom is the nitrogen atom N(9), which consistently demonstrates the ability to form

covalent bonds with metals in all studied environments. Solvents with high dielectric constants, such as water and methanol, contribute to the stabilization of the molecule and can be recommended for the synthesis of olanzapine metal complexes. The quantum-chemical approach provides the opportunity to predict the behavior of the

molecule under different conditions in advance, facilitating the selection of synthesis conditions and the interpretation of experimental data, including IR spectroscopy and structural analysis of complex compounds.

References

- [1] Stewart J.J.P. "Optimization of parameters for semiempirical methods. I. Method". // J. Comput. Chem., 1989. Vol. 10, No. 2, 209–220.
- [2] Boyd D.B. "Solvent effects in quantum chemistry". // Reviews in Computational Chemistry, 2007, Vol. 23, p.355–378.
- [3] Dewar M.J.S., Zoebisch E.G., Healy E.F., Stewart J.J.P. "Development and use of quantum mechanical molecular models. AM1: a new general purpose quantum mechanical molecular model" // J. Am. Chem. Soc., 1985, Vol. 107, No. 13, 3902–3909.
- [4] Jensen F. Introduction to Computational Chemistry. 3rd ed., Chichester: Wiley, 2017, 664 p.
- [5] Cramer C.J. Essentials of Computational Chemistry: Theories and Models. 2nd ed., Chichester: Wiley, 2004, 596 p.
- [6] Gogberashvili, Z., Tsintsadze, M., Kilasonia, N. Gegeshidze, N. "Synthesis of mixed ligand (2-amino-6-methylpyridine, azelaic acid dihydrazide) coordination compounds and study of physico-chemical properties". *International scientific conference "Chemistry-achievements and perspectives"* Tbilisi, Georgia, p.80, 2023

- [7] Tsintsadze, M., Gegeshidze, N., Kilasonia, N. Preparathion and characterization of some double complex compounds of metals with N,Ndimethylformamide." CHEMICAL AND TECHNOLOGICAL ASPECTS OF BIOPOYMERS. Book Volume IP. 26-35, Publishing House "UNIVERSAL
- [8] Kilasonia, N., Lochoshvili, D., Jokhadze, E., Tsintsadze, M. "Quantum-chemical study of caprylic acid hydrazide molecule by AM1 method in different solvents". 2nd InterlScient. Conf. "Science, Education, Innovation and Chemical Technologies from Idea to Implemention"Seasonal school for masters and doctoral students "Innovation - from Idea to Implemention". TSU, Tbilisi, Georgia, 2023
- [9] Tsintsadze, M., Giorgadze, T., Sharia, I., Tsintsade, G., "Coordination compounds of Co(II) and Ni(II) with nitrogen- and oxygen-containing ligands - derivatives of the heterocyclic series (meta-nitrobenzaldehyde hydrazones), Technical University, Tbilisi, 2021, 142 p. . ISBN 978-9941-28-700-8
- [10] Tsintsadze, G., Lochoshvili, D., Topuria, E., Tusiashvili, T. "Solvent effect on complex formation of dimethylacetamide and N,N-dimethylformamide", Herald of the National Academy of Sciences of Georgia. Chemistry series. 2016, vol. 42, N3 p. 320-324
- [11] Chanturia M.M., Giorgadze T.Z., Lochoshvili D.M., Gulbani D.V., "Energy, electronic and structural characteristics of alpha-pyridinaldehyde isonicotinoylhydrazone (Apainh) molecule in different solvents calculated by the quantum-chemical

Development of Graphene Production Technology

T. Qamushadze *, E. Khutsishvili, N. Kobulashvili, M. Darchiashvili

*LEPL Ferdinand Tavadze Metallurgy and Materials Science Institute, Tbilisi, Georgia 8 Elizbar Mindeli St, Tbilisi, 0186, Georgia E-mail:elzakhutsishvili@yahoo.com

Abstract. As is known, graphene is a two-dimensional (2D) form of carbon. It consists of a single layer of carbon atoms arranged in a hexagonal lattice structure with a sp²-hybridized electronic configuration. Unlike other configurational forms of bulk graphite, it is distinguished by such unique properties as the highest mechanical strength, the greatest resistance to chemical influences, the gigantic mobility of current carriers, and many others. Therefore, based on its properties, it can already be said today that in the near future, graphene will undoubtedly become the main element of many new unique innovative devices. One of the most pressing problems of modern high technologies is the refinement and modernization of methods for obtaining graphene and the discovery of its unknown properties. To partially solve these problems, graphene was obtained in the work. For this purpose equipment was developed based on the method of chemical deposition of carbon atoms from the air phase and manufactured. By numerous experiments methane was selected from various hydrocarbons for pyrolysis, which turned out to be optimal for the successful implementation of the intended technological process. Since the transportation, storage, and use of pure methane in experiments posed many technical problems, a 20% mixture of it with an inert gas (argon) was used. The composition and quality of the resulting layers were determined by electron microscopy. Energy Dispersive Spectroscopy (EDS) revealed that in addition to carbon and copper, traces of oxygen were also detected in the obtained samples, which is mainly due to copper rust on the surface of the coating and, in part, to oxygen molecules adsorbed on the surface of the coated graphene.

თ. ქამუშაძე, ე. ხუციშვილი, ნ. ქობულაშვილი, მ. დარჩიაშვილი - გრაფენის მიღების ტექნოლოგიის შემუშავება

რეზიუმე. როგორც ცნობილია, გრაფენი არის ნახშირბადის ორგანზომებილიანი (2D) ფორმა. იგი შედგება ნახშირბადის ატომების ერთი მარტივი ფენისგან, რომლებიც ${\sf sp}^2$ -ჰიბრიდიზაციის ელექტრონული კონფიგურაციით არიან განლაგებული ჰექსაგონალური მესრის სტრუქტურაში. მოცულობითი გრაფიტის სხვა კონფიგურაციული ფორმებისაგან განსხვავებით, იგი გამოირჩევა ისეთი უნიკალური თვისებებით, როგორიცაა უმაღლესი მექანიკური სიმტკიცე, უდიდესი მედეგობა ქიმიური ზემოქმედებების მიმართ, მასში დენის მატარებელთა გიგანტური ძვრადობა და მრავალი სხვა. ამრიგად, მისი თვისებებიდან გამომდინარე, დღეს უკვე შეიძლება ითქვას, რომ ახლო მომავალში გრაფენი უეჭველად მოგვევლინება არაერთი ახალი უნიკალური ინოვაციური მოწყობილობის ძირითად ელემენტად. თანამედროვე მაღალი ტექნოლოგიების ერთ-ერთი ყველაზე აქტუალური პრობლემაა გრაფენის მიღების მეთოდების დახვეწა-მოდერნიზაცია და მისი უცნობი თვისებების გამოვლენა. ამ პრობლემების ნაწილობრივ გადასაჭრელად სამუშაოში განხორციელდა გრაფენის მიღება. ამისათვის შემუშავებული იქნა პროექტი და დამზადდა აირფაზიდან ნახშირბადის ატომების ქიმიური დალექვის მეთოდზე დაფუძნებული დანადგარი, ჩატარებულ იქნა მრავალი ექსპერიმენტი, რის საფუძველზეც სხვადასხვა ნახშირწყალბადებიდან პიროლიზისთვის შეირჩა მეთანი, რომელიც ოპტიმალური აღმოჩნდა დასახული ტექნოლოგიური პროცესის წარმატებით ჩასატარებლად. რადგანაც სუფთა მეთანის ტრანსპორტირება, შენახვა და ექსპერიმენტებში გამოყენება მრავალ ტექნიკურ პრობლემებს მოიცავდა, ამიტომ გამოყენებულ იქნა ინერტულ აირთან (არგონი) მისი 20% -იანი ნარევი. ელექტრონული მიკროსკოპიით დადგინდა მიღებული ფენების შედგენილობა ენერგოდისპერსული სპექტროსკოპიის (Energy Dispersive Spectroscopy –EDS) მეთოდით დადგინდა, რომ მიღებულ ნიმუშებში, გარდა ნახშირბადისა და სპილენძისა, დაიმზირება ჟანგბადის კვალიც, რომელიც განპირობებულია ძირითადად საფენის ზედაპირზე არსებული სპილენძის ოქსიდით და, ნაწილობრივ, დაფენილი გრაფენის ზედაპირზე ადსორბირებული ჟანგბადის მოლეკულებით.

Keywords: deposition, carbon, layer, hydrocarbon, pyrolysis, substrate.

Introduction

One of the promising new materials needed for the further development of modern high technologies is graphene, which is the thinnest, purest, strongest, plastic, chemically inert, thermally stable material in the world. Graphene exhibits a high crystalline quality, where charged relativistic particles with zero mass move ballistically, without scattering, over long distances and are thus

characterized by a gigantic mobility of 10⁵ cm²/V·s (300K). Although the areas of application of graphene have not yet been fully identified, but based on its properties, it can already be said that in the near future it will become the main element of a number of new unique innovative devices. However unknown, unusual, unique properties of graphene are not yet fully understood.

The reason is that graphene is a two-dimensional form of carbon (2D), consisting of a single layer of carbon atoms arranged in a

hexagonal lattice structure with a sp²-hybridized electronic configuration [1]. The physical structure of graphene is a puzzle, because according to both theory and experiment [2-6], crystals cannot exist in a free state in a perfect two-dimensional 2D space. Graphene is the basic structural element of all other carbon materials such as graphite, carbon nanotubes, and fullerenes. It was unconsciously "produced" for centuries during pencil sharpening, but was first isolated in 2004 by the well-known method of micromechanical cleavage [7]. Although many works has been devoted to graphene production technology [8-15], its perfection is still associated with many problems. Improving and modernizing the methods for obtaining graphene, and revealing its unknown properties, which is so necessary to discover new areas of its use, is one of the most important and pressing problems today.

The goal of this work was to partially solve these problems and obtain mono- or multi-sheet graphene. To this end, a number of tasks were set:

- Selection of the optimal chemical deposition method from existing ones;
- Creation of appropriate equipment for the selected method;
- Selecting the optimal hydrocarbon for pyrolysis from various hydrocarbons;
- Investigation of obtained layers of graphene.

Experimental

Currently, various modifications of mechanical, chemical, epitaxial, and air-phase deposition methods are mainly used to obtain graphene. The air-phase deposition is attractive because graphene grows by this method on a metal surface, such as Cu, Pt, Ir, etc. Then graphene can be separated from the metal and transferred to different substrates according to the application.

Air-phase chemical deposition method. Among the metals on which graphene grows, copper is the most attractive. During the chemical deposition of carbon atoms from any carbon source at high temperatures completely different processes occur on the surface of polycrystalline copper compared to other metals. For example, the solubility of carbon in copper is 1000 times lower than in nickel. Because of this, carbon atoms deposited on the copper surface cannot diffuse throughout the volume. As the temperature of the substrate increases, the probability of the formation of a graphene layer on its surface increases and its area increases too. In addition, it is possible to obtain not only multilayer graphene sheets, but also monolayer graphene on copper, since copper acts as a catalyst during carbon deposition process. So after coating a copper surface with a monolayer of graphene, the probability of deposition of subsequent layers of graphene on it sharply reduces. This method is very promising for large-scale production of graphene.

Technological process. The main node of the equipment for production of graphene is a reactor.

It is possible to obtain a vacuum, introduce hydrogen and inert gases under controlled pressure, and conveniently place the copper substrate into the reactor. To conduct pyrolysis of hydrocarbon gas, the reactor is placed into a furnace, which ensures to obtain the appropriate temperature over a fairly wide temperature plateau. After pyrolysis, the equipment provided controlled cooling of the reactor and also supply of electricity and water

A schema of equipment for production of graphene is shown in Fig.1.

The equipment consists of two coaxial quartz tubes (1, 2), whose diameters are 80 mm and 50 mm, respectively. The tubes are horizontally rigidly fixed to a steel stand (3) by means of a two-groove flanged pipe system (4), the grooves of which are equipped with vacuum rubber pad. The flanges are cooled by technical water flowing through the fittings (6). The space

between the quartz tubes is connected to the vacuum and air supply systems via fittings (5). A cart (9) with a furnace (10) moves freely by rollers (8) along the pipe (7), which is attached to the stand. The furnace can move with the cart and heat the desired part of the tube (1) placed in it.

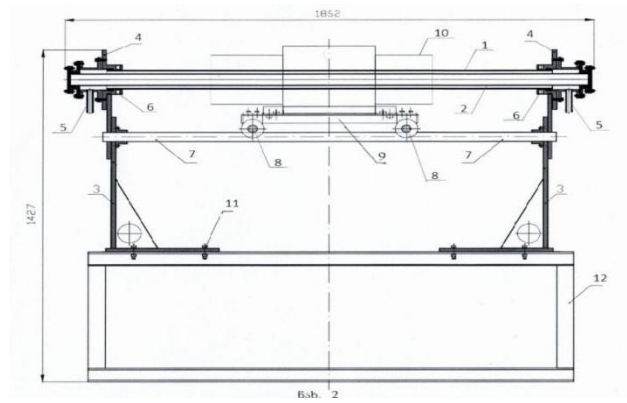


Fig. 1. A schema of equipment for production of graphene. 1,2- coaxial quartz tubes; 3- steel stand; 4-flanged pipe system; 6- fittings; 7- pipe; 8- rollers; 9-cart; 10- furnace; 11-nuts; 12- steel base.

The furnace is equipped with thermocouples that are connected to a thermostat and are used to regulate the temperature in the furnace. The stand is rigidly attached to a steel base (12) by means of bolts, and nuts (11). The length of the equipment is 1862 mm, and the height is 1427 mm.

Initially, studies were conducted to select hydrocarbons for pyrolysis. The studies were conducted using propane (C₃H₈), hexane (C₆H₁₄), and methane (CH₄). The final product of pyrolysis of all three hydrocarbons is carbon and hydrogen. However, during the pyrolysis of propane, an easily usable product, an oily residue remained on the copper substrate and reactor walls, which we explained by the fact that propane production involves the addition of aromatic oils to the product, which are very difficult to clean. Hexane pyrolysis begins at 600°C and, as with other heavy hydrocarbons, proceeds in a complex manner, with the formation of various intermediate hydrocarbons. Then process continues with decomposition of hydrocarbons into lighter ones, etc. The carbon atoms formed during the decomposition of each of these intermediate products deposited on the copper layer in portions, and therefore the thickness of the resulting graphite layer cannot be controlled. The best results were observed when using methane (CH₄), specifically, during the pyrolysis of a methane-argon mixture, in which the methane content was 20%. The use of the mixture dramatically reduced the expected risks not only during its transportation, but also during storage and technological processes. Therefore the aforementioned methane-argon mixture was chosen as the working material.

Before conducting the technological process, the reactor was purging first with argon, then with a 20% mixture of argon and methane (to a pressure of 1.5 atm). After inert argon purging the reactor, a vacuum was established in it, and then a 20% mixture of argon and methane was introduced into the reactor. Before the furnace was turned on, the pressure of the gas mixture in the reactor was +0.2 atm. During the heating process the pressure increased and reached +0.6 atm at approximately 700°C. Methane pyrolysis was carried out in the temperature range of 700°C -750°C in two regimes. During the first regime the copper foil was heated up with the furnace. During the second regime the furnace was heated up separately and then was rolled using a cart and the copper foil was placed in the already hot furnace. The difference between these two regimes is that since methane decomposes even at temperatures lower than 700°C (starting at

 450^{0} C), in the first case the sample undergoes deposition of carbon atoms for a much longer time than in the second case. In both regimes, the excerpt at the final temperature lasted the same amount of time - 10 minutes. Then the reactor was cooled. When the sample cooled with the furnace, then the deposition of carbon atoms on the sample continued until the furnace temperature dropped to 450° C. To prevent this, immediately after the process was completed, the sample was removed from the furnace using a cart and the reactor cooling fans were turned on. Typical graphite layers obtained experimentally by us are shown in Fig. 2.

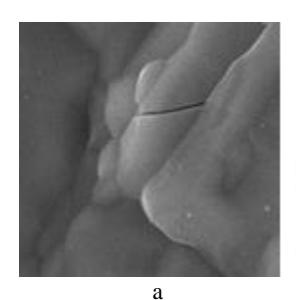


Fig. 2. Typical graphite layers obtained experimentally

Due to the nature of graphene layers, the most informative analysis is provided by an electron microscope SEM (Scanning Electron Microscope) with the LaB6-cathode TESCAN VEGA 3–XMU

Results and Discussion

The analysis of the composition of the layers was carried out by the SEM using the X-ray EDS (Energy Dispersive Spectroscopy) method, the sensitivity of which in average is 0.1 at.%. An electronic images of graphene layers shown in Fig. 2. are presented in Fig. 3. The images taken at different magnifications showed almost the same result for all of the layers, which indicates the presence of multilayer graphene scales on the copper layer (Figs. 3). The electronic images were taken near the graphene boundary, so the multilayered landscape of graphene "flakes" is clearly visible.



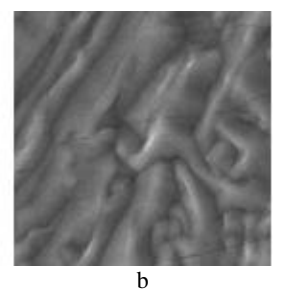


Fig. 3. SEM images of graphene surface layer taken at different magnifications; scale: $a-1\mu m$; $b-2\mu m$.

Figure 4 shows a typical energy dispersive spectrum of a graphene sample and Table 1 presents the copper, carbon, and oxygen contents in the layer.

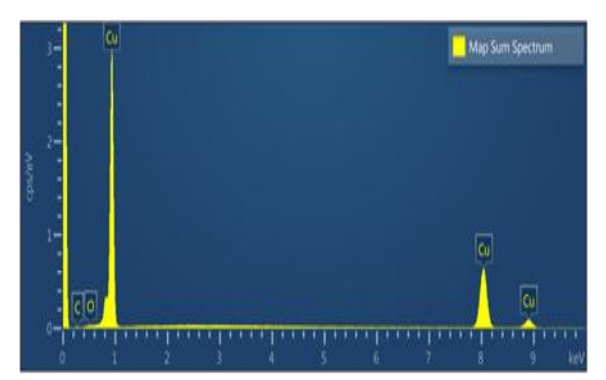


Fig. 4. Energy dispersive spectrum of graphene layer

Table 1. Elemental composition of graphene layer

Element	Weight %	Atomic %
Cu	97.23	87.16
0	0.25	0.87
C	2.52	11.97
Total	100.00	100.00

Energy Dispersive Spectroscopy (EDS) method revealed that copper, carbon, and oxygen, in certain percentages, were present in all of the layers we produced. At the same time, their carbon content varies within 10-12 atomic percent, while the oxygen content is 0.5-3 at.%. The presence of copper and carbon in the layers is clear. To determine the origin of oxygen, we also examined the surface of the copper foil used as a coating during the process using the same method. Naturally, no trace of carbon was visible on it, but oxygen in the order of 0-2 at.% was observed.

Conclusion

Compared to other hydrocarbons, methane is the most convenient for implementing this technology, as its pyrolysis produces multilayer graphene layers on the surface of copper foil. Energy-dispersive spectroscopy revealed that in addition to carbon and copper, traces of oxygen were also observed in the obtained samples, which is mainly due to copper rust on the surface of the coating and partially adsorbed oxygen molecules on the surface of the deposited graphene.

References

- [1] Yang, G., Li, L., Lee, W. B., Ng, M. C. « Structure of graphene and its disorders: a review", *Science and Technology of Advanced Materials*, 19(1) 2018, 613-648.
- [2] Peierls, R. R. « Quelques propriétes typiques des corps solidesé, *Ann. Inst. Henri Poincare*, 5,1935, 177-222.
- [3] Landau, L.D. and Lifshitz, E.M. Statistical Physics. Part 1, Pergamon, Oxford, 1980.
- [4] Mermin, N.D. Crystalline order in two dimensions, Phys. Rev., 176 (1968) 250-254.
- [5]Peierls, R.E. Bemerkungen uber Umwandlungstemperaturen, *Helv. Phys. Acta*, 7, 1934, pp. 81-83.
- [6] Novoselov, K.S. ,Jiang, D, Schedin, F. Geim, A.K. "Two-dimensional atomic crystals", *Phys. Sci.*, 102, 2005, pp. 10451-10453.
- [7] Novoselov, K.S., Geim, A.K., Morozov, S.V., Jiang, D., Zhang, Y., Dubonos, S.V., Grigorieva, I.V., Firsov, A.A. "Electric field effect in atomically thin carbon films", *Science*, 306, 2004, pp. 666-669.

- [8] Zhang, Y.B., Tan, Y.-W., Stormer, H.L., Kim, Ph. "Experimental observation of the quantum Hall effect and Berry's phase in graphene", *Nature*, 438 2005, pp. 201-204.
- [9] Kane, C.L., Mele, E.J. "Quantum spin Hall effect in graphene", *Phys. Rev. Lett.*, 95, 2005, 226801 (1-4).
- [10] Peres, N.M.R., Castro Neto, A.H., Guinea, F. "Conductance quantization in mesoscopic graphene", *Phys. Rev. B*, 73, 2006, 195411 (1-8).
- [11] Khveshchenko, D.V. "Coulomb-interacting Dirac fermions in disordered graphene", *Phys. Rev. B*, 74, 2006, 161402 (R1-R4).
- [12] Morozov, S.V., Novoselov, K.S., Katsnelson, M.I. Schedin, F., Ponomarenko, L.A., Jiang, D. and Geim, A.K. "Strong suppression of weak localization in graphene", *Phys. Rev. Lett.*, 97, 2006, 016801 (1-4).
- [13] Pisana, S., Lazzeri, M., Casiraghi, K.S., Novoselov, C., Geim, A.K., Ferrari, A.C., Maur, F. "Breakdown of the adiabatic Born–Oppenheimer approximation in graphene", *Nat. Mater.*, 6, 2007, pp. 198-201.
- [14] Abanin, D.A., Lee, P.A. and Levitov, L.S. "Randomness-induced *XY* ordering in a graphene quantum Hall ferromagnet", *Phys. Rev. Lett.*, 98 2007, 156801 (1-4).
- [15] Miao, F., Wijeratne, S., Zhang, Y., Coskun, U.C., Bao, W. and Lau, C.N. "Phase-coherent transport in graphene quantum billiards", Science, 317 2007, pp. 1530-1533.